KAUNAS UNIVERSITY OF TECHNOLOGY

SIGITA KAŠĖTAITĖ

BIODEGRADABLE PHOTOCROSS-LINKED POLYMERS AND POLYMER COMPOSITES OF GLYCEROL DIGLYCIDYL ETHER

Doctoral dissertation
Technological sciences, Chemical Engineering (05T)

2018, Kaunas

KAUNO TECHNOLOGIJOS UNIVERSITETAS

SIGITA KAŠĖTAITĖ

BIOSKAIDŪS TINKLINIAI GLICEROLIO DIGLICIDILETERIO POLIMERAI IR POLIMERINIAI KOMPOZITAI

Daktaro disertacija
Technologijos mokslai, chemijos inžinerija (05T)

2018, Kaunas

Disertacija rengta 2014–2018 metais Kauno technologijos universiteto Cheminės techologijos fakultete Polimerų chemijos ir technologijos katedroje. Mokslinius tyrimus rėmė Lietuvos mokslo taryba.

Mokslinė vadovė:

Prof. dr. Jolita OSTRAUSKAITĖ (Kauno technologijos universitetas, technologijos mokslai, chemijos inžinerija, 05T).

Interneto svetainės, kurioje skelbiama disertacija, adresas:
http://ktu.edu

Redagavo:

Gavin Stewart (Užsienio kalbų centras, Kauno technologijos universitetas)

CONTENTS

ABBREVIATIONS

3D – three-dimensional
3DLL – 3D laser lithography
ACE – activated chain end
AM – activated monomer
BAPO – phenylbis(2,4,6-trimethylbenzoyl)phosphine oxide
CAD – computer-aided design
CAE – 3',4'-epoxycyclohexylmethyl-3,4-epoxycyclohexanecarboxylate
CG – crude glycerol
CPI – cationic photoinitiator
DGEBA – bisphenol A diglycidyl ether
DMA – dynamic mechanical analysis
DMTA – dynamic-mechanical thermal analysis
DPL – dynamic projection lithography
DSC – differential scanning calorimetry
E – irradiance energy dose
E' – storage modulus (determinated in a tension mode)
ER – epoxy resin
FRPCP – free radical promoted cationic photopolymerization
FT-IR – Fourier transform infrared
G" – loss modulus
G' – storage modulus (determinated in a shear mode)
GDGE – glycerol diglycidyl ether
HM – horn meal
IR – infrared
LA – photolithography
LDPE – low density polyethylene
ŋ* – complex viscosity
OWRK – Owens-Wendt-Rabel-Kaelble
PG – phosphogypsum
PI – photoinitiator
pK_a – dissociation constant
PVA – poly(vinyl alcohol)
RC – rapeseed cake
RD – reactive diluent
SLA – stereolithography
tanδ – loss factor
$T_{dec.-10\%}$ – thermal decomposition temperature at the 10 % weight loss
T_g – glass transition temperature
TGA – thermogravimetric analysis
t_{gel} – gel point
TPO – diphenyl(2,4,6-trimethylbenzoyl)phosphine oxide
UV – ultraviolet
UV/Vis – ultraviolet/visible

INTRODUCTION

Relevance of the work

The estimated world production of plastics for 2017 was 400 million tons and is expected to increase to 1800 million tons by the year 2050 [1]. Petroleum resources are extensively used for the production of these plastics [2], which are typically stable in the environment for a long time and in many application fields this could be a disadvantage. This could be avoided by using bioplastics. Bioplastics are either biobased, biodegradable, or feature both properties [3], therefore they are more environmentally friendly compared to petroleum-based plastics. The world production of bioplastics for 2017 was 2.05 million tons and is expected to increase 20 % by the year 2022 [3]. The European Commission initiated the "*Europe 2020*" strategy which determines the exploitation of materials from renewable resources as the main direction towards innovative and sustainable development of the economy [4]. Such materials have features including less dependency on limited and increasingly expensive fossil resources, low toxicity and high biodegradability, potentially better recovery and recycling options. Glycerol, as a by-product of biodiesel production [5], or glycerol derivatives can be used as starting materials for the preparation of biodegradable plastics.

The usage of three-dimensional (3D) printing technology in the production of plastics attracts attention due to flexibility of the process and fast production compared to the traditional manufacturing methods, which reduces time-to-market [6]. The production time is reduced by applying ultraviolet/visible (UV/Vis) light irradiation technology, which increases production speed involving less direct labor and higher production capacity [7]. This leads to increased productivity and better exploitation of equipment [7].

The use of petroleum-based plastic mulching films in agriculture produces a huge amount of wastes to be disposed of at the end of their lifetime [8]. Biodegradable plastic mulching films could solve this environmental pollution problem. The incorporation of nitrogen and phosphorus containing waste materials, e.g. rapeseed cake (RC), phosphogypsum (PG), and horn meal (HM) into biodegradable plastic mulching films can increase their biodegradability and act as mulch or slow-release fertilizers for plants [9].

The aim of this work was the synthesis of novel biodegradable glycerol diglycidyl ether-based photocross-linked polymers, formation of polymeric biocomposites, characterization, and exploring of their potential applications in optical 3D printing and mulching coatings.

The tasks proposed for the achievement of the aim were as follows:

1. Synthesis of novel biodegradable photocross-linked polymers of glycerol diglycidyl ether and epoxy reactive diluents and investigation of their properties.

2. Synthesis and properties investigation of novel biodegradable photocross-linked polymers of glycerol diglycidyl ether and di- or trihydroxyl compounds.
3. Evaluation of compositions based on glycerol diglycidyl ether on applicability in optical 3D printing.
4. Formation and properties investigation of novel biodegradable photocross-linked polymer composites of glycerol diglycidyl ether and biobased industrial waste materials (rapeseed cake, phosphogypsum, and horn meal), as well as the evaluation of their potential application for mulching coatings.

Scientific novelty of the work

1. Novel biodegradable photocross-linked polymers of glycerol diglycidyl ether and epoxy reactive diluents were synthesized. The composition of glycerol diglycidyl ether and 3',4'-epoxycyclohexylmethyl-3,4-epoxycyclohexanecarboxylate was found to be suitable for optical 3D printing.
2. Novel biodegradable photocross-linked polymers of glycerol diglycidyl ether and di- or trihydroxyl compounds were synthesized. The addition of di- or trihydroxyl compounds into the compositions accelerated photocross-linking of glycerol diglycidyl ether.
3. Novel biodegradable composites of glycerol diglycidyl ether-based photocross-linked polymer and biobased industrial waste materials (rapeseed cake, phosphogypsum, and horn meal) were produced. The composites are suitable as biodegradable mulching coatings.

Practical value of the work

Novel photocurable system based on glycerol diglycidyl ether and 3',4'-epoxycyclohexylmethyl-3,4-epoxycyclohexanecarboxylate was selected and tested by dynamic projection lithography (DPL) and direct femtosecond 3D laser lithography (3DLL) by using 3D optical printer *Ember* and *Laser Nanofactory* setup. The selected photoresin was found to be suitable for producing 3D microstructures by DPL and 3DLL.

The main statements of the dissertation

1. Novel photocurable systems based on glycerol diglycidyl ether and epoxy reactive diluents are applicable as renewable biodegradable photoresins for rapid optical 3D printing on demand.
2. The addition of di- or trihydroxyl compounds accelerates the photocross-linking of glycerol diglycidyl ether and improves biodegradability of the resulting polymers.
3. Novel biocomposites of glycerol diglycidyl ether-based photocross-linked polymer and biobased industrial waste materials (rapeseed cake, phosphogypsum, and horn meal) are applicable as biodegradable mulching coatings.

Approval and publication of research results

The results on the topic of this dissertation have been published in 4 scientific articles in the journals indexed in *Clarivate Analytics Web of Science* database and 12 papers presented in the proceedings of international scientific conferences.

Structure and content of the dissertation

The dissertation consists of an introduction, literature review, experimental part, results and discussion, conclusions, a list of references, and a list of publications. The dissertation consists of 118 pages, 26 tables and 50 figures, 14 mathematical expressions and equations. The list of references consists of 289 bibliographic sources.

Contribution of the author

The author has designed, synthesized, and characterized 3 different series of glycerol diglycidyl ether-based photocross-linked polymers and polymeric composites. The author has also performed the real time photorheometry curing tests, mechanical testing, dynamic-mechanical thermal analysis, swelling experiments, measurements of contact angle, determined the yield of insoluble fraction, calculated the cross-linking density and surface free energy. Infrared spectroscopy, differential scanning calorimetry, and thermogravimetric analysis were performed by the corresponding technicians of the Department of Polymer Chemistry and Technology, Kaunas University of Technology. Dynamic mechanical analysis was performed with the assistance of Dr. Egidija Rainosalo (Technology Center Ketek Ltd. and Centria University of Applied Sciences, Finland). Biodegradability experiments were performed by Dr. Danguolė Bridžiuvienė (Biodeterioration Research Laboratory, Nature Research Center, Lithuania). The author has analyzed and described all the data of the investigations mentioned above. Photolithography and dynamic projection lithography were performed and the data were analyzed by Edvinas Skliutas with the assistance of Dr. Mangirdas Malinauskas (Laser Research Center, Vilnius University, Lithuania). 3D laser lithography was performed and the data were analyzed by Linas Jonušauskas (Femtika, UAB, Lithuania).

1. LITERATURE REVIEW

1.1. Glycerol

Glycerol (propan-1,2,3-triol according to IUPAC) is a liquid compound containing three hydrophilic hydroxyl groups that are responsible for hygroscopicity and solubility in water [10]. It is also commercially called as glycerin, 1,2,3-propanotriol, trihydroxypropane, glyceritol or glycidic alcohol [11]. The term glycerin is used to name purified commercial products with content $\geq$ 95 % of glycerol [12]. Synthetic glycerol is petroleum-based [13] and can be produced by chemical reactions [14] starting from propylene (Fig. 1.1). The most important process involves the chlorination of propylene resulting in allyl chloride (path a) [15]. Then allyl chloride is oxidized using hypochlorite to dichlorohydrins which reacts with a strong base resulting in epichlorohydrin. Glycerol is the product of epichlorohydrin hydrolysis. Chlorine-free processes include the synthesis from acrolein and propylene oxide (paths b and c) [15]. Propylene is oxidized to acrolein which is reduced to allyl alcohol (path b). Then, in the presence of hydrogen peroxide, glycidol is formed through an epoxidation. Glycidol is converted to glycerol through the hydrolysis. Due to the large production of biodiesel where glycerol is a by-product, the market is filled of glycerol. Therefore, the synthetic reactions are not economical. Natural glycerol obtained from biodiesel production could be an alternative to synthetic petroleum-based glycerol.
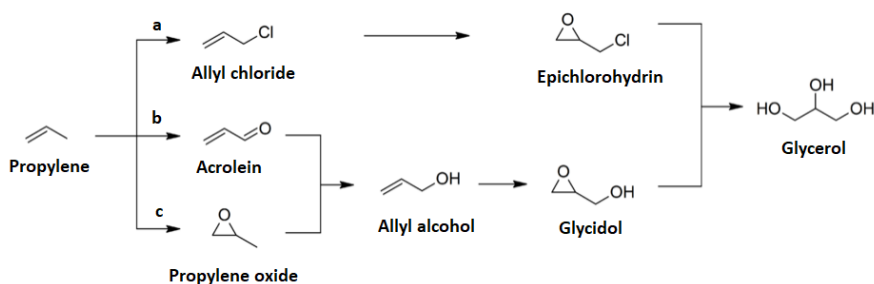
Fig. 1.1 Glycerol synthesis from propylene

1.1.1. Glycerol as a by-product of biodiesel production

Biodiesel is an alternative renewable fuel to conventional petroleum diesel derived from fossil materials, which are unsustainable and non-renewable and contribute to global warming [16-18]. Biodiesel is described as mono alkyl esters of long chain fatty acids derived from renewable lipid feedstocks [19] such as animal fats and vegetable oils [20]. Therefore, it has advantages against petroleum diesel such as renewability, non-toxicity, biodegradability, clean burning, and lower sulfur and aromatic content [21, 22]. In addition, the use of biodiesel instead of petroleum diesel could reduce the global warming [23]. In Europe rapeseed oil is mainly used for biodiesel production [24, 25]. European and global biodiesel production from 2013 till 2022 is presented in Fig. 1.2 [26]. Biodiesel production has grown

gradually in European Union countries and the rest of the world. The production has risen from 11 billion l to 14 billion l in European Union countries and from 29 billion l to 33 billion l in the world until the year of 2017. The estimated world production of biodiesel for 2017 is 33 billion l and is expected to increase until 41 billion l by the year of 2022 [26].
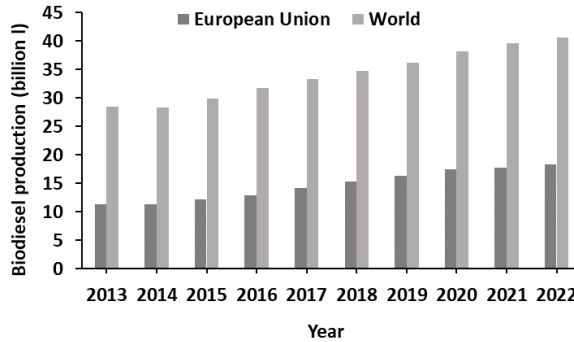
Fig. 1.2 Biodiesel production from 2013 till 2022 in European Union countries and world [26]

The list of countries that produced most of biodiesel in 2016 is shown in Fig. 1.3 [27]. The USA was the world largest biodiesel producer with 5.5 billion l of biodiesel. 2nd world largest biodiesel producer was Brazil with 3.8 billion l. Argentina, Germany and Indonesia shared 3rd place as the biggest biodiesel producing countries with a 3 billion l of biodiesel per year. The remaining countries such as France, Thailand, Spain, Belgium, and Colombia have produced 1.5, 1.4, 1.1, 0.5, 0.5 billion l of biodiesel in 2016, respectively.
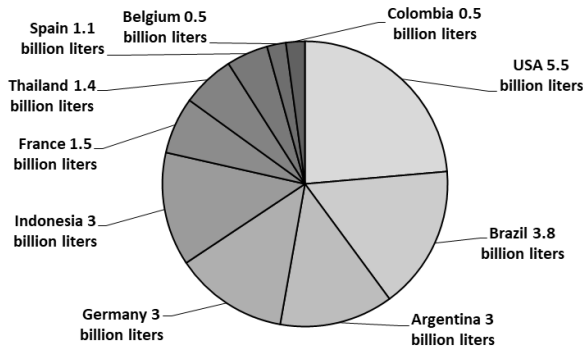
Fig. 1.3 Biggest biodiesel producing countries in 2016

Biodiesel production generates about 10 wt. % of glycerol as the main by product [28-32]. This suggests that in 2017 about 3.3 billion l of glycerol was produced. As the production of biodiesel increases, the amount of glycerol as a by-product also will be higher, and the problem of utilization is more relevant. The use of glycerol in the food, pharmaceutical or cosmetics industry and converting

12

glycerol into chemicals [33], which could be used as monomers for production of polymers, is the most useful utilization solution.

Crude glycerol (CG) is obtained as by-product from biodiesel production via trans-esterification reaction with methanol in the presence of a catalyst (acid or base) [34-37]. The schematic biodiesel production reaction from vegetable oil (triglyceride) is shown in Fig. 1.4.
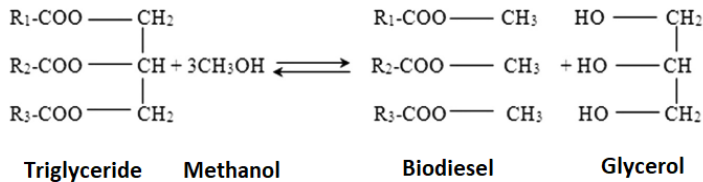
Fig. 1.4 Glycerol as by-product of biodiesel production [38]

1.1.1.1. Purification of crude glycerol

Only about 40-88 % of CG is pure glycerol [39]. The other components are the following: water, fatty acids and their esters, methanol, catalyst [40]. They must be removed before use of glycerol in food, pharmaceutical or cosmetics industry [41]. A number of ways is applicable to remove the impurities and increase the purity of glycerol. Glycerol refinement could be divided into two steps [42]. The preliminary purification is the first step, when non-glycerol compounds are neutralized and removed. A considerable amount of methanol is present in CG as it is added in excess to increase efficiency of trans-esterification process [25]. Methanol is generally recovered by heating and reused in the biodiesel production process as it is considered as ecological way [43]. The pH value is settled during acidification/neutralization. During the second step, selective purification through vacuum distillation, elimination of free ions with ion exchange resins, absorption on activate carbon, and densification is carried out in order to obtain the desired purity of the final product [42]. Glycerol of high quality (up to 99.5 %) is obtained during the mentioned purification [44]. Distillation using vacuum is applied in case of material is liable to polymerize at high temperatures [45]. Vacuum is required in the distillation process as refined glycerol polymerizes above 200 °C. This process requires high energy quantities due to high heat capacity of glycerol [46]. In order to remove free ions of glycerol, anion and cation exchangers can be used. As ion exchangers need to maintain efficiency, high amount of waste water is produced [47]. These purification methods consume high energy quantities, therefore selective separation using different types of membranes can be used [48]. Membrane separation is used to purify CG as alternative method to mentioned above, as it does not require water and is considered as an ecofriendly process [49] based on the differences in concentration or electric potential between two mediums. A process flow diagram of trans-esterification reaction and purification of CG is shown in Fig. 1.5.
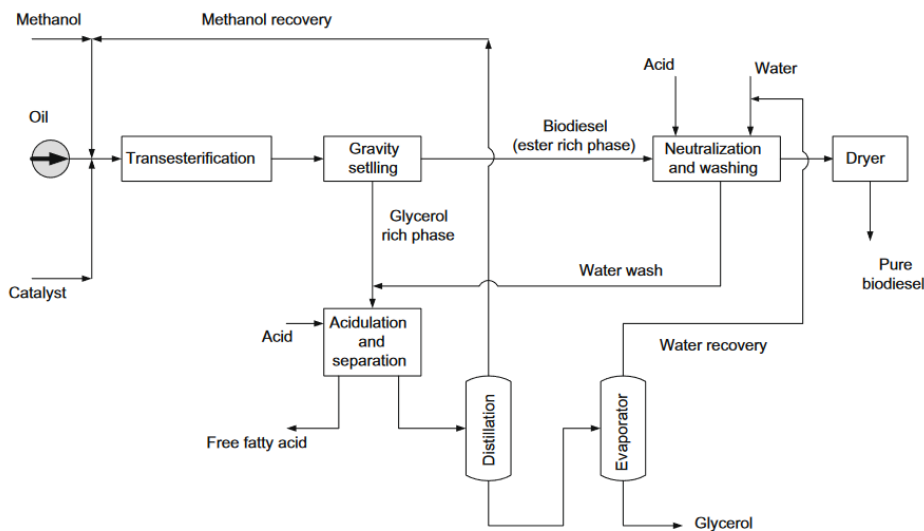
Fig. 1.5 Process flow diagram of trans-esterification reaction and crude glycerol purification [19]

After the oil trans-esterification reaction with methanol in the presence of catalyst (e.g. sodium hydroxide (NaOH), potassium hydroxide (KOH), and sodium methoxide (NaOCH$_3$)), the reaction mixture is allowed to cool and settle down [19]. The glycerol rich phase settles at the bottom and the ester rich phase forms the upper layer. Gravity separation is used to minimize the formation of emulsion and is based on the density difference between polar and non-polar phases. In this case, the glycerol rich phase is polar, and the ester rich phase is non-polar. By adding water to the ester rich phase, catalyst residue, small amount of monoglyceride and diglyceride is removed. The cost of the separation equipment is increased as 10 l of waste water are produced for 1 l of biodiesel [50]. The wash water is evaporated and methanol is returned back to the process. The salts are neutralized with an acid (e.g. with aqueous hydrochloric or phosphoric acid) [12]. The glycerol is purified during the distillation process. The methanol is evaporated and glycerol is obtained.

1.1.1.2. Application of crude glycerol in industry

The properties and versatile structure allows the use of glycerol in various industrial areas. At present, it is estimated that there are more than two thousand uses for glycerol. However, glycerol is used in small amounts in the majority of products [12]. The utilization of CG includes the production of different chemical products, hydrogen production, additives for automotive fuels, ethanol or methanol production, animal feed, and waste treatment [51]. The availability to use CG in animal nutrition industry is attractive as a larger volume of glycerol is expected to be utilized. CG could replace corn grain in diets fed to lactating dairy cattle [52]. Also glycerol can be a source of organic carbon for the denitrification of a municipal

waste water treatment plant [53]. Finally, CG can be used as a concrete additive to improve mechanical properties of the cement [54]. The industrial areas for the use of refined glycerol are summarized in Fig. 1.6.
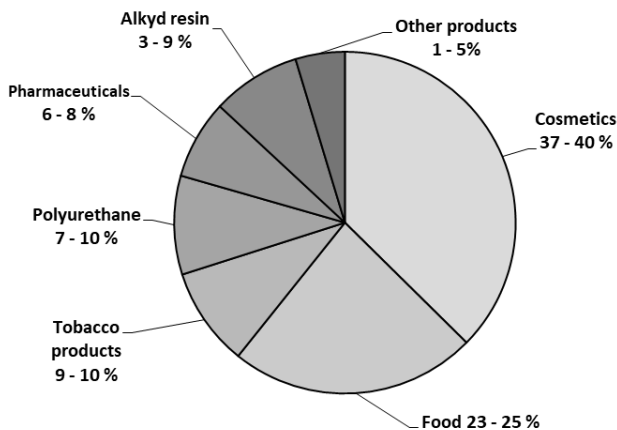
Fig. 1.6 Industrial areas for the use of glycerol [12, 55]

The majority (37-40 %) of all refined glycerol is used in cosmetics area for skin, hair care products [36] and food industry – (23-25 %) of all refined glycerol are used as sweetener, thickening agent, solvent, filler, sugar substitute, and preserve food [36]. Also purified glycerol can be used in production of tobacco (9-10 %) and polyurethane (7-10 %). The smaller quantities of glycerol are used in pharmaceutical and personal care products (6-8 % for production of cough syrups, allergen immunotherapies, toothpaste, mouthwashes, fiber softener, etc. [36]), for production of alkyd resin (3-9 %) and for the other products (1-5 %).

1.1.2. Glycerol derivatives

The excess of glycerol as a by-product of biodiesel production challenges scientists to design new products via modification of its functional groups [12]. The structure and properties of glycerol allows them to perform various chemical and microbial fermentation reactions to get chemicals and chemical intermediates. Glycerol can be easily modified through halogenation, reduction, cyclization, esterification, etc. reactions to get alternative green chemicals [56-58]. The conversion reactions of CG into chemicals and polymers are summarized in Fig. 1.7.
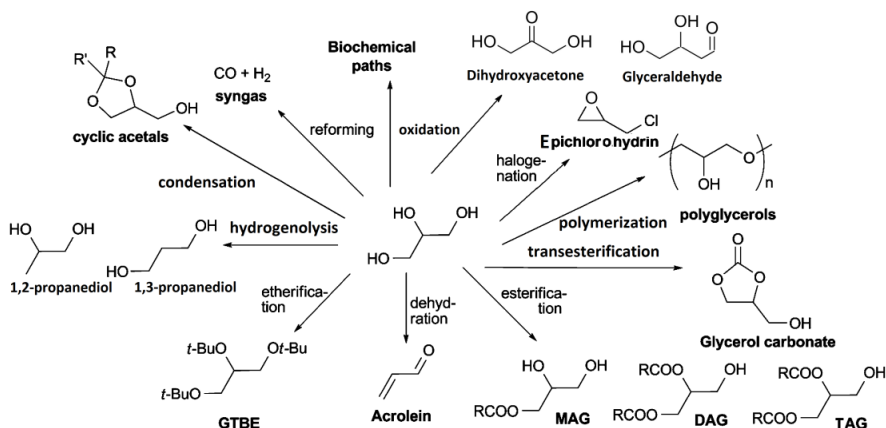
Fig. 1.7 Conversion reactions of crude glycerol into chemicals and polymers [59]

1.1.2.1. Glycerol derivatives obtained by microbial fermentation reactions

CG can be utilized by microbial fermentation as a carbon source in biochemical paths [60, 61]. Aerobic and anaerobic reactions are carried out to produce 1,2-propanediol, 1,3-propanediol, citric acid, lactic acid, dihydroxyacetone, ethanol, n-butanol, mannitol, polyhydroxybutyrate, hydrogen, etc. [62] (Fig. 1.8) Various microorganisms such as genera *Klebsiella*, *Enterobacter*, and *Lactobacilli* are used for bacterial fermentation of glycerol. Glycerol derivatives obtained by microbial fermentation are used in various areas such as food, cosmetics and personal care, pharmaceutical industry, and production of other chemicals and polymers. The pathogenicity of microorganisms, strict anaerobic conditions, and impurities could be limiting factors for the fermentation of CG [29]. The main products, used microorganisms, and the application of obtained products by microbial CG fermentation are listed in Table 1.1.
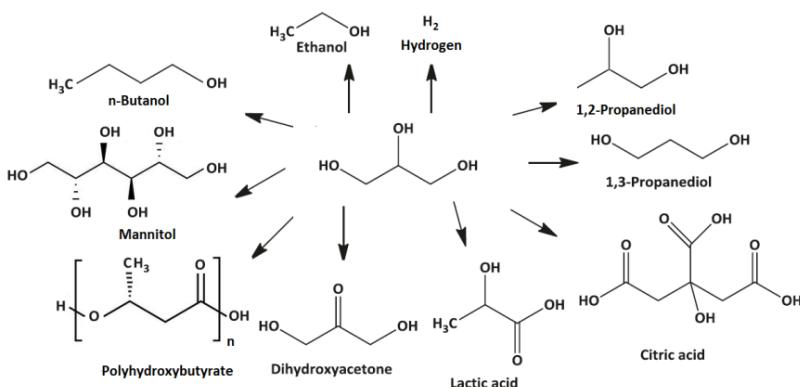
Fig. 1.8 Products obtained by microbial fermentation of crude glycerol

16

Table 1.1 List of products obtained by crude glycerol microbial fermentation using various microorganisms and their application in industry

Product	Microorganisms	Application in the industry
1,2-Propanediol	*Klebsiella, Citrobacter, Enterobacter, Clostridi, Lactobacilli* genera [63-66]	Production of polyester resin, as an additive in cosmetics and pharmaceuticals [67, 68]
1,3-Propanediol		Production of aliphatic polyesters, polyurethanes, sealants, coatings, paints [25, 69]
Citric acid	*Aspergillus niger Yarrowia lipolytica* [70]	Production of ice creams, in pharmaceutical and cosmetics industry, and as a cleansing agent [71]
Lactic acid	*E. coli, Lactobacillus rhamnosus, Klebsiella pneumonia* [29, 72]	Production of biodegradable polymers, non-toxic esters [73]
Dihydroxyacetone	*Gluconobacter oxydans* [74]	Cosmetics, food, pharmaceutical area, and in the synthesis of chemicals and biodegradable polymers [29, 59, 75]
Ethanol	*E. coli, Enterobacter aerogenes, S. cerevisiae, Ogataea polymorpha* [76, 77]	As sustainable bio-fuel [29]
n-Butanol	*Clostridium pasteurianum* [78]	Production of nitrocellulose, urea-formaldehyde or melamine-formaldehyde resins [79]
Mannitol	*Candida magnolia, Yarrowia lipolytica* [80, 81]	Production of ingredients of chewing gums, sweeteners for diabetics and polyesters [25, 82, 83]
Polyhydroxybutyrate	*Cupriavidus necator, Pseudomonas oleovorans* [84, 85]	Production of medical elements for internal sutures and packaging materials [25, 86]
Hydrogen	*Citrobacter freundii, Bacillus subtilis, Shigella sonnei nterobacter ludwigii*, etc. [87]	Production of hydrochloric and formic acid, cyclohexane, methanol, ammonia, urea, etc. and as a potential fuel [29]

1.1.2.2. Glycerol derivatives obtained by chemical reactions

CG can also be converted by chemical reactions into many products, such as dihydroxyacetone, glycerol carbonate, mono-, di-, triacetylglycerol (MAG, DAG, TAG), acrolein, glycerol tertiary butyl ether (GTBE), propanediols, cyclic acetals, syngas, polyglycerols, and epichlorhydrin [12, 51, 88] (Fig. 1.7). The disadvantage of chemical conversion is that the impurities of CG may take part in reactions and have an influence on product properties [89].

Oxidation reactions of CG using different catalysts as Pt, Pd, Au [88] results in the large number of products such as dihydroxyacetone, glyceraldehyde and their derivatives [90]. These compounds are potential materials for polymer synthesis which could be applied in biomedical area, e.g. dihydroxyacetone acid together with lactic acid is used for synthesis of biodegradable polymers [91]. Also, dihydroxyacetone is widely applied in cosmetics area as ingredient for sunless tanners [88].

The production of glycerol carbonate can be carried out via trans-esterification with dimethyl carbonate, carbonation using CO_2, and glycerolysis with urea [92-96]. Due to high toxicity and corrosive nature of phosgene [97], the catalytic trans-esterification reaction of glycerol with dimethyl carbonate is usually carried out concerning mild reaction conditions. Different homogeneous (KOH, NaOH, and K_2CO_3) or heterogeneous (as NaOH/γ-Al_2O_3, K_2CO_3/MgO) base catalysts can be employed to trans-esterification reaction of glycerol [88, 98, 99]. The application of glycerol carbonate in industry includes various areas, such as production of surface coating agents, emulsifiers, polymers, e.g. polyurethane. Also, glycerol carbonate is used as electrolyte in the semiconductors, plant activating agent, solvent in cosmetics, personal care, and pharmaceutical area, curing agent in cement and concrete, etc. [100, 101].

Esterification reaction of CG with acetic acid using conventional acids as homogeneous catalysts results in MAG, DAG, TAG [102]. MAG and DAG are used for production of biodegradable polyesters applied in cosmetics and biomedicine [103]. Regarding the ability to improve the fuel viscosity, TAG is applied as biodiesel additive [104].

The production of acrolein from CG is performed through aqueous glycerol dehydration using a heterogeneous acid catalyst [88]. Acrolein is applied as a starting material for the production of acrylic acid and superabsorbent polymers [105].

Etherification reaction of CG with isobutylene results in mono-GTBE, di-GTBE, and tri-GTBE [88]. The homogeneous catalysts, e.g. p-toluene sulfonic acid, methane sulfonic acid and heterogeneous acid catalysts such as zeolites is used for the etherification of CG [102]. GTBE is used as additive for biodiesel to decrease in the cloud point of biodiesel [106].

1,2-Propanediol and 1,3-propanediol can be obtained through hydrogenolysis in the presence of metallic catalyst and hydrogen [25, 107]. Metals such as Pt, Pd, Ru, Ir, Cu, and Ni are used as catalysts [108]. The application of 1,2-propanediol and 1,3-propanediol is summarized in Table 1.1.

Cyclic acetals are obtained by reaction of CG with aldehydes. Condensation reaction of CG with furfural in the presence of acidic catalyst results in 1,3-dioxolane and 1,3-dioxane [88]. Glycerol acetals are used as flavors [109], as additives for fuel to decrease carbon monoxide, unregulated aldehydes emissions, anti-freezing agents [110-112]. Also glycerol acetals are applied as disinfectants and solvents for cosmetic and medical products [113].

The catalytic steam reforming of glycerol at a high temperature (850-900 °C) [114] produces hydrogen and carbon monoxide, named as syngas (synthesis gas) [115]. Metals such as Ru, Rh, Ni, Ir, Co, Pt, Pd and Fe are used as catalysts in glycerol steam reforming [116-118]. The syngas can be used for the synthesis of chemicals such as methanol [119].

Oligomerization and polymerization of CG open up a large area for utilization of glycerol-based polymers. Base catalysts such as carbonates [120] are used for the production of polyglycerol via self-etherification at elevated temperature.

Polyglycerol is widely used for the production of polymeric materials such as polyurethanes, polyesters, epoxy resins, and different copolymers [25, 121, 122].

Halogenation reaction of CG with hydrogen chloride in the presence of acid catalysts results in a mixture of 3-chloro-1,2-propanediol and 2-chloro-1,3-propanediol as primary products [123]. The mixture of secondary products (1,3-dichloro-2-propanol and 1,2-dichloro-3-propanol) is converted to epichlorohydrin using NaOH [124] which is widely used for the production of adhesives, elastomers, and epoxy resins [125].

1.2. Photocross-linking of epoxy resins

1.2.1. Epoxy resins

Epoxy resins (polyepoxides) (ERs) are described as low-molecular-weight pre-polymers containing at least two epoxide (oxirane) groups [126] and were discovered in 1909 [127]. ERs are attractive due to their excellent engineering properties [126]:

- Versatile structure allows various polymerization reactions,
- No separation of volatiles during polymerization reaction,
- Very low shrinkage during polymerization,
- Possibility to obtain products with low and high T_g,
- Very high adhesion to many surfaces due to polar groups.

ERs are used as monomers for production of thermosetting polymers by cross-linking reactions [128]. Mechanical, thermal properties, and swelling of polymers can be improved to the desired direction by cross-linking [129]. The cross-linking restricts the motion of the chains and increases the strength of the polymer [130]. This means that polymer becomes more rigid and less elastic and might even become brittle by increasing the number of cross-links between polymer chains (cross-linking density). Brittleness can be avoided by toughening ERs with hardeners (curing or cross-linking agents) such as thermoplastic polymers [131-134] or inorganic nanoparticles [135, 136], but the most important hardeners are aliphatic and aromatic amines, anhydrides, and polyamides [137]. Basically, molecules which can react with epoxy groups are known as hardeners.

1.2.1.1. Typically used epoxy resins

Chemical structures of typically used ERs are shown in Fig. 1.9. About 75-90 % of all ERs are mostly produced from epichlorohydrin and bis(4-hydroxyphenylene)-2,2-propane, known as bisphenol A [138, 139]. Aromatic compounds are used in the production of ERs due to their stability and toughness, which reaches good thermal and mechanical properties [140]. However, bisphenol A is considered as a toxic material and can cause diseases such as reproductive and cardiovascular disorders, diabetes, and cancer [141-143]. Consequently, the use of bisphenol A diglycidyl ether (DGEBA) for the production of polymers might be limited in the future. However, according to the data from U. S. Food and Drug Administration (FDA), bisphenol A is considered as safe to use [144]. In February of 2018, the U.S. National Toxicology Program released the results of a research

program which indicate that Bisphenol A is unlikely to cause health effects to people when exposed to very low levels [145].

Bisphenol A diglycidyl ether (DGEBA)   **Bisphenol F diglycidyl ether**   **Epoxy Novolac**

4-Epoxycyclohexylmethyl 3,4 -epoxycyclohexanecarboxylate (CAE)
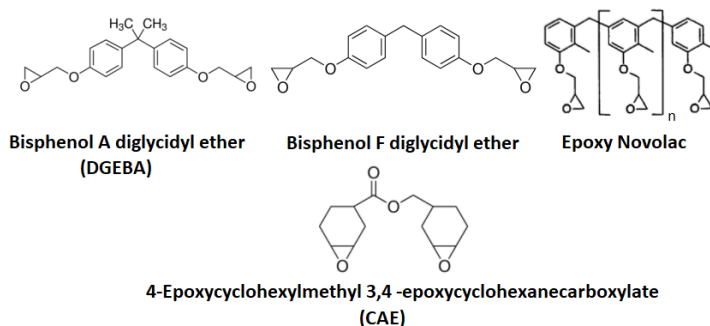
Fig. 1.9 Chemical structures of typically used epoxy resins

Bisphenol F diglycidyl ether has lower viscosity, higher reactivity, and better hardening properties at low temperatures compared with bisphenol A diglycidyl ether [146]. However, bisphenol F (bis(4-hydroxyphenyl)methane) is also considered as a cause of diseases and cancer [147, 148].

Epoxy novolac resin is glycidyl ether of phenolic novolac and is produced by the reaction of phenolic novolac resin with epichlorohydrin [149]. Epoxy novolac can be highly cross-linked due to many epoxy groups, which results in excellent thermal and chemical resistance properties, but low flexibility [150]. Also, phenol is considered as toxic compound even at low concentrations and is one of the major pollutants in wastewater [151].

Cycloaliphatic ER, 3',4'-epoxycyclohexylmethyl-3,4-epoxycyclohexanecarboxylate (CAE), is produced by reaction of 3'-cyclohexenylmethyl-3-cyclohexenecarboxylate and peracetic acid [149]. CAE has better weather resistance and less tendency to yellow than aromatic resins [152].

The research for alternative materials which have better performance, better commercial availability or lower cost, and are safer attracts a lot of attention. A number of bio-based alternatives to avoid the mentioned disadvantages of typically used ERs have been investigated [138, 153, 154]. Polymers derived from renewable natural resources, such as oil, lignin, tannins, etc. have attracted interest because of their low cost and biodegradability. The utilization of glycerol, derived from oil as a by-product of biodiesel production, to production of glycerol-based ER expands the market of ERs. Glycerol-based ER, e.g. glycerol diglycidyl ether (GDGE) (Fig. 1.10), is produced by the reaction of glycerol with epichlorohydrin [155]. Glycerol-based ER is more flexible than conventional Bisphenol A ER.
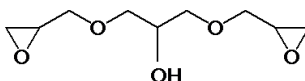
Fig. 1.10 Chemical structure of glycerol diglycidyl ether

1.2.1.2. Application of epoxy resins in industry

The properties and versatile structure allow the use of ERs in different areas ranging from coatings to aerospace industry [156]. Due to low shrinkage on cure, excellent solvent and chemical resistance, mechanical and corrosion resistance ERs are used as anticorrosion coatings. Epoxy layers are used as a protective barrier in metal containers to prevent canned foods from becoming spoiled or contaminated with bacteria or rust [157]. ERs are also used as coatings for decorative flooring applications [158].

ERs are used as adhesives in the construction of every day products such as bicycles, cars, boats, planes, golf sticks, skis, snowboards, and other applications where high strength is required [149]. ER reinforced with carbon fiber is used as laminate in aerospace industry due to high strength. In the production of cars, ER is used as glue which replaces welding procedure. It is also used for production of press tools in the manufacturing of new car models [156].

Epoxy nanocomposites are used in electronic equipment over molding integrated and hybrid circuits, and making printed circuit boards [159]. Also capacitors, diodes, and transistors are produced from epoxy-based materials [160]. Due to excellent electrical insulator properties, epoxy nanocomposites protect electrical components and integrated circuit from dust, moisture, short circuiting, and mechanical damage in semiconductor devices [161]. Epoxy composites filled with silica have been used for materials in electronic packaging applications [162].

ERs are widely used for construction. A composite material produced from organic polymer resin and inorganic aggregates is used as a concrete due to fast hardening, high strength, chemical and water resistance, and adhesiveness [163]. Bisphenol A-type ERs usually are used as concrete additives in the construction industry. Epoxy asphalt concrete has excellent strength properties, high temperature stability, good fatigue resistance [164] and is used not only for the highway pavement, but also for the railroad trackbeds [165].

ERs are widely used in biomedical applications as well. ERs reinforced with nano diamond particles having low electrical and high thermal conductivities, wide optical transparency, extreme hardness, and chemical inertness have been used in various biomedical systems [166]. Collagen-based epoxy derivatives are exploited as wound dressings, vascular grafts, and aortic heart valves [167].

1.2.2. Photoinitiated cationic polymerization

A process in which the monomer is transformed into polymer under effect of UV light irradiation by a chain reaction [168] is considered as photoinitiated polymerization. The photocurable formulation consists of [169]: photoinitiator (PI), which absorbs the light and generates the reactive species, monomer, and reactive diluent (RD), which reduces the viscosity and participates in the reaction. The initiating species and the growing chain ends in most cases are radicals or cations, and rarely anions [168-170]. UV curing technology shortens the curing time from hours to minutes and the process is more sequential and easier to control compared

to the other curing processes, e.g. thermal polymerization [171, 172]. Also, UV light-initiated polymerization is advantageous for reasons such as solvent free process, consuming of little energy, and curing is possible under ambient conditions [173]. The mentioned advantages allow the use of UV-cured materials in various areas, such as adhesives and sealants, coatings, photochromic and imaging materials, photoresists, optics and electronics, dental care, nail polish, stereolithography, etc. [174]. Cationic photopolymerization [168] and free radical promoted cationic photopolymerization (FRPCP) [175] mechanisms are well known and will be discussed.

Photoinitiated cationic polymerization is attractive due to insensitivity to oxygen, low volume shrinkage during polymerization, and low levels of toxicity and irritation of monomers [169, 176]. Also one more advantage so called "dark reaction" when the UV light source has been removed and the chain reaction continues to proceed for a considerable time should be mentioned [169]. Firstly, cationic photoinitiator (CPI) is excited by the absorption of UV light and generates cationic initiating species (cations) via homolytic or heterolytic bond cleavage. In this way, the cationic chain polymerization of monomers is initiated. By selecting the appropriate monomer (mono-, di-, or multifunctional), the ability to get linear or 3D polymer network is possible [177, 178].

The most commonly used CPIs are onium salts (On^+X^-) (Table 1.2) which consist of an organic cation (On^+) and a counter anion (X^-) [177]. The organic cation absorbs the UV light and is the source of photochemistry [169]. The counter anion determines the strength of the acids formed during photolysis and reactivity of the propagating ion pair in the polymerization [169]. The reactivity of counter anions is as follows: $BF_4^- < PF_6^- < AsF_6^- < SbF_6^-$ [179]. Onium salts are used in the photocurable formulatios due to excellent latency, good thermal stability, and solubility in most of the cationically polymerizable monomers [180]. Moreover, they are efficient PIs of cationic polymerization when irradiation is carried out using light in the short- to mid-wavelength UV regions (230-300 nm) [181].

Table 1.2 List of onium salts photoinitiators and their structures [182]

Name	Structure*
Aryldiazonium salts	$ArN_2^+X^-$
Diaryliodonium salts	$Ar_2I^+X^-$
Triarylsulfonium salts	$Ar_3S^+X^-$
Triarylselenonium salts	$Ar_3Se^+X^-$
Dialkylphenacylsulfonium salts	$ArCOCH_2S^+R_2X^-$
Dialkyl-4-hydroxyphenyl-sulfonium salts	$HOArS^+R_2X^-$

* $X = BF_4^-, PF_6^-, AsF_6^-, SbF_6^-$

A wide range of monomers is polymerizable by a photoinitiated cationic polymerization and include unsaturated monomers such as vinyl ethers, styrene, N-vinylcarbazole, and epoxy monomers [169]. Usually DGEBA and CAE are used for cationic photoinitiated polymerization [183-185]. The amount of CPI used in these

studies ranged between 0.5 and 5 wt. %. The mentioned cycloaliphatic ER display higher rates of polymerization compared to other types of ERs [186] due to the high level of ring strain. CAE shows lower reactivity than would be predicted from the reactivity of model compounds such as cyclohexane oxide due to an intramolecular interaction of the epoxy groups with the ester carbonyl group during epoxy ring-opening process when less reactive cyclic dialkoxycarbenium ions are formed [169]. The ester or ether groups in epoxy resins reduces their reactivity. The ring opening polymerization of epoxy monomers by epoxy RDs and hydroxyl compounds will be discussed in subsections 1.2.2.1. and 1.2.2.2.

1.2.2.1. Ring opening polymerization of epoxy monomers by epoxy reactive diluents

Cationic ring opening photopolymerization of epoxy monomer via activated chain end mechanism (ACE) is presented in Fig. 1.11. Triarylsulfonium salt is excited by UV light and forms a sulfonium radical cation, resulting in production of highly acidic photoacid [187]. The photoacid attacks the nucleophilic oxygen of epoxy group resulting in ring opening. Since the counter ion is close with the growing cationic center, the propagation reaction at the beginning is increasing slowly. When reaction proceeds, the counter ion gets separated from the cationic center due to increase in viscosity with conversion. This results in an increase in rate of propagation reaction. The reaction stops when the molecular weight is high enough to prevent the diffusion of the unreacted species.
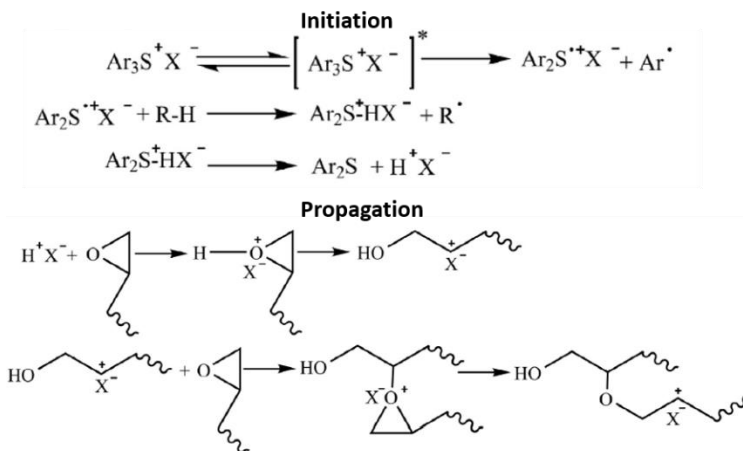
Fig. 1.11 Photoinitiated polymerization of epoxy monomer via activated chain end mechanism [187]

RDs are one of the most important components of photoinitiated polymerization formulations and are used to reduce the viscosity, control cross-linking density, and improve mechanical properties [188, 189]. RD weakens the interaction between the epoxy resin molecules and increases the homogeneity of the reaction mixture thereby decreasing the viscosity of the mixtures [190]. In this case, the mobility of the monomer molecules and growing chains increases resulting in

increase of the reaction rate and cross-linked material becomes more homogeneous and shows better mechanical properties. Diluents are classified into non-reactive and reactive. Non-reactive diluents, such as toluene or xylene, and various phenolic compounds [191] do not participate in the reaction. RDs chemically bind to the resin and become a part of cross-linked polymer. Consequently, they are less volatile than non-reactive diluents and therefore, more environmentally friendly [137]. RDs can be divided into epoxy-based and non-epoxy-based. Epoxy RDs significantly influence the properties of ERs.

The photoinitiated polymerization of GDGE involving phenyl glycidyl ether were carried out in the presence of triarylsulfonium hexafluorophosphates as CPI at 50 °C, 60 °C, 70 °C and under UV light at intensity of 35 mW·cm^{-2} [192]. The structures of phenyl glycidyl ether and sulfonium salts are shown in Fig. 1.12. The formulations with 6 wt.% of CPI containing GDGE:phenyl glycidyl ether in the weight ratios 3:1, 1:1, and 1:3 were prepared and the final conversion of the reaction and thermal stability of resulted polymers were studied. The obtained neat GDGE film was rigid probably due to the presence of higher cross-linking associated with the diglycidyl ether moieties. The addition of phenyl glycidyl ether resulted in flexible films and the flexibility increased with an increase in phenyl glycidyl ether content. With increase of temperature, the polymerization conversion of GDGE:phenyl glycidyl ether in 1:1 ratio increased (reached 70 %) due to increase in mobility of reactive species and viscosity of formulation. When phenyl glycidyl ether content was increased, the T_g of formulations, cured at 50 °C with UV light, decreased and were 18.9 °C, 7.2 °C, 2.5 °C for GDGE:phenyl glycidyl ether in the weight ratios of 3:1, 1:1, 1:3, respectively. While T_g of neat GDGE polymer was 23.5 °C. This shows the effect of plasticization with increase of phenyl glycidyl ether content. The T_g values show that photocross-linked polymers are non-vitrifying as the analysis temperatures are higher than the resulting T_g values [193].

Phenyl glycidyl ether (PGE)   **Triarylsulfonium hexafluorophosphate salts**
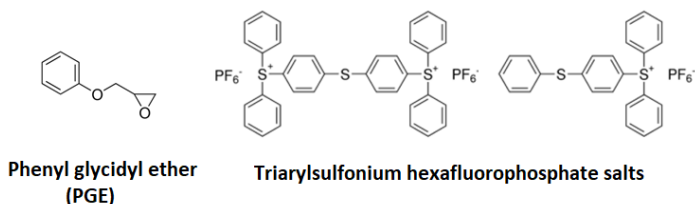
Fig. 1.12 Chemical structures of phenyl glycidyl ether and triarylsulfonium hexafluorophosphate salts

Similar research was carried out involving GDGE and poly(propylene glycol) diglycidyl ether which structure is presented in Fig. 1.13 [194]. In this case, difunctional RD was used. The formulations with GDGE:poly(propylene glycol) diglycidyl ether in the weight ratios of 3:1, 1:1, and 1:3 containing 6 wt.% of CPI were polymerized at 30 °C, 40 °C, 50 °C, 60 °C, 70 °C and under UV light at intensity of 45 mW·cm^{-2}. When the temperature was increased, the polymerization conversion of GDGE:poly(propylene glycol) diglycidyl ether in 3:1 ratio increased (reached 70 %) due to an increase in mobility of reactive species and viscosity of formulation. The T_g values of photocross-linked polymers of GDGE:poly(propylene

glycol) diglycidyl ether in the weight ratios of 3:1, 1:1, and 1:3 were 12.9 °C, 3.2 °C, -7.4 °C, respectively and decreased in addition of poly(propylene glycol) diglycidyl ether. The effect of plasticization was observed when the T_g of neat GDGE polymer was 22.8 °C. The thermogravimetric analysis (TGA) showed increasing stability with an increase in GDGE content due to higher T_g, better cross-linking by activated monomer (AM) mechanism (it will be discussed later in subsection 1.2.2.2.). AM mechanism takes place due to the presence of hydroxyl group in the GDGE structure and could be the reason of enhanced thermal stability of GDGE backbone as compared to poly(propylene glycol) diglycidyl ether. The durometer hardness (Shore A) of the photocross-linked polymers was 67, 66, 63, and increased with the increase of GDGE content which had more rigid backbone compared to more flexible poly(propylene glycol) diglycidyl ether.
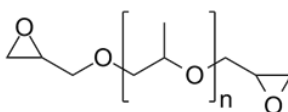
Fig. 1.13 Chemical structure of poly(propylene glycol) diglycidyl ether

The photocross-linking of epoxidized oils, such as linseed, rapeseed, and fish oil with aromatic diepoxy RDs in the presence of diphenyliodonium hexafluorophosphate or triarylsulfonium hexafluoroantimonates as CPI was carried out [195]. DGEBA, bisphenol A propoxylate diglycidyl ether, and CAE were chosen as RDs. The chemical structures of bisphenol A propoxylate diglycidyl ether and CPIs are shown in Fig. 1.14. The formulations with epoxidized natural oil and different amount (from 20 wt. % to 50 wt. %) of RD, containing 5 wt. % of CPI were polymerized at room temperature under UV light. The polymeric films with 60 μm to 370 μm were obtained. When diphenyliodonium hexafluorophosphate was used for the photocross-linking, the polymeric films were heterogeneous and opaque. Consequently, the triarylsulfonium hexafluoroantimonate was more suitable for the photocross-linking of oils. The obtained polymeric films with DGEBA were brittle, therefore the investigation of properties with smooth films prepared with other RD was carried out. The insoluble fraction of polymers after extraction with acetone for 24 h ranged from 59 % to 87 %. The higher insoluble fractions were obtained when bisphenol A propoxylate diglycidyl ether was used as RD compared to CAE due to rigid aromatic backbone in the structure. The Young's modulus ranged from 1.6 MPa to 320.1 MPa and was higher when CAE was used as RD which had more flexible structure compared to bisphenol A propoxylate diglycidyl ether. Thermal decomposition temperatures at the 10 % weight loss ($T_{dec-10\%}$) of polymers prepared using RDs ranged from 250 °C to 420 °C and were higher than those of the polymers without RD. The addition of RD increased the number of reactive species and more cross-linked structures have been formed. Biodegradation results after 5 months exposition in soil showed that the polymeric films prepared without RDs decomposed more than containing RDs. The Young's modulus and thermal decomposition temperatures increased with an increase of RD content.
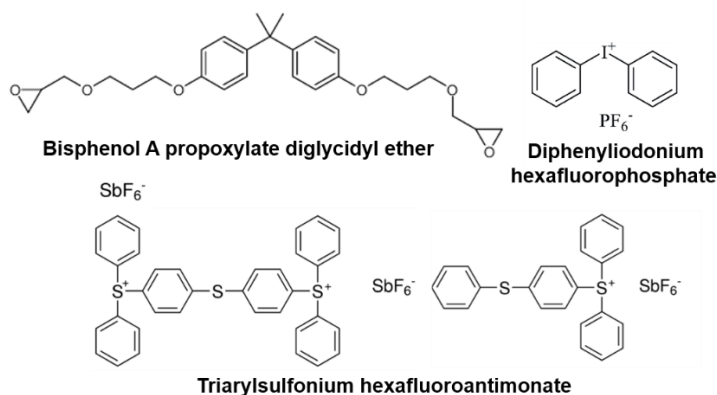
Fig. 1.14 Chemical structures of bisphenol A propoxylate diglycidyl ether, diphenyliodonium hexafluorophosphate, and triarylsulfonium hexafluoroantimonate

The photocross-linking of epoxidized linseed oil was carried out with the different amount (10 mol. %, 20 mol. %, and 30 mol. % with respect to the epoxidized linseed oil) of epoxy RDs in the presence of 3 mol. % of triarylsulfonium hexafluoroantimonates at room temperature under UV light with intensity of 310 mW·cm^{-2} [196]. CAE, 1,4-cyclohexanedimethanol diglycidyl ether, DGEBA, trimethylolpropane triglycidyl ether, and bis[4-(glycidyloxy)phenyl]methane were used for the photopolymerization reaction (Fig. 1.15). The smooth, transparent, flexible, and wrinkle-free polymeric films were obtained after 2-5 min of UV light irradiation when CAE and bis[4-(glycidyloxy)phenyl]methane were used as RDs. The (69-91) % conversion of epoxy groups was reached when RDs were used for cross-linking. It was higher than that of polymer without RD. The highest conversion of epoxy groups was observed when 10 mol. % of RDs was used. The yield of insoluble fraction after the extraction with chloroform ranged from 91 % to 99 % and was independent from RD content. The hardness values varied from 71 N·mm^{-2} to 1248 N·mm^{-2}. The elongation at break was in the range of (1.29-6.27) %. Tensile strength ranged from 0.67 MPa to 6.21 MPa. Young's modulus was in the range between 6.97 N·mm^{-2} and 26.02 N·mm^{-2}. In most cases, RD improved mechanical properties of epoxidized linseed oil resin. The highest values of mechanical properties were obtained when 10 mol. % of RD was used. RDs had no significant effect on $T_{dec-10\%}$ values which were in the range of (300-325) °C. The photocross-linked polymers swallowed up more in chloroform (200-300 %) than in toluene (133-233 %).

Fig. 1.15 Chemical structures of 1,4-cyclohexanedimethanol diglycidyl ether, trimethylolpropane triglycidyl ether, and bis[4-(glycidyloxy)phenyl]methane

1.2.2.2. Ring opening polymerization of epoxy monomers by hydroxyl compounds

Epoxy-based coatings and films should be smooth and without cracks when applied in the industry. These features are especially important when coatings are used for decorative applications. Brittleness and wrinkles can be avoided or limited by curing ERs with hydroxyl compounds [197]. Photoinitiated polymerization of ER with hydroxyl compounds proceeds via AM mechanism [198]. AM of photocationically polymerized epoxy monomer in the presence of hydroxyl containing compound is shown in Fig. 1.16. In the propagation reaction, the hydroxyl compound attacks the ionic chain resulting in a protonated ether [199]. The mechanism includes termination of a growing chain and the proton transfer to the monomer, which could start another chain growing process. AM mechanism is considered as faster than ACE mechanism of the pure epoxy monomer [200].

Fig. 1.16 Polymerization of epoxy monomer via activated monomer mechanism [199]

The properties of polymers can be modified by adding hydroxyl compounds of different structures and functionality because hydroxyl compounds act as flexibilisers (plasticizers) [201]. When hydroxyl compound molecules are incorporated into polymer chains, the T_g is decreased [202] due to increased free volume between chains resulting in easer movement and rotation of chain segments. In addition to this, the mechanical properties may be improved by adding hydroxyl compounds including increased elongation, decreased Young's modulus and tensile strength [203]. The decreasing of polymer T_g is necessary when it is used for biomedical applications such as drug delivery systems. In this case, the degradation

of the drug at higher temperatures is avoided [204]. Various hydroxyl compounds with a 1, 2, 3, or more hydroxyl groups were tested in photoinitiated polymerization of DGEBA and cycloaliphatic epoxy resins [205-211].

The photocross-linking of DGEBA with different amount (10 wt.%, 20 wt.%, and 30 wt.%) of hydroxyl hemi-spiroorthocarbonate and dihydroxyl spiroorthocarbonates (Fig. 1.17) in the presence of 2 wt.% of triarylsulfonium hexafluoroantimonates at room temperature under UV light with intensity of 35 mW·cm^{-2} was carried out [207]. In the presence of 10 wt.% of the used hydroxyl compounds the epoxy groups conversion was slightly increased while conversion of neat DGEBA reached 74 %. This can be explained by the plasticization effect due to flexible structure of spiroorthocarbonates resulting in an increase of the reactive species mobility. A decrease of epoxy group conversion with increase of dihydroxyl spiroorthocarbonates above 10 wt.% was noticed. This can be due to a large amount of nucleophilic hydroxyl groups release which competes with protonation of epoxy ring, decreasing the amount of reactive oxirane cationic groups formed by photoacid addition. The gel fraction of photocross-linked polymers with hydroxyl compound fragments ranged from 95 % to 98 % after extraction with chloroform and was lower or the same as gel fraction of neat DGEBA (98 %). The polymers containing 20 wt.% of hydroxyl compound fragments reached the highest gel fraction. The T_g values of photocross-linked polymers with hydroxyl compound fragments ranged from 95 °C to 154 °C while T_g of neat DEGBA polymer was 145 °C. Only 10 wt.% of dihydroxyl spiroorthocarbonates increased the T_g of DGEBA. The T_g was shifted towards lower values when amount of spiroorthocarbonate was increased. When 20 wt.% and 30 wt.% of hydroxyl hemi-spiroorthocarbonate were used, the storage modulus decreased noticeably, although storage modulus was increased when 10 wt.% hydroxyl hemi-spiroorthocarbonate was used due to obtained higher conversions of epoxy groups. The addition of dihydroxyl spiroorthocarbonates resulted in the higher storage modulus values than hydroxyl hemi-spiroorthocarbonate due to two hydroxyl groups leading to a higher cross-linking density.

| Hydroxyl hemi-spiroorthocarbonate | Dihydroxyl spiroorthocarbonate 1 | Dihydroxyl spiroorthocarbonate 2 |
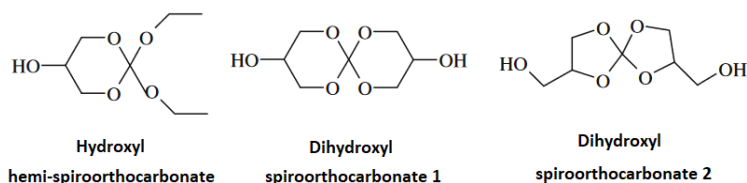
Fig. 1.17 Chemical structures of hydroxyl hemi-spiroorthocarbonate and dihydroxyl spiroorthocarbonates

The photocross-linking of CAE with different hydroxyl compounds (Fig. 1.18) was carried out in the presence of 0.3 wt.% of iodonium hexafluoroantimonates at 30 °C under UV light with intensity of 50 mW·cm^{-2} [211].
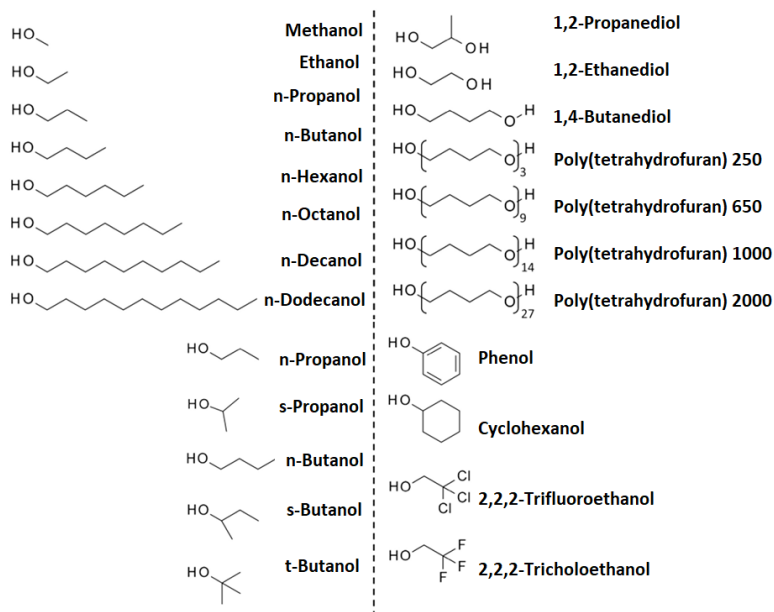
Fig. 1.18 Chemical structures of hydroxyl compounds tested in the photocross-linking of 3',4'-epoxycyclohexylmethyl-3,4-epoxycyclohexanecarboxylate

The formulations in the mole ratio of hydroxyl groups to oxirane ranged from 0 to 1. The effect of hydroxyl groups number and structure of hydroxyl compounds on resulting properties of photocross-linked polymers was investigated. Also, the effect of n-decanol and 1,2-propanediol on conversion of epoxy groups was tested. Both, n-decanol and 1,2-propanediol, increased the epoxy group conversion with increase of alcohol or diol content. The opposite results were obtained when curing of cycloaliphatic ER with 10 mol.%, 30 mol.%, and 50 mol.% of 1,2-propanediol was carried out in the presence of 3 wt.% triarylsulfonium hexafluorophosphate [206]. The addition of diol resulted in an approximate 40 % decrease of epoxy group conversion. The reason of opposite results could be in the difference of propagation reactions via ACE and AM mechanisms. During AM mechanism, a large number of protons released are trapped by diol molecules and cannot continue the chain growth reaction, resulting in a decreased degree of epoxy group conversion. The addition of n-decanol decreased the T_g about 40 °C per 0.1 hydroxyl equivalents, while 1,2-propanediol reduced the T_g about 20 °C per 0.1 hydroxyl equivalents. Rubbery modulus of polymer containing 0.3 hydroxyl equivalents of n-octanol was 5 MPa and rubbery modulus of 0.3 hydroxyl equivalents of 1,2-propanediol reached 20 MPa, while neat CAE had a rubbery modulus of 70 MPa. The worst properties were reached when n-decanol was used due to the propagation reaction via AM mechanism. Hydroxyl group attacks the ionic chain resulting in ether bond in the chain and therefore the chain transfer ability of another hydroxyl group at the chain end is restricted. In case of diols, the polymer can continue to react because it has hydroxyl groups at the chain end. By increasing the size of alcohols or diols, the

epoxy group conversion was affected minimally and the T_g values were decreased. The polymer with the fragments of methanol reached T_g of 130 °C, while the T_g of the polymer with the fragments of n-dodecanol reached T_g of 80 °C. The plasticization effect was increased with the increase of alkyl chains. The diols did not reduce the T_g as alcohols, e. g. T_g of the polymer with the 1,2-propanediol and poly(tetrahydrofuran) 2000 fragments was 170 °C. The rubbery modulus values of alcohols ranged from 4 MPa to 8 MPa, while diols had values of 18 MPa.

As all discussed compounds are primary hydroxyl compounds and have similar nucleophilicities, the primary, secondary, and tertiary alcohols were tested. The lower epoxy group conversions were observed when t-butanol was used. This could be explained by the increased steric hindrance, which delays the ring opening reactions between t-butanol and protonated monomer in comparison to the other alcohols. The polymer with the fragments of n-butanol reached the lowest T_g value of 100 °C and the highest with t-butanol of 115 °C. The backbone of t-butanol limits chain-end mobility, which is the reason of increasing T_g value. Hydroxyl compounds which have lower dissociation constant (pK_a) (acidic) are less nucleophilic and less reactive, therefore produce lower conversion of epoxy groups. Phenol with $pK_a \approx 10$, 2,2,2-trifluoroethanol with $pK_a \approx 11$, and 2,2,2-tricholoethanol with $pK_a \approx 12$ decreased the epoxy groups conversion in comparison to cyclohexanol with $pK_a \approx$ 18. The charge and nucleophilicity of hydroxyl compound are reduced due to electronic effects and steric crowding. The hydroxyl groups of phenol molecule donate some of electron density via resonance into π system of benzene ring. The hydroxyl groups of 2,2,2-trifluoroethanol and 2,2,2-tricholoethanol lose electron density via induction from the highly electronegative groups. The polymers with the fragments of acidic hydroxyl compounds and cyclohexanol reached the silimar T_g values which ranged from 110 °C to 120 °C. The polymers with the fragments of acidic hydroxyl compounds had higher rubbery modulus values of (20-60) MPa than polymer with cyclohexanol which rubbery modulus was 10 MPa.

1.2.3. Photoinitiated free radical promoted cationic polymerization

Nowadays, many devices are designed with lasers emitting light in long wavelength UV and visible regions [212] (300-405 nm). Consequently, the performance of CPI should be moved towards long light wavelengths. The onium salts can be indirectly activated to absorb light at long wavelengths by using radical sources which are sensitive to visible light via FRPCP mechanism [175].

The photocross-linking of CAE, using diphenyliodonium hexafluorophosphate (Ph$_2$I$^+$) as CPI, phenylbis(2,4,6-trimethylbenzoyl)phosphine oxide (BAPO) and diphenyl(2,4,6-trimethylbenzoyl)phosphine oxide (TPO) as radical PI in the presence of N-vinylcarbazole (NVK) (Fig. 1.19) as an additive for FRPCP was carried out under visible light (>400 nm) at intensity of 8 mW·cm^{-2} [175]. 1 wt.% or 3 wt.% of NVK, 1 wt.% of BAPO or TPO, and 2 wt.% of Ph$_2$I$^+$ was used in the formulations.
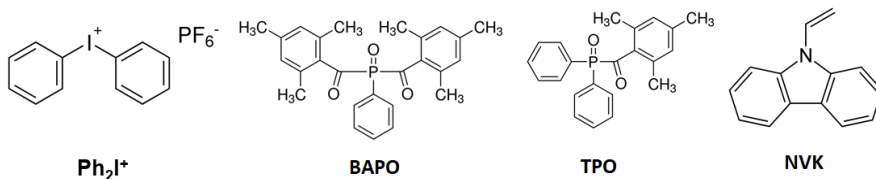
Fig. 1.19 Chemical structures of diphenyliodonium hexafluorophosphate (Ph$_2$I$^+$), phenylbis(2,4,6-trimethylbenzoyl)phosphine oxide (BAPO), diphenyl(2,4,6-trimethylbenzoyl)phosphine oxide (TPO), and N-vinylcarbazole (NVK)

The general scheme of FRPCP is presented in Fig. 1.20. Under visible light BAPO or TPO produces benzoyl and phosphinoyl radicals which can be easily oxidized by Ph$_2$I$^+$. The resulting cations initiate the ring opening reaction of CAE (path 1). The addition of benzoyl and phosphinoyl radicals to NVK double bond results in NVK radicals which can be oxidized by Ph$_2$I$^+$ salt. The resulting NVK cation initiates the ring opening reaction of CAE (path 2). NVK cation can be easier oxidized by Ph$_2$I$^+$ salt than phosphinoyl or benzoyl radicals due to lower ionization potential which are 4.7 eV, 6.6 eV, 8.3 eV, respectively. Consequently, the addition of NVK into formulations increased the epoxy groups conversion compared with the formulations consisting of BAPO or TPO and Ph$_2$I$^+$. Also, the conversion increased via a boost of NVK content in the formulations. The formulation of NVK and Ph$_2$I$^+$ without additive was no capable to polymerize CAE and formulation with BAPO or TPO and Ph$_2$I$^+$ absorbed only UV light. In addition, BAPO increased the epoxy group conversion more than TPO due to lower ionization potential which is compatible with the faster oxidation process.
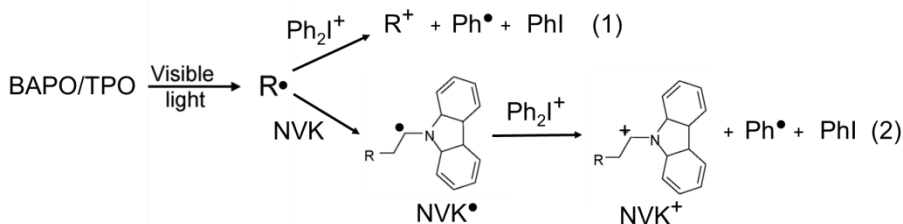
Fig. 1.20 General scheme of photoinitiated free radical promoted cationic polymerization (FRPCP) [175]

1.3. 3D printing

3D printing, also known as additive manufacturing, solid freeform fabrication, and rapid prototyping, is described as computer-controlled process when materials layer by layer are joined together to make parts from 3D model data and was introduced during 1980s [213, 214]. 3D printing has advantages such as design freedom, low startup costs, fast production processes, and local production [213]. By using 3D printers, the production and maintenance of the products can be carried out everywhere. These advantages enable people to replace many traditional manufacturing methods. 3D printing is believed to be the industrial revolution as it affects technology and economy. Additive manufacturing can be carried out directly

at a customer's house, therefore the manufacturing location is moved to the location of demand, resulting in an effect on the usual manufacturing processes. Consequently, a large number of small investments are distributed in manufacturing locations instead of a small number of centralized manufacturing sites with high investments [214].

3D printing process begins with sliced 3D computer model which is created by structures built in computer-aided design (CAD) software and the obtained data are sent to the 3D printer via a command file that directs the printing process [215]. The general scheme of 3D printing process by the example of a coffee mug is shown in Fig. 1.21. In the first step, a coffee mug is transformed into digital data by means of CAD or analysis of geometric data by means of 3D scanning. In the second step, a virtual model is sliced into layered data. The overhanging objects such as a handle of a coffee mug are designed with temporary support structures to prevent collapse during the build process. The data are sent to the 3D printer and in the third step, 3D printing of product layer by layer is performed by an additive manufacturing process. Also, postprocessing is performed to remove typical artifacts such as support structures and surface roughness due to staircase effects [214].
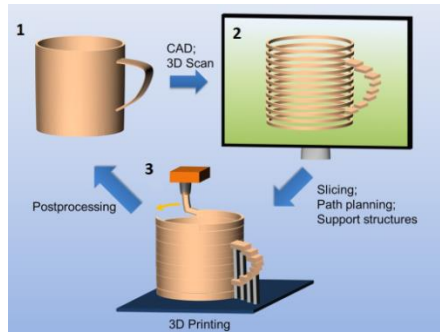
Fig. 1.21 General scheme of 3D printing process by example of a coffee mug [214]

3D printing technology has been widely used in many industries to produce various objects such as houses, bridges, cars, tissues and organs, dental materials, jewelry, clothes, food, etc. [213, 216-220]. The main materials used for additive manufacturing process are metals and alloys, polymers and composites, ceramics, and concrete [221]. The processes, used polymers, and benefits of the main technologies of additive manufacturing are summarized in Table 1.3. Additive manufacturing technology based on extrusion process is fused decomposition modeling. Thermoplastics such as polycarbonate, acrylonitrile butadiene styrene, poly(lactic acid), and nylon are used due to low melting temperature. The molten thermoplastic filaments are extruded layer by layer onto the build platform and fuses instantly after leaving the printing nozzle. Fused decomposition modeling is considered as low cost, simple process with high speed and obtained products have good strength. Other technologies, based on the solidification of powder, are selective laser sintering, powder bed and inkjet head 3D printing, and 3D plotting. In selective laser sintering technology, the powder of a thermoplastic polymer such as polycaprolactone and polyamide is sintered (hardened) with a CO_2 laser by heating.

32

In powder bed and inkjet head 3D printing, any polymers which can be supplied as powder are used as starting materials. In this case, the binder is required. The mixture is distributed by inkjet unit which is able to move in X-Y direction. In these selective laser sintering and powder bed and inkjet head 3D printing methods, the platform lowers, and the next layer of powder or powder and binder mixture is spread and hardened until the object is finished. In powder bed and inkjet head 3D printing, the platform is stationary, and the syringe head can move in three dimensions extruding materials layer by layer. Hardening reactions can be generated by heat, UV light, or by mixing two reactive components. Benefits of selective laser sintering are fine resolution, obtained products have good quality and strength, while powder bed and inkjet head 3D printing is considered low-cost technology as a wide range of materials can be used. Both methods take advantage of easy removal of unbounded powder. The key advantage of 3D plotting is the possibility to obtain soft materials. Laminated object manufacturing is based on layer by layer cutting and lamination of polyvinyl chloride sheets. This technology has a compact desktop 3D printer. In laser lithography or stereolithography (SLA), a liquid photocurable epoxy or acrylate based resin is hardened with UV light using lasers in a vat or container. The platform lowers, a sweeper distributes a layer of the photopolymerizable resin, and the process is repeated until the object is finished. One of the main advantages of SLA is the high printing resolution provided by the spot size of the focused laser beam. When laser beams the UV light through a mask, the technology is called as dynamic projection lithography (DPL). DPL is less affected by oxygen inhibition as compared to SLA, because the layer is on the bottom of the vat and has no direct contact with air.

Table 1.3 List of used polymers, processes, and advantages of the main technologies of additive manufacturing [213-215, 221]

Technology	Process	Polymer	Advantages
Fused decomposition modeling	Extrusion	Polycarbonate, acrylonitrile butadiene styrene, poly(lactic acid), nylon	Low cost, high speed, good strength, multi-material capability
Selective laser sintering	Solidification of powder	Polycaprolactone and polyamide	Fine resolution, high quality, good strength, easy removal of unbounded powder
Powder bed and inkjet head 3D printing		Which can be supplied as powder	Low cost, multi-material capability, easy removal of unbounded powder
3D plotting		Polycaprolactone, poly(lactic acid), hydrogel	High printing resolution, soft materials capability
Laminated object manufacturing	Sheet lamination	Poly(vinyl chloride)	Compact desktop 3D printer
Stereolithography (SLA)	Photopolymerization	Photocurable epoxy or acrylate based resin	High printing resolution
Dynamic projection lithography (DPL)			Low oxygen inhibition

The most commonly used additive manufacturing technologies such as SLA are limited in resolution. High quality objects with thickness in the range of 50-150 μm can be printed by SLA, while direct 3D laser lithography (3DLL) allows to produce objects with thickness below 1 μm [222]. 3DLL technology is considered as capable to produce 3D micro- and nanostructures with sizes in the order of 100 nm [223]. 3DLL is based on curing of photocurable resin with a tightly focused laser beam. The resolution depends on light-matter interaction and localization of photons [224]. This technology is supported by femtosecond (10^{-15} s) laser pulses with very high peak intensities.

1.3.1. Stereolithography

The term "stereolithography" comes from the Greek words "stereo" and "(photo)lithography" which means solid and the form of "writing" with light [225]. SLA is one of the earliest methods of additive manufacturing and was developed in 1986 [226]. General scheme of SLA setup is presented in Fig. 1.22. There are two variants of setup structure. One of them is when the object is built bottom-up from a fabrication platform which is fitted out below the resin surface (Fig. 1.22a) [215, 226]. In this case, the laser is using the CAD file and the UV light beam of the laser is focused into the photocurable resin surface. The resin forms a solid single layer to a defined depth and sticks to the fabrication platform which is moved away, and another uncured layer is ready for the polymerization [226]. The process is repeated until the 3D object is finished. The scanning of the built layers allows to follow the accuracy of the process, by comparing the scanned data and the design [226]. The other variant is when the object is built top-down from a fabrication platform which is fitted out above the resin surface (Fig. 1.22b) [226]. In this case, the process is based on DPL technology when a digital mirror device is used. The laser beam is split of up to several millions of mirrors through a mask, which will expose the whole layer with UV light at once. The laser light is projected into transparent coated plate which is in the bottom of resin container. Printing time is greatly reduced, as it is independent of the number of structures being built simultaneously. The printing resolution and time is affected by scan speed, intensity of the laser power, and the duration of UV light exposure [227]. The cure depth is determined by the energy of the light which is used when the layer is polymerized [226].
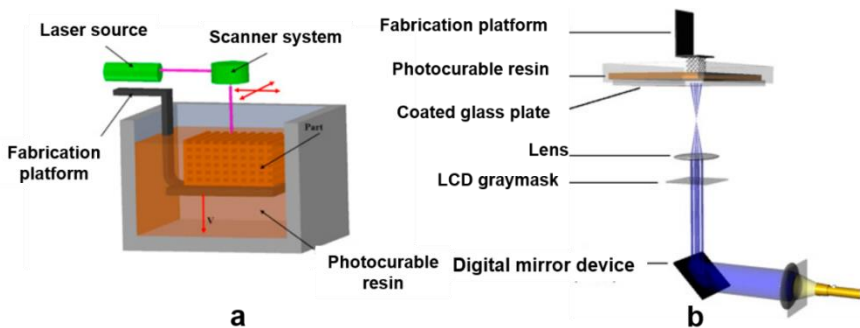
Fig. 1.22 General scheme of stereolithography setup: (a) a bottom-up setup with scanning laser, (b) a top-down setup with digital light processing [215, 226]

The acrylate and ERs are the most commonly used in materials of the SLA technology. Most of them have commercial names and the compositions of the SLA materials in most cases are not specified. The mechanical characteristics, glass transition temperatures, and water absorption of materials printed by SLA technology is presented in Table 1.4. For the determination of mechanical characteristics standard method ASTM D638 with some modifications was used. T_g temperatures were determined with different methods such as differential scanning calorimetry (DSC) and dynamic mechanical analysis (DMA) in tension mode. The values of T_g, elongation at break, tensile strength, and Young's modulus of fresh printed and post-cured objects are different. The materials listed in the table were post-cured with heat or UV light. The mechanical and thermal characteristics usually increase when post-cure is applied. The preparation of material is indicated by the manufacturer. One of the most used acrylate materials for SLA is PR48 [228], containing TPO as PI. PR48 is formulated for 3D printers with SLA and DLP technology using lasers with 385-405 nm wavelength light. SL5170 [229] is the mixture of acrylate and epoxy resins, containing CAE resin and triarylsulfonium salt as PI. SU8 2000 [230] is epoxy novolac based resin formulated for SLA technology using lasers with 350-400 nm wavelength light. The other materials listed in the table are epoxy based resins of SOMOS® brand [231-233]. SOMOS 9120 is flexible and common to polypropylene, while SOMOS® 18420 is heat resistant and acrylonitrile butadiene styrene-like material. SOMOS® NeXt and SOMOS®WaterShed XC 11122 are tough and strong and are common to polycarbonate. SOMOS®Taurus has thermal and mechanical characteristics that until now have only been achieved using thermoplastic technologies, such as fused decomposition modeling and selective laser sintering. SOMOS®Accura Bluestone is a nanocomposite material and has high strength. The desired thermal and mechanical characteristics of printed object can be achieved by choosing the resins and PI.

Table 1.4 The mechanical characteristics, glass transition temperatures, and water absorption of materials printed by stereolithography [228-233]

Material	T_g (ºC)	Elongation at break (%)	Tensile strength (MPa)	Young's modulus (MPa)	Water absorption (%)
PR48	-	3-5	16-28	600-1400	-
SL5170	65-90	7-19	59-60	3737-4158	-
SU8 2000	210	6.5	60	2000	0.65
SOMOS® 9120	-	15-25	30-32	1227-1462	-
SOMOS® 18420	57-96	8-16	42.2-68.1	2180-2960	0.61-0.68
SOMOS® NeXt	43-47	8-10	31.0-34.6	2370-2490	0.40
SOMOS® Taurus	53-54	17-24	46.9-49.0	2206-2310	0.70-0.75
SOMOS® WaterShed XC 11122	39-46	11-20	47.1-53.6	2650-2880	0.35
SOMOS® Accura Bluestone	71-83	1.4-2.4	66-68	7600-11700	-

1.4. Non-degradable and biodegradable plastic mulching films

The term "mulch" comes from the German word "molsch", which means soft, melted or beginning to decay [234]. Mulch is a layer of material applied to the surface of soil [235] and mulching is a water conservation method which increases the infiltration of water into the soil, improves the fertility, prevents soil from erosion, and reduces surface runoff [236]. Materials used as mulches can be classified into main two groups [237]:

- Organic materials (plant products and animal wastes),
- Inorganic materials (gravel, concrete, and plastic films).

The plastic films are most commonly used as mulch. The main advantages of plastic mulching film are the increase of the soil temperature, decrease of water evaporation and the use of chemicals in weed control, and the increase of the yield [238]. Plastic mulching films are most commonly made from petroleum-based plastics, usually from low density polyethylene (LDPE) [239], due to good mechanical properties and low cost [240]. The tensile strength of LDPE is 15.37 MPa and elongation at break is 208.81 % [241]. However, LDPE is non-degradable. The mass loss of LDPE after 45 days exposition in soil is 0 % [240]. Even during the exposition in soil for many years, the biodegradation is very low [242]. Furthermore, since erosion of wind and rain breaks down plastic mulching film into pieces, the collection becomes the waste of time [243]. Consequently, the plastic pieces are left in the field, buried or burned, which leads to environmental pollution [244]. In order to avoid the mentioned disadvantages, biodegradable plastic mulching films have been developed using raw materials from renewable resources.

Biodegradable plastic mulching films are degradable by microorganisms into carbon dioxide or methane, water and biomass at the end of their use [245] and can be used as an alternative to LDPE mulching films. Biodegradable mulching films can be produced using natural or synthetic biodegradable polymers such as poly(lactic acid) [246], poly(vinyl alcohol) (PVA) [247], starch [247], or various polyesters [249]. Synthetic polymer poly(butylene adipate-co-terephthlate) displays similar mechanical properties to LDPE mulching films. The tensile strength of poly(butylene adipate-co-terephthlate) is 30 MPa and elongation at break is 700 % [250]. Plastic mulching films produced from renewable materials usually have lower elongation at break values, showing a brittle fracture behavior [246]. Poly(lactic acid) films exhibits a low elongation at break of 4 %, but a high Young's modulus of 432.4 MPa and tensile strength of 18.8 MPa [246]. Various additives such as organic and inorganic fillers can be used for polymer composites to modify the properties of biodegradable mulching films.

1.4.1. Biodegradable plastic mulching coatings filled with industrial waste materials

Agriculture and other sectors of industry generate a huge quantity of natural waste materials which cause certain environmental problems. Rapeseed cake (RC), a by-product of biodiesel production [251], phosphogypsum (PG), a by-product in production of phosphorus fertilizers [252], and keratin-based materials such as

animal feathers, hair, hoof, horns, and nails [253] are the most common natural industrial waste materials. Horns contain 15 % of nitrogen and 1 % of phosphorus [254]. Since nitrogen and phosphorus in horns are present as components of organic compounds, the plants cannot assimilate them directly. The microorganisms of soil should convert them into inorganic compounds at first. The slow degradation of keratin-based waste materials can be explained by the presence of cistein amino acid, which has sulphur and forms intramolecular and intermolecular physical bonds [255]. PG cannot be used as nutrient for most of the soil microorganisms. However, sulfate-reducing bacteria can convert gypsum ($CaSO_4 \times 2H_2O$), the main component of PG, to hydrogen sulfide gas under anaerobic conditions that can be created in the moist soil [256]. RC contains lysine amino acid [257], which is important for the growth and metabolic processes. The biodegradability of such wastes depends on the microorganisms present in the soil and on the nature of waste material. These nitrogen and phosphorus containing waste materials can be used for the preparation of biodegradable polymeric composites which would act as mulch or as slow-release fertilizers for plants.

The polymer composites were prepared from PVA, horn meal (HM) and glycerol for mulching coatings [258]. The composites with the mass ratio PVA:HM: glycerol of 4:6:3, 4:6:6, and 4:6:9 and water up to 100 g were prepared at 80–85 °C. In this case, PVA as biodegradable polymer was used as a binder, constant amount of HM with the particle size of ≤0.16 mm was used as the nitrogen containing filler, and glycerol was used as a plasticizer. The mechanical characteristics and contact angle of polymer composites are listed in Table 1.5. The elongation at break values ranged from 5.36 % to 255 % and increased with the increase of glycerol content. The tensile strength values reached (2.28-10.37) MPa, contact angle of water was in the range of (17.91-50.4) ° and increased with the decrease of glycerol content. The wettability of composites increased with the increase of glycerol content. Also, the composites with the mass ratio of 4:6:9 containing particle of HM with size of 0.40-0.25 mm, 0.25-0.16 mm, 0.16-0.09 mm, and ≤0.09 mm were prepared. The mechanical characteristics increased with decrease of the particle size. These polymeric composites were used for the preparation of coatings for the mulching of tomato sprouts cultivated in pots. When the polymeric composites with the HM were used as coatings, the vegetation rate of sprouts increased compared to cultivated sprouts without the mulch.

Table 1.5 The mechanical characteristics and contact angle of polymer composites prepared from polyvinyl alcohol, horn meal, and glycerol [258]

Composite (PVA:HM:glycerol)	Elongation at break (%)	Tensile strength (MPa)	Contact angle (°)
4:6:3	5.36 ± 0.67	10.37 ± 0.24	50.4 ± 1.44
4:6:6	87.58 ± 17.4	3.19 ± 0.37	22.99 ± 1.36
4:6:9	255 ± 22.8	2.28 ± 0.11	17.91 ± 0.74

The similar polymeric composites were prepared from PVA, HM and CG with the mass ratio PVA:HM:CG of 4:6:0, 4:6:2, 4:6:3, 4:6:4, 4:6:6, and 4:6:9 and water up to 100 g [259]. Two fractions with the particles of HM with size of 250–160 μm

and ≤ 90 μm were used. The most interesting of the performed tests were degradation in soil and isolation of fungi. The mass loss of the composites after 60 days exposition in soil ranged from 20 % to 50 % and increased with the decrease of CG content in the composites. The mass of the composites with the smaller particles of HM (90 μm) decreased about 20 % more than the composites with the bigger particles of HM (160–250 μm). *Penicillium* genus was a dominating fungi in the substrate mulched with the composite without CG, while a dominating fungi in the substrate mulched with the composite containing highest amount of CG was *Geomyces pannorum*.

The film-forming polymeric composites for the encapsulation of mineral fertilizers were prepared from PVA, CG, RC, PG, and HM at 85 °C [260]. Although these composites were prepared not for the mulching purposes, their mechanical characteristics are still meaningful. The mechanical characteristics of polymeric composites are listed in Table 1.6. The elongation at break values were found to be 5.58 %, 4.14 %, and 121 % when the mass ratio of PVA:HM, PVA:RC, PVA:PG was 4:6, respectively. The tensile strength values were following: 10.2 MPa, 14.0 MPa and 4.95 MPa, while Young's modulus values were 442 MPa, 432 MPa and 152 MPa, respectively. These observations show that PG enhanced elasticity as compared to the composite films filled with HM and RC. The mass ratio of HM and RC had no significant influence to the mechanical properties.

Table 1.6 The mechanical characteristics of polymeric composites prepared from polyvinyl alcohol, rapeseed cake, phosphogypsum, horn meal, and crude glycerol [260]

Mass ratio of the components	Elongation at break (%)	Tensile strength (MPa)	Young's modulus (MPa)
PVA:HM:RC:CG			
4:6:0:3	5.58 ± 0.44	10.20 ± 0.60	442 ± 22
4:4:2:3	3.45 ± 0.41	11.30 ± 0.50	345 ± 24
4:2:4:3	4.62 ± 0.40	11.00 ± 0.60	325 ± 16
4:0:6:3	4.14 ± 0.20	14.00 ± 0.80	432 ± 21
PVA:HM:PG:CG			
4:4:2:3	7.01 ± 0.65	10.20 ± 0.10	454 ± 26
4:2:4:3	79.00 ± 6.90	7.41 ± 0.30	249 ± 16
4:0:6:3	121.00 ± 8.00	4.95 ± 0.28	152 ± 7
PVA:RC:PG:CG			
4:4:2:3	6.13 ± 0.52	12.10 ± 0.60	539 ± 25
4:2:4:3	30.90 ± 2.00	6.64 ± 0.24	328 ± 14
10:0:0:3	262.00 ± 18.00	35.40 ± 3.80	216 ± 8

1.5. Summary of literature review and justification of the work aim

As environmental pollution is rising due to the use of synthetic petroleum-based stable plastics, the renewable materials such as glycerol, a by-product of biodiesel production or glycerol derivatives, e.g. GDGE are a good alternative for production of biodegradable plastics. GDGE is attractive due to excellent engineering properties, such as versatile structure, which allows to perform various polymerization reactions, high adhesion to many surfaces due to polar groups, and low shrinkage during polymerization.

UV/Vis light initiated polymerization has many advantages against thermal polymerization, including easy control of the process, consumption of little energy, and curing under ambient conditions, but one of the greatest benefits is that the curing time is shortened from hours to minutes and the process is more sequential. However, there is still little data available on the use of GDGE in the photoinitiated polymerization reactions.

Optical 3D printing technologies, which involve UV/Vis light, such as SLA, DPL, and 3DLL are unique fabrication methods which offer unmatched material processing precision, flexibility and variety of used substances. These technologies has advantages against other 3D printing technologies such as low oxygen inhibition and high printing resolution.

Biodegradable plastic mulching films can be used as an alternative to stable LDPE mulching films thus eliminating the environmental pollution problem in agriculture. Incorporation of biobased industrial waste materials such as RC, PG, and HM into plastic mulching film could improve the fertility of the plants.
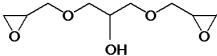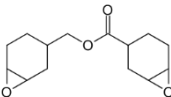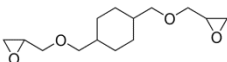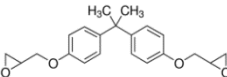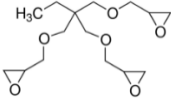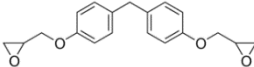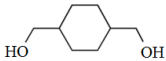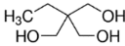
After considering the advantages of GDGE, UV/Vis light initiated polymerization, optical 3D printing technologies, and biodegradable plastic mulching films, it was decided to synthesize novel biodegradable GDGE-based photocross-linked polymers, to form polymeric composites and investigate their suitability to be applied in optical 3D printing and mulching coatings. Therefore, synthesis of photocross-linked polymers of GDGE and epoxy reactive diluents, of GDGE and di- or trihydroxyl compounds and formation of photocross-linked polymer composites of GDGE and biobased industrial waste materials (rapeseed cake (RC), phosphogypsum (PG), horn meal (HM)) was carried out. The thermal, mechanical, thermomechanical, swelling, wettability, and biodegradability properties were investigated in terms of potential application.

2. EXPERIMENTAL PART

2.1. Materials
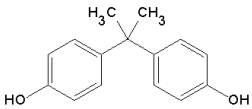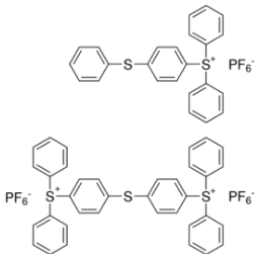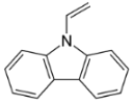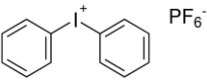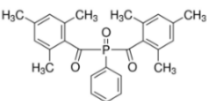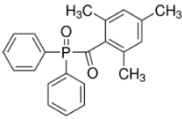
The materials used in the experiments are listed in Table 2.1. All materials and solvents were used as received and were not additionally purified before the use.

Table 2.1 Structure and characteristics of the used materials

Material (abbrevation), *supplier*	Chemical structure	Notes
Glycerol diglycidyl ether (2,3-bis(oxiran-2-ylmethoxy)propan-1-ol) (GDGE), *Sigma-Aldrich*		Technical grade, weight per epoxide equivalent 138-160, $n20/D$ 1.482
3',4'-Epoxycyclohexylmethyl-3,4-epoxycyclohexanecarboxylate (RD1), *Sigma-Aldrich*		$n20/D$ 1.498
1,4-Cyclohexanedimethanol diglycidyl ether (RD2), *Sigma-Aldrich*		mixture of *cis* and *trans* isomers, technical grade, $n20/D$ 1.481
Bisphenol A diglycidyl ether (2,2-bis[4-(glycidyloxy)phenyl]propane) (RD3), *Sigma-Aldrich*		Weight per epoxide equivalent 172-176, m.p.= 40-44 °C
Trimethylolpropane triglycidyl ether (RD4), *Sigma-Aldrich*		Technical grade, $n20/D$ 1.477
Bisphenol F diglycidyl ether (bis[4-(glycidyloxy)phenyl]methane) (RD5), *Sigma-Aldrich*		m.p.= 43-48 °C
1,4-Cyclohexanedimethanol (A1), *Sigma-Aldrich*		mixture of *cis* and *trans* isomers, 99 %, m.p.= 31.5 °C
1,1,1-Tris(hydroxymethyl)propane (A2), *Sigma-Aldrich*		98 %, m.p.= 56-61 °C
Hydroquinone (1,4-benzenediol) (A3), *Sigma-Aldrich*		99 %, m.p.= 172-175 °C

Table 2.1 (continuation of the table). Structure and characteristics of the used materials

Material (abbrevation), *supplier*	Chemical structure	Notes
Bisphenol A (2,2-Bis(4-hydroxyphenyl)propane) (A4), *Sigma-Aldrich*		99 %, m.p.= 158-159 °C
Triarylsulfonium hexafluorophosphate salts *Sigma-Aldrich*		mixed, 50 wt. % in propylene carbonate, $n20/D$ 1.5
N-Vinylcarbazole (NVK), *Sigma-Aldrich*		98 %, m.p.= 60-65 °C
Diphenyliodonium hexafluorophosphate (Ph_2I^+), *Sigma-Aldrich*		98 %, m.p.=140-144 °C
Phenylbis(2,4,6-trimethylbenzoyl)phosphine oxide (BAPO), *Sigma-Aldrich*		97 %, m.p.=131-135 °C
Diphenyl(2,4,6-trimethylbenzoyl)phosphine oxide (TPO), *Sigma-Aldrich*		97 %, m.p.=88-92 °C
Commercial resin PR48, *Autodesk*	–	–
Rapeseed cake (RC), *Mestilla*	–	Particle size of 150-200 μm
Phosphogypsum (PG), *Lifosa*	–	Particle size of 80-100 μm
Horn meal (HM), *ĮĮ of V. Karkazas*	–	Particle size of 100-150 μm

The solvents, i.e. tetrahydrofuran (99.9 %), dichloromethane (99.7 %), chloroform (98.5 %), toluene (99.2 %), isopropanol, acetone were purchased from *Eurochemicals*, diiodomethane (99 %) was purchased from *Sigma-Aldrich*.

2.2. Preparation of compositions

2.2.1. Preparation of compositions for photoinitiated cationic polymerization

The compositions (see Table 2.2) were prepared by mixing glycerol diglycidyl ether (GDGE) with selected amount (10 mol.%, 20 mol.%, and 30 mol.% with respect to GDGE) of epoxy reactive diluent (RD) (RD1, RD2, RD3, RD4, RD5) either di- or trihydroxyl compounds (A1, A2, A3, A4), or different amount (5 wt.%, 10 wt.%, 15 wt.%, 20 wt.% with respect to GDGE) of fillers (rapeseed cake (RC), phosphogypsum (PG), horn meal (HM)) and the cationic photoinitiator (CPI) (3 mol.% relative to amount of GDGE). Neat compositions without RD, hydroxyl compound, or filler were prepared by mixing GDGE with the CPI. Dichloromethane was used for preparation of compositions with epoxy RDs. Tetrahydrofuran was used for preparation of compositions with di- or trihydroxyl compounds. Compositions with fillers were prepared without the solvent. Compositions were applied on a plastic substrate with a glass Pasteur pipette and cured for 2-4 min under UV/Vis light using a 500 W Helios Italquartz, model GR.E UV lamp with a wavelength range of (250-450) nm at an intensity of 310 mW·cm^{-2} at 78 °C.

Table 2.2 Composition formulations with different percentages of reactive diluents, di- or trihydroxyl compounds or fillers, and 3 mol.% of cationic photoinitiator

Composition	RD or di- or trihydroxyl compound (mol.%), or filler (wt.%)
Neat1	-
10RD1	10
20RD1	20
30RD1	30
10RD2	10
20RD2	20
30RD2	30
10RD3	10
20RD3	20
30RD3	30
10RD4	10
20RD4	20
30RD4	30
10RD5	10
20RD5	20
30RD5	30
Neat2	-
10A1	10
20A1	20
30A1	30
10A2	10
20A2	20
30A2	30

Table 2.2 (continuation of the table). Composition formulations with different percentages of reactive diluents, di- or trihydroxyl compounds or fillers, and 3 mol.% of cationic photoinitiator

Composition	RD or di- or trihydroxyl compound (mol.%), or filler (wt.%)
10A3	10
20A3	20
30A3	30
10A4	10
20A4	20
30A4	30
Neat3	-
5RC	5
10RC	10
15RC	15
20RC	20
5PG	5
10PG	10
15PG	15
20PG	20
5HM	5
10HM	10
15HM	15
20HM	20

2.2.2. Preparation of compositions for photoinitiated free radical promoted cationic polymerization

The compositions (see Table 2.3) were prepared by mixing GDGE with 30 mol.% of RD1 (with respect to GDGE), different percentages of radical photoinitiator (PI) BAPO or TPO (1-5 wt.% relative to amount of GDGE), 3 wt.% of NVK as promoter, and 2 wt.% of Ph_2I^+ as CPI. The compositions for the FRPCP were prepared without the solvent and mixed for 48 hours (except **1** – **2BAPO** and **1** – **4TPO**, which were mixed for 24 hours) until the homogeneous solution was obtained.

Table 2.3 Formulation of compositions with 30 mol.% of RD1, different percentages of BAPO or TPO, 3 wt.% of NVK, and 2 wt.% of Ph_2I^+

Composition	RD1 (mol.%)	BAPO/TPO (wt.%)
1BAPO		1
2BAPO		2
3BAPO	30	3
4BAPO		4
5BAPO		5
1TPO		1
2TPO		2
3TPO	30	3
4TPO		4
5TPO		5

2.3. Research techniques

2.3.1. Fourier transformed infrared spectroscopy

Fourier transformed infrared (FT-IR) measurements of the cured photocross-linked polymers and polymer composites were performed on a *Perkin Elmer Spectrum BX II* FT-IR spectrometer. The reflection was measured during the test. The spectra were acquired from 10 scans. The range of wavenumber was (400-4000) cm^{-1}.

2.3.2. Photorheometry

UV/Vis real time photorheometry curing tests were carried out with *MCR302* rheometer from *Anton Paar* equipped with the plate/plate measuring system. Peltier-controlled temperature chamber with the glass plate (diameter of 38 mm) and the top plate PP08 (diameter of 8 mm) was used. Measuring gap was set to 0.5 mm. The samples were irradiated at room temperature by UV/Vis radiation in a wavelength range of (250-450) nm through the glass plate of the temperature chamber using UV/Vis spot curing system *OmniCure S2000*, Lumen Dynamics Group Inc. Intensity of the UV irradiation was 9.3 $W \cdot cm^{-2}$ (high pressure 200 W mercury vapor short arc). Shear mode with the frequency of 1 Hz and shear strain of 2 % was used in all cases. Storage modulus G', loss modulus G", loss factor tanδ (tanδ = G"/G'), and complex viscosity ŋ* were recorded as a function of irradiation time. G', G", and ŋ* values were taken after 10 min of composition irradiation by UV/Vis radiation. The gel point t_{gel} was defined as crossover point between G" and G' modulus. The experiment was carried out once.

2.3.3. Soxhlet extraction

The amount of insoluble polymer fraction (Y) was determined by Soxhlet extraction. The samples of the photocross-linked polymers and polymer composites (0.2 g) were put into a filter package and placed in a Soxhlet apparatus. Extraction was performed with chloroform for 24 hours. Insoluble fractions were dried under

vacuum to constant weight. The experiment was carried out once. The yield of insoluble fraction was calculated according to the formula:

$$Y = \frac{m}{m_0} \cdot 100 \qquad\qquad (2.1)$$

where Y is the yield of insoluble fraction (%), m is the mass of the sample after extraction (g), m_0 is the mass of the sample before the extraction (g).

2.3.4. Differential scanning calorimetry

Glass transition temperatures (T_g) of the photocross-linked polymers and polymer composites were estimated by differential scanning calorimetry (DSC). The measurements were performed on a *Perkin Elmer DSC 8500* apparatus with the heating-cooling-heating rate of 10 °C·min^{-1} under nitrogen atmosphere from -25 °C to 95 °C (nitrogen flow rate 50 mL·min^{-1}). The T_g was determined as the middle point of the transition which appeared as a step in the baseline of the recorded DSC signal and were taken from the second heating scan. The experiment was carried out once.

2.3.5. Thermogravimetric analysis

Thermal decomposition temperatures at the 10 % weight loss ($T_{dec.-10\%}$) and residue yield after thermal degradation in N_2 atmosphere (Res.) of the photocross-linked polymers and polymer composites were determined by thermogravimetric analysis (TGA). The measurements were performed on a *Perkin Elmer TGA 4000* apparatus in the temperature range from room temperature to 900 °C at a heating rate of 20 °C·min^{-1} under nitrogen atmosphere (nitrogen flow rate 100 mL·min^{-1}). The experiment was carried out once.

2.3.6. Mechanical testing

Mechanical properties of the photocross-linked polymers and polymer composites were estimated by tensile test on a *BDO-FB0.5TH (Zwick/Roell)* testing machine at 22 °C using the ASTM method D882 with some modifications. Strain rate of 1 mm/min was used in all cases. Mechanical testing was performed on dog bone shaped samples with the length of 45 mm and width of 5 mm. to determine tensile strength, elongation at break, and Young's modulus.

2.3.7. Dynamic-mechanical thermal analysis

Dynamic-mechanical thermal analysis (DMTA) was performed in a shear mode using *MCR302* rheometer from *Anton Paar* equipped with the plate/plate measuring system. Temperature was ramped from -20 °C to 40 °C (for the photocross-linked polymers of GDGE and di- or trihydroxyl compounds) and from 10 °C to 50 °C (for the photocross-linked polymers of GDGE and RDs) at a rate of 2 °C·min^{-1}. Frequency of 1 Hz and strain of 0.5 % were used in all cases. G', G'', and tanδ were recorded as a function of temperature. The T_g was defined by the maximum peak of tanδ curve. G' modulus was determined at the glassy state, at 20 ºC, and rubbery (viscoelastic) state. The experiment was carried out once.

2.3.8. Dynamic mechanical analysis

Dynamic mechanical analysis (DMA) of the polymer composites was carried out using dynamic mechanical analyser *Netzsch DMA 242C* in the temperature range from 0 °C to 50 °C at a heating rate of 2 °C·min⁻¹. Tension mode with the oscillation frequency of 1 Hz was used. Tests were performed with the samples of the following size: 10 mm × 5 mm. Storage modulus (E'), loss modulus (E''), and tanδ were recorded as a function of temperature. The T_g was defined by the maximum peak of tanδ curve. E' modulus was determined at the glassy state, at 20 °C, and rubbery (viscoelastic) state. The experiment was carried out once.

2.3.9. Swelling measurements

The swelling degree (α) of photocross-linked polymers and polymer composites was estimated by measuring the weight of the samples swollen in distilled water, chloroform, and toluene at room temperature (18 °C). The weighed 20 mm × 20.00 mm samples were placed in a 20 ml glass beaker containing the solvent and stored at room temperature. Every 15 min (for the polymer composites) and 30 min (for the photocross-linked polymers of GDGE and RDs or di- or trihydroxyl compounds) the samples were removed and the surface was wiped dry and weighed. The experiment was performed until the equilibrium of swelling was reached. The experiment was carried out once. The following formula has been used:

$$\alpha = \frac{m - m_0}{m_0} \cdot 100 \qquad\qquad (2.2)$$

where α is the swelling degree (%), m is the mass of the swollen sample (g), m_0 is the mass of the sample before the swelling experiment (g).

2.3.10. Contact angle measurements

Contact angle measurements of photocross-linked polymer composite films were perfomed on *OneAttension Theta Lite* apparatus. A static sessile drop method was used. Distilled water and diiodomethane with the known surface free energy of 72.8 mN/m and 50.8 mN/m respectively, were used for the measurements. The drop volume was (2-6) µl. The average values of contact angle were taken from at least three film samples.

2.3.11. Biodegradability assessment by soil burial test

Biodegradability experiments were carried out by soil burial test under laboratory conditions at (26 ± 2) °C according to the standard test method ISO 846:1997. The samples of the photocross-linked polymers and polymer composites with the dimensions of (10 mm × 10 mm) were weighed, placed into poly(vinyl chloride) bags with 0.05 mm mesh diameter, and buried into the soil for 3 months. Five liter volume chambers filled with composting soil (pH$_{KCl}$ – 6.6; the moisture content (20-30) %) were used for the biodegradability experiment. The samples were removed monthly, washed with sterile water, and weighed. The experiment

was carried out in triplicates. For the estimation of soil microbial activity, cotton wool (1 g) was buried and its mass loss made up 31 % after 3 months. Biodegradability of photocross-linked polymers and polymer composites was estimated according to the formula:

$$ML = \frac{m_0 - m}{m_0} \cdot 100 \qquad (2.3)$$

where ML is the mass loss (%), m_o is the mass of the sample before the biodegradability experiment (g), m is the mass of the sample after 1, 2 or 3 months exposition in soil (g).

2.3.12. Photolithography

Photolithography (LA) and selective LA experiments were performed with the composition **30RD1** with 3 mol.% of the CPI by *Thorlabs* UV curing light-emitting diode (LED) system *CS2010* with 270 mW power and intensity of 1.8 mW·cm^{-2} (Fig. 2.1a). 10 μl droplets of the composition was casted on the glass for the LA process (Fig. 2.1b) or glass coated with 200 nm gold layer (the gold was selectively removed with a femtosecond pulsed laser to form a binary mask) for the selective LA (Fig. 2.1c) and irradiated with 365 nm wavelength UV light. The width of abraded lines was from 150 μm to 400 μm, and the opaque slits between them were of 150 μm. Acetone was used to dissolve uncured composition **30RD1**, leaving only the formed microstructures (rinsing duration 1 min) and isopropanol was used to leach out noncross-linked monomers from the objects printed out of standard resin PR48. The curing time and the absorbed irradiance energy dose of the composition **30RD1** was determined and compared with the commercial resin PR48. The irradiance energy dose (E) was calculated according to the formula:

$$E = \frac{P}{S} \qquad (2.4)$$

where E is the irradiance energy dose (J·m^{-2}), P is the UV LED power (W), S is the irradiated area (m^2) calculated using the formula:

$$S = \pi(D \cdot tan\,\alpha)^2 \qquad (2.5)$$

where D is the distance between a sample and LED chip (m), α is divergence from the optical axis (°).
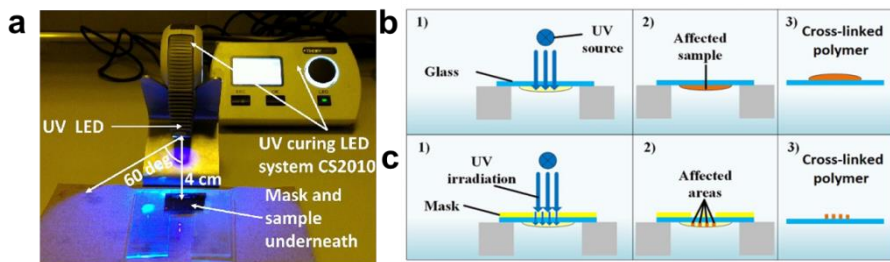
Fig. 2.1 Thorlabs UV curing LED system CS2010 (a), LA setup (b), and selective LA setup (c) [261]

2.3.13. Dynamic projection lithography

Dynamic projection lithography (DPL) experiments were performed with the compositions **1BAPO** – **5TPO** containing 30 mol.% of RD1 and different amount of BAPO or TPO as radical PI by *Autodesk's* 3D optical printer *Ember* (Fig. 2.2a). Projector *Wintech PRO4500* with 5W power and 405 nm wavelength was used as the light source. The digital mirror device consisted of 1280×800 (total 1.024 million) micromirrors. One micromirror pitch size is 7.6 μm, which creates a 50×50 μm^2 projection of a single image pixel, which defines device resolution in X, Y plane. Such an optical system ensured 18.61 mW·cm^{-2} light intensity projected through the UV light transparent polydimethylsiloxane window where the printing process occurred. Ember's principle working scheme is shown in Fig. 2.2b. Irradiation from the projector reflects to the mirror and exposes resin through the polydimethylsiloxane window (Fig. 2.2b I), after irradation, the tray slides (1) and the build head rises up (Fig. 2.2b II), and the tray comes back in primary position (1) and the build head lowers (2) (Fig. 2.2b III). Glass substrates were used to cast 10 μl droplets of the samples on them. The substrates with samples were placed on the polydimethylsiloxane window. Autodesk AutoCAD 2017 student version software was used as CAD. The model was created corresponding to Ember resolution test results and consisted of 50 μm to 400 μm width layers with 50 μm to 500 μm (both increasing every 50 μm width slits in between). The light intensity through the PDMS substrate was increased to the maximum and reached 26.54 mW·cm^{-2} value. Optical profilometer *SENSOFAR PLμ 2300* was used to obtain formed features profiles and determine their height dependence on absorbed irradiance energy dose. Isopropanol was used to dissolve out noncross-linked monomers from the objects printed out of standard resin PR48 (rinsing duration from 10 to 15 min). Acetone was used to dissolve uncured compositions **1BAPO** – **5TPO** (rinsing duration from 1 to 2 min). Scanning electron microscope (SEM) *HITACHI TM-1000* was employed for characterization.
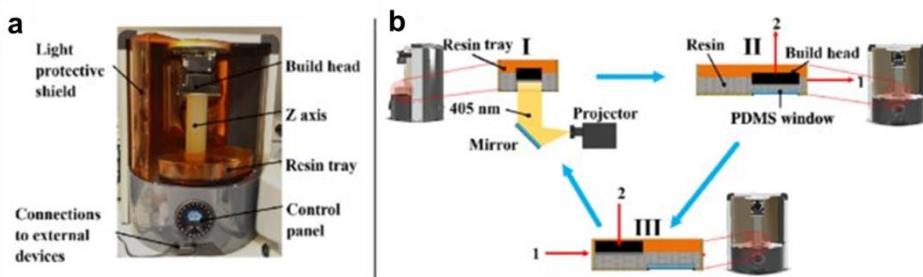
Fig. 2.2 3D optical printer Ember (a), Ember's principle working scheme (b), and selective SLA technology (c) [261]

2.3.14. 3D laser lithography

3D laser lithography (3DLL) experiments for the formation of 3D hexagonal structure was performed with the composition **3BAPO** containing 30 mol.% of RD1, 3 wt.% of BAPO as radical PI, 3 wt.% of NVK as promoter, and 2 wt.% of

48

Ph$_2$I$^+$ as CPI by *Laser Nanofactory* setup developed by *Femtika* (Fig. 2.3). Components in the system were Pharos laser with the power of 0.35 mW, power attenuator consisting of λ/2 phase plate (PP$_1$) and polarizer out of two glass slides (G$_1$, G$_2$) angled at Brewster angle, mirrors (M), Hiro harmonic generator, removable power meter (RPM), telescope (T), objective lens (Obj) and illuminating LED. In order to start structure production at the polymer-glass interface, focusing was done in polymer drop-up configuration. Laser was operating at 200 fs pulse duration and 200 kHz repetition rate. Fundamental 1030 nm radiation was converted to II harmonic (515 nm). Such exposure characteristics were chosen as representing what is used in standard 3D nanopolymerization. The system also doubled as an imaging unit, allowing monitoring fabrication process in real time. The chosen translation velocity was 1 mm/s as it matches the lowest one used for structuring standard photopolymers.
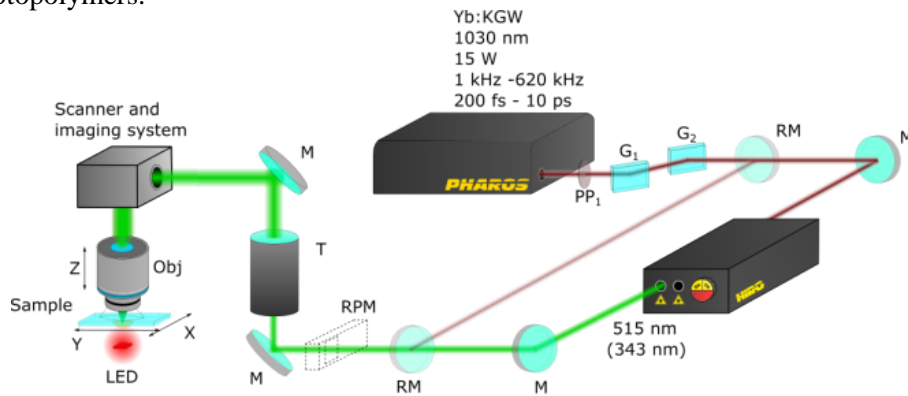
Fig. 2.3 Scheme of *Laser Nanofactory* setup developed by Femtika

2.4. Calculations

2.4.1. Calculation of cross-linking density

Calculation of cross-linking density (N) of the photocross-linked polymers and polymer composites was performed according to the theory of rubber elasticity using the following formula:

$$N = \frac{G'}{RT} \tag{2.6}$$

where N is the cross-linking density (mol/m^3), G′ is the steady-state (plateau) value after 10 minutes of storage modulus taken from real time photorheometry measurements (Pa), R is the universal gas constant (8.314 J/K·mol), T is the temperature (K) [262].

2.4.2. Estimation of tensile strength, elongation at break, and Young's modulus

Calculation of tensile strength, elongation at break, and Young's modulus was performed with „testXpert V11.02 Standard" program. The tensile strength, elongation at break, and Young's modulus values reported are mean values of ten

measurements with calculated standard deviation. The following equation for calculating of the elongation at break was used:

$$\varepsilon = \frac{\varepsilon_R}{\varepsilon_0} \cdot 100 \qquad (2.7)$$

where ε is elongation at break (%), ε_R is elongation at rupture (m), ε_0 is initial length of the sample (m).

Tensile strength was calculated according to formula:

$$\sigma_B = \frac{F}{S} \qquad (2.8)$$

where σ_B is tensile strength (MPa), F is load at break (N), S is cross-sectional area of the sample (m^2).

Young's modulus was calculated according to formula:

$$E_{mod} = \frac{F \cdot l_0}{S \cdot \Delta l} \qquad (2.9)$$

where E_{mod} is Young's modulus (MPa), F is force applied (N), l_0 is length of the sample without force (m), S is area of a section of the sample (m^2), Δl is change in the length of the sample after a force is applied (m).

2.4.3. Estimation of surface free energy

Calculation of surface free energy of photocross-linked polymer composites was perfomed on *OneAttension Theta Lite* apparatus. The average values of contact angle for the surface free energy calculations were taken from at least three film samples. The Equation of State [263, 264], Owens-Wendt-Rabel-Kaelble (OWRK) [265, 266], and Wu [267, 268] methods were chosen for the surface free energy calculation. Surface free energy was calculated according to Young's equation [269]:

$$\sigma_s = \sigma_{sl} + \sigma_l \cdot cos\theta \qquad (2.10)$$

where σ_s is surface free energy of the solid (mN/m), σ_{sl} is the interfacial tension between liquid and solid (mN/m), σ_l is the surface tension of the liquid (mN/m), θ is the contact angle between the solid and the measuring liquid ($^\circ$).

The following equation for calculating of the surface free energy is used in the Equation of State method:

$$\sigma_{sl} = \sigma_s + \sigma_l - 2\sqrt{\sigma_l \cdot \sigma_s} \cdot e^{-\beta(\sigma_l - \sigma_s)^2} \qquad (2.11)$$

where β is empirically determined constant (0.0001247).

According to the OWRK method, the estimation of interfacial tension σ_{sl} is based on two surface tensions, σ_s and σ_l, and the similar interactions between the phases. These interactions are interpreted as the geometric mean of a disperse part σ^D and a polar part σ^P of the surface tension or surface free energy:

$$\sigma_{sl} = \sigma_s + \sigma_l - 2(\sqrt{\sigma_s^D \cdot \sigma_l^D} + \sqrt{\sigma_s^P \cdot \sigma_l^P}) \qquad (2.12)$$

According to the Wu method, interactions are interpreted as the harmonic mean of a disperse part σ^D and a polar part σ^P of the surface tension or surface free energy:

$$\sigma_{sl} = \sigma_s + \sigma_l - 4(\frac{\sigma_s^D \cdot \sigma_l^D}{\sigma_s^D + \sigma_l^D} + \frac{\sigma_s^P \cdot \sigma_l^P}{\sigma_s^P \cdot \sigma_l^P}) \qquad (2.13)$$

In the OWRK and Wu methods at least two liquids with known disperse and polar parts of the surface tension are required to determine the surface free energy of the solid.

2.4.4. Statistical data analysis

Standard deviation (SD) was used to explain variations in experimental data:

$$SD = \sqrt{\frac{\sum_{i=1}^{n}(x_i - x)^2}{n-1}} \qquad (2.14)$$

where SD is standard deviation, $\{x_1, x_2, ..., x_n\}$ are observed values of the parameters, x is the arithmetic average of observed values, n is number of the repeated experiments.

3. RESULTS AND DISCUSSION

3.1. Biodegradable photocross-linked polymers of glycerol diglycidyl ether and epoxy reactive diluents

Five different epoxy reactive diluents (RDs) were selected in order to evaluate the effect of their chemical structure and amount on the photocross-linking of glycerol diglycidyl ether (GDGE) and on the properties of the resulting polymers. The photocross-linked polymers **Neat1** – **30RD5** were synthesized by the reaction of GDGE with different molar amount (10 mol.%, 20 mol.%, and 30 mol.%) of different epoxy RD under UV/Vis light, using 3 mol.% of cationic photoinitiator (CPI) (see Table 2.2). Such concentrations of RD and CPI were chosen based on the previous results [196]. The obtained photocross-linked polymeric films of GDGE and epoxy RDs (thickness of 250 ± 35 µm) were transparent and smooth.

The chemical structures of the photocross-linked polymers **Neat1** – **30RD5** were identified by FT-IR spectroscopy:

IR (cm^{-1}) of photocross-linked polymer **Neat1**: 3430 (ν O–H), 2919 (ν CH$_2$ aliph.), 2870 (ν C–H aliph.), 1074 (ν C–O–C).

IR (cm^{-1}) of photocross-linked polymers **10** – **30RD1**: 3455–3403 (ν O–H), 2929–2920 (ν CH$_2$ aliph), 2877–2870 (ν C–H aliph.), 1728–1724 (ν C=O aliph.), 1074 (ν C–O–C).

IR (cm^{-1}) of photocross-linked polymers **10** – **30RD2**: 3460–3439 (ν O–H), 2920–2918 (ν CH$_2$ aliph), 2868–2863 (ν C–H aliph.), 1078–1074 (ν C–O–C).

IR (cm^{-1}) of photocross-linked polymers **10** – **30RD3**: 3458–3445 (ν O–H), 3042–3039 (ν C–H ar.), 2923–2917 (ν CH$_2$ aliph.), 2870–2869 (ν C–H aliph.), 1078–1075 (ν C–O–C).

IR (cm^{-1}) of photocross-linked polymers **10** – **30RD4**: 3443–3433 (ν O–H), 2919 (ν CH$_2$ aliph), 2869–2867 (ν C–H aliph.), 1076–1073 (ν C–O–C).

IR (cm^{-1}) of photocross-linked polymers **10** – **30RD5**: 3443–3433 (ν O–H), 3041–3039 (ν C–H ar.), 2920 (ν CH$_2$ aliph), 2870 (ν C–H aliph.), 1074 (ν C–O–C).

The signals of epoxy group which was present at 985 cm^{-1} in the FT-IR spectrum of GDGE and at 975 cm^{-1} present in the spectrum of RD1 disappeared in the FT-IR spectrum of GDGE, RD1, and the photocross-linked polymer **10RD1** (Fig. 3.1). The characteristic C–O–C group stretch at 1073-1078 cm^{-1} appeared in the IR spectra of all photocross-linked polymers with the fragments of RDs.
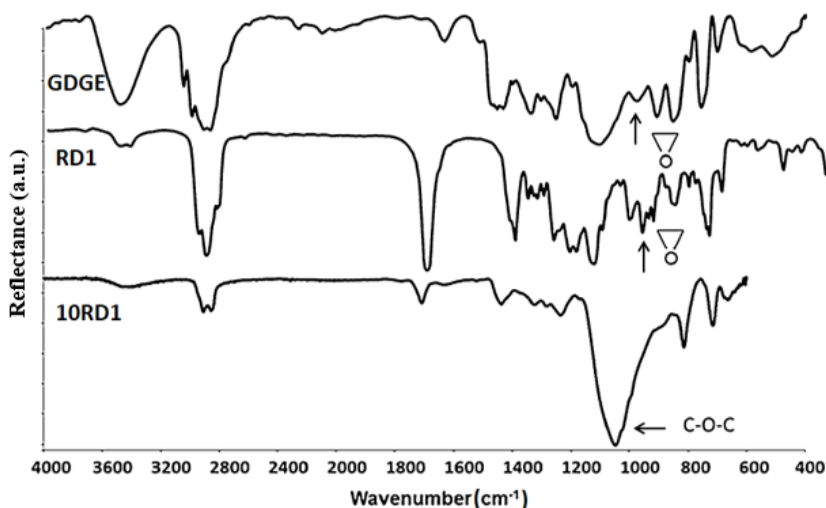
Fig. 3.1 IR spectra of glycerol diglycidyl ether, 3',4'-epoxycyclohexylmethyl-3,4-epoxycyclohexanecarboxylate, and the photocross-linked polymer **10RD1**

As the CPI triarylsulfonium hexafluorophosphate salts was not sensitive to 405 nm wavelength of Vis light used in the dynamic projection lithography (DPL) and 3D laser lithography (3DLL), the cationic photopolymerization was changed to free radical promoted cationic photopolymerization (FRPCP) [175]. The photocross-linked polymers **1BAPO** – **5TPO** (see Table 2.3) were synthesized by the reaction of GDGE with 30 mol.% of RD1, using different percentages of radical photoinitiator (PI) BAPO or TPO (1-5 wt.%), 3 wt.% of NVK as promoter, and 2 wt.% of Ph_2I^+ as CPI. Such concentrations of the radical PI, promoter, and CPI were chosen based on the previous results [175].

Photorheometry is a powerful technique to monitor changes of rheological and mechanical properties such as viscosity and shear modulus during polymerization of monomers with UV/Vis light [270]. The storage modulus (G') is the stored energy, representing the elastic portion and loss modulus (G'') is the energy dissipated as heat, representing the viscous part [271]. The ratio between the G'' and G' modulus in a viscoelastic material is defined as the loss factor (tanδ), which provides a measure of damping in the material. The G' modulus characterizes the rigidity of the thermosetting resin [272]. Changes of G' and G'' modulus as a function of irradiation time can be monitored in real time when a sample undergoes transition from liquid to solid [273]. The G' and G'' modulus, tanδ, and complex viscosity (ŋ*) versus irradiation time curves of the photocross-linked polymer **30RD1** are shown in Fig. 3.2.
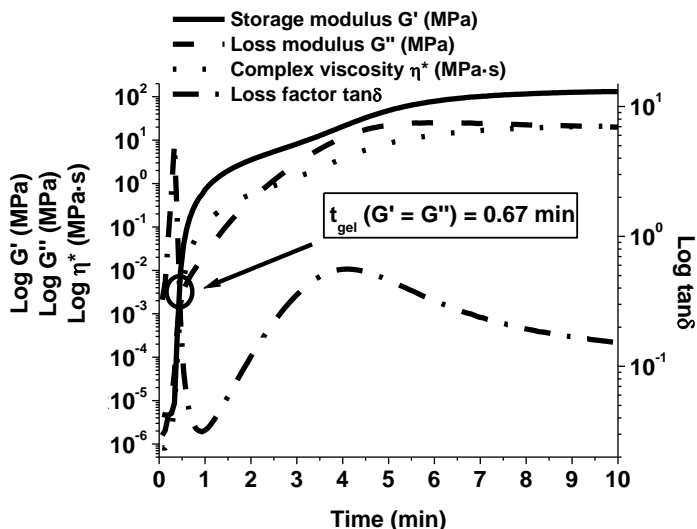
Fig. 3.2 Curves of storage modulus G', loss modulus G", loss factor tanδ, and complex viscosity η* versus irradiation time of the photocross-linked polymer **30RD1**

When the irradiation of the composition started, G" > G' and tanδ > 1 occured which means that sample was a viscoelastic liquid. The G', G", tanδ, and η* increased very fast indicating a growth of the chain size and network formation in the initial stage of photopolymerization. The sample consolidation time or the crossover point between G" and G' modulus is characterized as gel point (t_{gel}) at which tanδ = 1 [274]. The composition **30RD1** reached t_{gel} after 0.67 min irradiation of UV/Vis light. The G' increased faster and exceeded G" while tanδ started to decrease in the intermediate stage (when G" < G' and tanδ < 1) and the sample started behave as a viscoelastic solid. During the late stage, G' and G" continued to increase with time due to gel aging and settled down into steady-state (plateau) indicating the end of the gelation process. All the photocross-linked polymers **Neat1 – 30RD5** showed the same behaviours.

Real time photorheometry data of photocross-linked polymers **Neat1 – 30RD5** are listed in Table 3.1. The addition of RDs into the compositions led to the higher values of G', G", and η* and thus accelerated the photocross-linking of GDGE as t_{gel} was reached much more faster. By increasing the amount of RD in the compositions, the G', G", and η* increased and t_{gel} decreased in all cases. This observation shows that the higher amount of the reactive species was produced with the increase of the RD amount in the composition which results in the increase of the overall reaction rate and in the formation of the more rigid network. As G' modulus characterizes the rigidity of the polymer, the G' modulus curves versus irradiation time of the photocross-linked polymers with the diferent amount of RD1 and the same amount (30 mol.%) of different RDs are presented in Fig. 3.3. The more rigid photocross-linked polymers **30RD1**, **20 – 30RD3** and **10 – 30RD5** with the highest G' modulus were obtained due to the high cross-linking density (Table 3.3). The photocross-linking of GDGE was the fastest (t_{gel} = 0.5 min) and the most rigid photocross-

linked polymer **30RD3** with 154 MPa of G' modulus was obtained when the 30 mol.% of RD3 (DGEBA) was used.

Table 3.1 Real time photorheometry data of photocross-linked polymers **Neat1** – **30RD5**

Photocross-linked polymer	Storage modulus G' (MPa)	Loss modulus G'' (MPa)	Complex viscosity η^* (MPa·s)	Gel point t_{gel} (min)
Neat1	0.17	0.01	0.03	6.67
10RD1	3.15	0.04	0.50	1.83
20RD1	7.12	1.40	1.15	1.00
30RD1	131.00	20.00	21.1	0.67
10RD2	7.74	5.30	1.49	2.25
20RD2	8.34	6.58	1.69	1.83
30RD2	14.20	11.70	2.93	1.25
10RD3	7.07	6.74	1.55	1.67
20RD3	128.00	16.40	20.60	0.75
30RD3	154.00	16.60	27.70	0.50
10RD4	27.00	18.40	5.20	1.83
20RD4	56.30	32.70	10.40	1.58
30RD4	63.50	37.50	11.70	1.25
10RD5	119.00	24.30	19.30	1.25
20RD5	122.00	25.10	19.80	1.08
30RD5	128.00	26.60	20.30	0.92
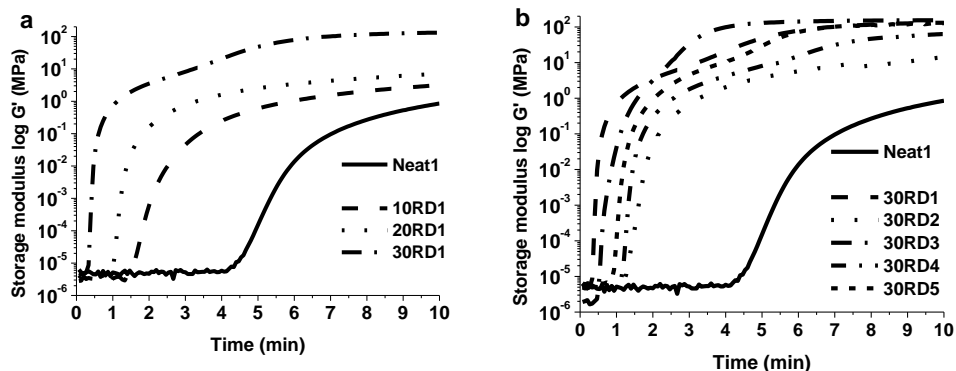
Fig. 3.3 Curves of storage modulus G' versus irradiation time of the following photocross-linked polymers: polymer **Neat1** without RD, polymers with the different amount of RD1 (a), and polymers containing 30 mol.% of different RDs (b)

Photorheometry was used to monitor the photocross-linking kinetics of compositions **1BAPO** – **5TPO** during photoinitiated FRPCP. When BAPO was used, the photocross-linking of GDGE and 30 mol.% of RD1 was faster and the photocross-linked polymers had better rheological properties such as viscosity and rigidity characterized by G' modulus than those when TPO was used (Table 3.2). This observation is similar to the previous results when BAPO increased the epoxy groups conversion more than TPO due to the lower ionization potential which is compatible with the faster oxidation process [175].

Table 3.2 Real time photorheometry data of photocross-linked polymers **1BAPO** – **5TPO**

Photocross-linked polymer	Storage modulus G' (MPa)	Loss modulus G'' (MPa)	Complex viscosity η* (MPa·s)	Gel point t_{gel} (min)
1BAPO	10.30	6.66	1.95	2.20
2BAPO	7.91	5.25	1.51	3.24
3BAPO	3.72	1.78	0.66	3.36
4BAPO	1.00	0.24	0.16	4.16
5BAPO	0.17	0.04	0.03	6.48
1TPO	3.03	1.50	0.54	3.80
2TPO	0.39	0.07	0.06	5.52
3TPO	0.04	0.02	0.01	9.16
4TPO	-	-	-	-
5TPO	-	-	-	-
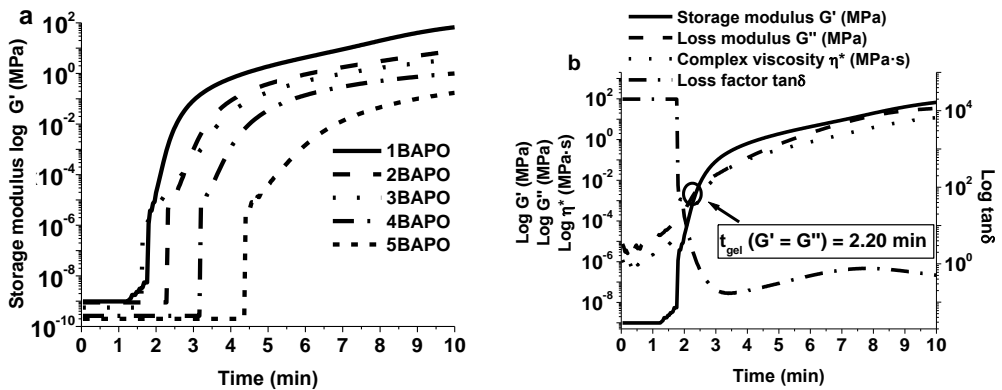
Fig. 3.4 Curves of storage modulus G' versus irradiation time of photocross-linked polymers with the different amount of BAPO (a) and curves of storage modulus G', loss modulus G'', loss factor tanδ, and complex viscosity η* versus irradiation time of the photocross-linked polymer **1BAPO** (b)

The compositions containing 4 wt.% and 5 wt.% of TPO did not solidify after 10 min of irradiation with UV/Vis light. The photocross-linking of GDGE and 30 mol.% of RD1 was faster and obtained photocross-linked polymers were more rigid when the lower amount of BAPO was used (Fig. 3.4a). The photocross-linking was the fastest (t_{gel} = 2.20 min) and the most rigid photocross-linked polymer **1BAPO** with 10.3 MPa of G' modulus was obtained when 1 wt.% of BAPO was used (Fig. 3.4b). When the cationic photopolymerization was used, the composition **30RD1** containing 30 mol. % of RD1 hardened faster (t_{gel} = 0.67 min) and had better rheological properties (G' = 131 MPa, G'' = 20 MPa, η* = 21.1 MPa·s) (Table 3.1) than that when the FRPCP was used for the analogical composition **1BAPO** containing 30 mol. % of RD1 (t_{gel} = 2.20 min, G' = 10.3 MPa, G'' = 6.66 MPa, η* = 1.95 MPa·s) (Table 3.2).

The photocross-linked polymers obtained from GDGE and RDs were insoluble in all common organic solvents. To confirm their cross-linked structure, the Soxhlet extraction was performed and cross-linking density values were calculated according

to the theory of rubber elasticity. The yields of insoluble fraction of the photocross-linked polymers with the fragments of RDs after the extraction with chloroform for 24 h were in the range of 84-99 % while the yield of insoluble fraction of polymer **Neat1** without RD was 90 % (Table 3.3) and were higher when analogical RDs were used for the photocross-linking of epoxidized linseed oil (69-91 %) [196]. The cross-linking density values of the photocross-linked polymers were also higher than of polymer **Neat1** (69 mol/m^3) and ranged from 1280 mol/m^3 to 62578 mol/m^3. These values showed that both GDGE and RD participated in the formation of the cross-linked structure.

Table 3.3 Yields of insoluble fraction and cross-linking densities of photocross-linked polymers **Neat1** – **30RD5**

Photocross-linked polymer	Yield of insoluble fraction Y (%)	Cross-linking density N (mol/m^3)
Neat1	90	69
10RD1	92	1280
20RD1	93	2893
30RD1	98	53232
10RD2	84	3145
20RD2	85	3389
30RD2	87	5770
10RD3	93	2873
20RD3	94	52013
30RD3	99	62578
10RD4	85	10971
20RD4	86	22877
30RD4	88	25803
10RD5	91	48355
20RD5	94	49574
30RD5	97	52013

The dependence of the chemical structure and amount of the RD on the yield of insoluble fraction and cross-linking density was observed. The yields of insoluble fraction of above 90 % were observed for the polymers **10** – **30RD1** with cycloaliphatic RD1 (CAE) fragments which is known as a very reactive compound displaying higher rates of polymerization [186]. Also the higher yield of insoluble fraction and cross-linking density values were observed for the polymers **10** – **30RD3** and **10** – **30RD5** with the fragments of aromatic RDs due to the rigid backbone of diglycidyl ethers of bisphenol A and F. The lower yields of insoluble fraction of 84-88 % were observed for the polymers **10** – **30RD2** and **10** – **30RD4** with the fragments of saturated RDs. This can be explained by the plasticization effect due to the flexible structure of RD2 ad RD4. Also the activated monomer (AM) mechanism could occure due to the presence of hydroxyl group in the GDGE structure which results in a large amount of nucleophilic hydroxyl groups released and competes with the protonation of epoxy ring, decreasing the amount of reactive oxirane cationic groups formed by photoacid addition [207]. The highest yield of insoluble fraction and cross-linking density were observed for the photocross-linked

polymer **30RD3** when the 30 mol.% of RD3 (DGEBA) was used. Three epoxy groups of RD4 had no influence on the yield of insoluble fraction, but cross-linking density was higher as compared to the other aliphatic RD1 and RD2 bearing two epoxy groups. By increasing the amount of RD fragments in the polymer structure, the yield of insoluble fraction and cross-linking density increased in all cases which is due to the restrictions of the chain mobility. This observation shows that the ring opening polymerization of GDGE by epoxy RDs occured via activated chain end (ACE) mechanism.

3.1.1. Thermal properties

The temperature range in which the polymers can be used is very important for their applications. Thus, thermal characteristics of the photocross-linked polymers **Neat1** – **30RD5** investigated by DSC, DMTA, and TGA are summarized in Table 3.4.

Table 3.4 DSC, DMTA, and TGA data of photocross-linked polymers **Neat1** – **30RD5**

Photocross-linked polymer	Glass transition temperature T_g (°C)		Temperature at the weight loss of 10 % $T_{dec.-10\%}$ (°C)	Residue yield after thermal degradation Res. (%)
	estimated by DSC	estimated by DMTA		
Neat1	33	18	308	6.1
10RD1	43	35	316	5.4
20RD1	52	38	320	5.4
30RD1	68	43	281	4.4
10RD2	34	22	330	6.5
20RD2	27	20	336	5.2
30RD2	34	20	336	5.6
10RD3	49	29	335	8.1
20RD3	56	30	330	8.0
30RD3	47	45	331	8.9
10RD4	36	29	339	5.2
20RD4	35	31	320	4.9
30RD4	20	28	325	5.5
10RD5	41	27	328	7.7
20RD5	56	33	345	9.4
30RD5	54	37	336	10.4

The DSC and DMTA data confirmed that photocross-linked polymers are amorphous materials as only the glass transitions were observed. The glass transition temperature (T_g) is one of the most important parameters of physical properties of polymers as in the highly viscous region above the T_g, polymers are soft and rubbery and below the T_g, polymers are hard and brittle [275]. The T_g values of the photocross-linked films with the fragments of RDs estimated by DSC were in the range of 20-68 °C while the T_g of polymer **Neat1** was 33 °C (Table 3.4). These T_g values were determined as the middle point of the transitions which appeared as a small step in DSC curves (Fig. 3.5a). The more appropriate DMTA method to define T_g with a clearly visible maximum peak of tanδ curves (Fig 3.5b) was also applied.

58
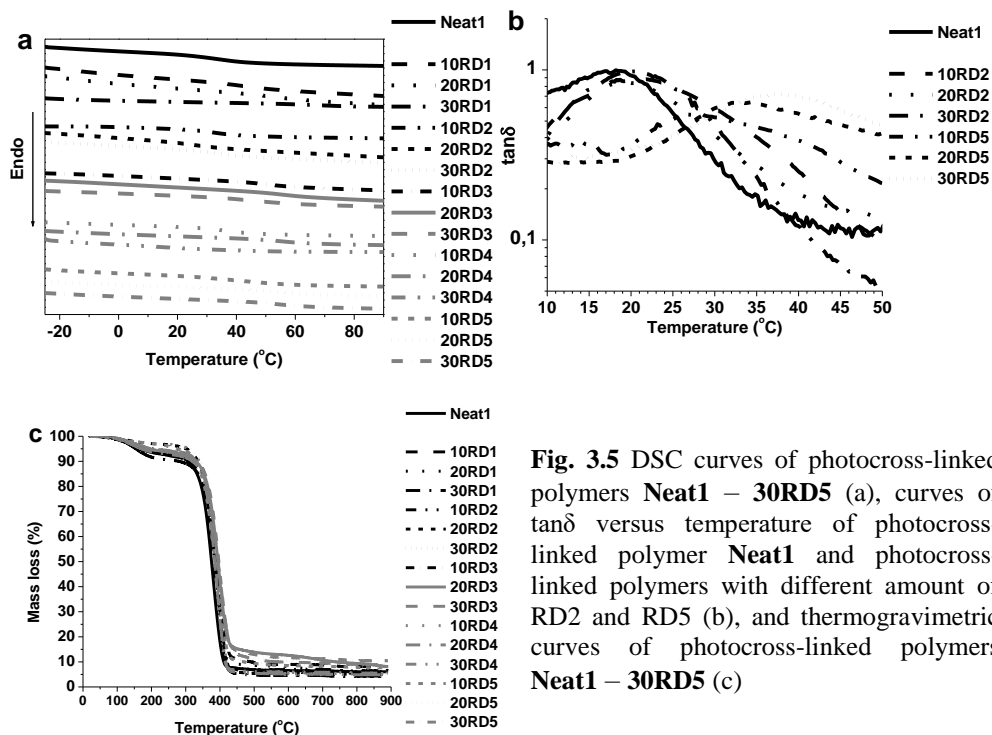
Fig. 3.5 DSC curves of photocross-linked polymers **Neat1** – **30RD5** (a), curves of tanδ versus temperature of photocross-linked polymer **Neat1** and photocross-linked polymers with different amount of RD2 and RD5 (b), and thermogravimetric curves of photocross-linked polymers **Neat1** – **30RD5** (c)

The T_g values estimated by DMTA were different than those obtained by DSC apparently because of the oscillating frequency effect in DMTA and the different heating rates used in both methods. The frequency effect changes molecular relaxations of polymer chains and provides different glass transition behavior [276]. The T_g values of the photocross-linked films with the fragments of RDs estimated by DMTA were in the range of 20-45 °C while the T_g of polymer **Neat1** was 18 °C (Table 3.4). The higher T_g values were observed for the polymers **10** – **30RD1** with the fragments of aliphatic RD1 (35-43 °C) and for the polymers **10** – **30RD3** (29-45 °C), **10** – **30RD5** (27-37 °C) with the fragmets of aromatic RDs due to higher yields of insoluble fraction (Table 3.3) and the higher amount of cross-linked moieties which restricted rotational motions and raised the T_g. These T_g values were lower than the commercial SL5170, SU8 2000 and SOMOS® brand materials based on ERs obtained by stereolithography (SLA) (53-210 °C) [229-233], but comparable to SOMOS® NeXt and SOMOS® WaterShed XC 11122 (43-47 °C) [232]. The photocross-linked polymer **30RD3** with the 30 mol.% of RD3 (DGEBA) exhibited the highest T_g = 45 °C. No clear dependence of the T_g on the amount of the RD was observed.

The cross-linked polymers **Neat1** – **30RD5** exhibited high thermal stability. Thermal decomposition temperatures at the 10 % weight loss ($T_{dec-10\%}$) of the photocross-linked films with the fragments of RDs ranged from 316 °C to 345 °C, while the $T_{dec-10\%}$ of polymer **Neat1** was 308 °C (Table 3.4), and were higher comparing to those of the photocross-linked polymers of epoxidized linseed oil with analogical RDs (300-325 °C) [196]. The photocross-linked polymer **20RD5** with the

20 mol.% of bisphenol F diglycidyl ether exhibited the highest $T_{dec-10\%} = 345$ °C. No clear dependence of the $T_{dec-10\%}$ on the amount of the RD was observed. Thermal decomposition of all polymers proceeded in one step (Fig. 3.5c). The residue yield after thermal degradation of the photocross-linked films with the fragments of RDs ranged from 4.9 % to 10.4 % while the residue yield of polymer **Neat1** was 6.1 % (Table 3.4). The residue yields of above 6.1 % were observed for the polymers **10 – 30RD3** and **10 – 30RD5** with the fragments of aromatic RDs having the highest cross-linking densities. The lower residue yields of 4.9-5.6 % were observed for the polymers **10 – 30RD1, 20 – 30RD2**, and **10 – 30RD4** due to the aliphatic structure of RDs.

3.1.2. Mechanical properties

The mechanical characterization of the prepared materials is indispensable in designing their future applications. Thus, the mechanical characteristics of the photocross-linked polymer **Neat1 – 30RD5** films estimated by tensile test are summarized in Fig. 3.6. In most cases, fragments of RD improved mechanical properties of GDGE resin. The addition of RDs in the compositions increased the elongation at break which ranged from 3.3 % to 8.3 % while the elongation at break of polymer **Neat1** was 0.4 %. These values were similar to those of epoxidized linseed oil polymers with analogical RDs tested with the same tensile test method (1.29-6.27 %) [196] and comparable to the commercial acrylate material PR48 obtained by SLA technology (3-5 %) [228] and SL5170, SU8 2000, and SOMOS® brand materials based on ERs (1.4-25.0 %) [229-233]. This observation showed that polymers **Neat1 – 30RD5** have the similar ductility as epoxidized linseed oil polymers and commercial acrylate and epoxy based materials obtained by SLA technology. Tensile strength of polymer **Neat1** was 11.0 MPa. Fragments of RD2 and RD4 decreased the tensile strength which was in the range of 4.4-7.9 MPa. The polymers with the fragments of RD1, RD3, RD5 exhibited higher tensile strength (11.5-21.7 MPa) due to the higher amount of cross-linked moieties which restricted the motion of the chains and increased the strength of polymer. These values were slightly higher than those of epoxidized linseed oil polymers with analogical RDs (0.67-6.21 MPa) [196] and were comparable to the commercial acrylate material PR8 (16-28 MPa) [228], but lower than commercial SL5170, SU8 2000, and SOMOS® brand materials (30.0-68.1 MPa) [229-233]. Polymer **Neat1** exhibited Young's modulus of 10.8 MPa while the addition of RDs increased Young's modulus (27-88 MPa). However, commercial acrylate material PR8 has higher values of 600-1400 MPa and commercial SL5170, SU8 2000, and SOMOS® brand materials have much more higher Young's modulus of 1227-11700 MPa [229-233]. The photocross-linked polymer **30RD5** having the fragments of aromatic RD5 (bisphenol F diglycidyl ether) exhibited the highest Young's modulus (88 MPa), while polymer **30RD1** having fragments of aliphatic RD1 (CAE) had a similar Young's modulus (74 MPa). The Young's modulus increased with an increase of the amount of the fragments of RD in the polymer structure in all cases. However, no clear dependence of RD amount on elongation at break and tensile strength was observed.
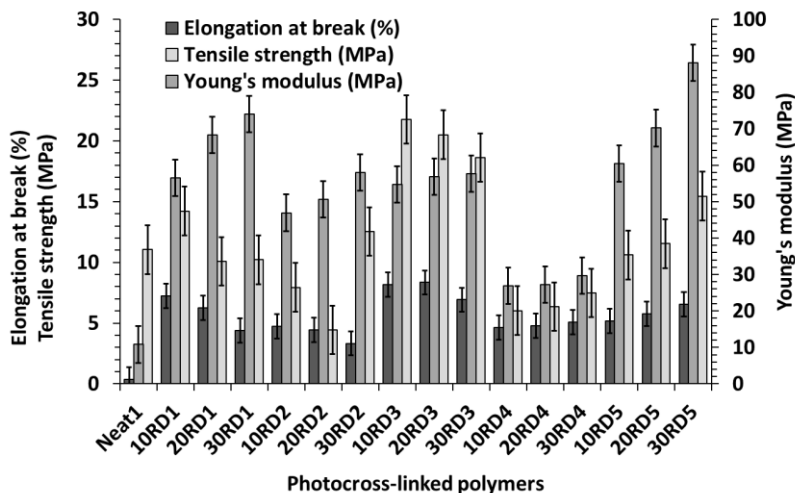
Fig. 3.6 Mechanical characteristics of the photocross-linked polymers **Neat1** – **30RD5**

3.1.3. Thermomechanical properties

The photocross-linked polymers were characterized by DMTA in order to evaluate their viscoelastic properties. The changes of rigidity (G' modulus) when temperature was increased are summarized in Fig. 3.7.
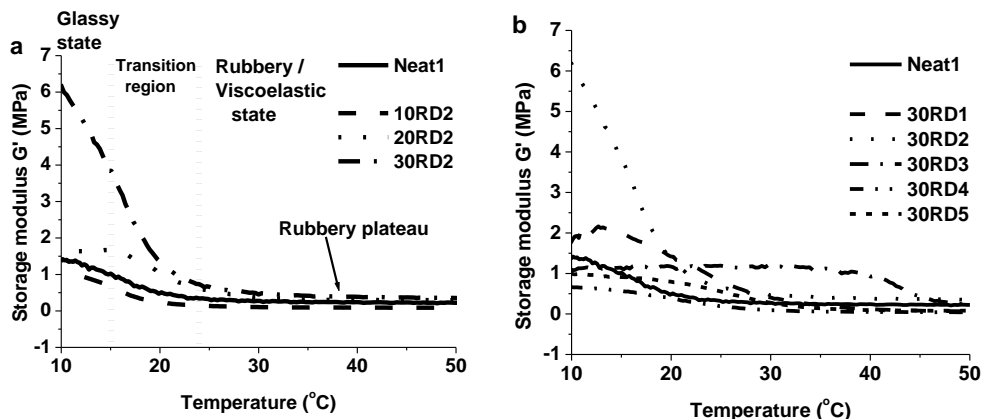
Fig. 3.7 Curves of storage modulus G' versus temperature of the photocross-linked polymer **Neat1** without RD and of the following photocross-linked polymers: polymers **10** – **30RD2** with the different concentrations of RD2 (a) and polymers containing 30 mol.% of different RDs (b)

At low temperatures (from 10 to 15 ℃) below the T_g, the movement of molecular chain segment was restricted [277] and was unable to resonate with the oscillatory loads and polymers remained rigid and brittle (Fig. 3.7a). The polymers were in the glassy or elastic state. G' modulus started to decrease as the molecules gained more free volume resulting in more molecular motions when temperature increased [278]. The glassy state changed into the rubbery/viscoelastic state (15-23

61

ºC). The polymers transited to the rubbery/viscoelastic state (23-50 ºC) and were soft and rubbery. This region had a clearly visible rubbery plateau with relatively stable G' modulus. The appearance of a rubbery plateau is the result of cross-linking [279]. The photocross-linked polymers with 30 mol. % of RDs exhibited a rubbery plateau at different temperatures depending on cross-linking density (Fig. 3.7b). The polymer **30RD3** with the 30 mol.% of RD3 (DGEBA) exhibited a rubbery plateau at 45 ºC due to the highest cross-linking density (Table 3.3).

The G' modulus of the photocross-linked polymers **Neat1** – **30RD5** at different temperatures is summarized in Table 3.5. The G' modulus in the glassy state (at 10 ºC) of the polymers with the fragments of RDs were in the range of 0.27-6.00 MPa while the G' modulus of polymer **Neat1** was 1.42 MPa. At room temperature (20 ºC), the G' modulus decreased greatly. Polymer **Neat1** had G' modulus of 0.51 MPa and polymers with the fragments of RDs had G' modulus of 0.25-1.36 MPa. In the rubbery (viscoelastic) state (at 50 ºC) polymers with the fragments of RDs were soft and rubbery with G' modulus of 0.04-0.65 MPa while the G' modulus of polymer **Neat1** was 0.22 MPa. At 50 ºC, the polymer **30RD1** containing the fragments of RD1 (CAE) had the highest G' modulus (0.65 MPa) due to the high cross-linking density and obtained high G' modulus during real time photorheometry. The G' modulus was higher in most cases when the amount of RD was increased in composition.

Table 3.5 Storage modulus G' of the photocross-linked polymers **Neat1** – **30RD5** in the glassy state (at 10 ºC), at 20 ºC, and rubbery (viscoelastic) state (at 50 ºC)

Photocross-linked polymer	Storage modulus G' (MPa) at temperature of		
	10 ºC (glassy state)	20 ºC	50 ºC (rubbery (viscoelastic) state)
Neat1	1.42	0.51	0.22
10RD1	0.27	0.25	0.06
20RD1	0.54	0.53	0.23
30RD1	1.47	1.20	0.65
10RD2	1.00	0.23	0.09
20RD2	1.85	1.04	0.29
30RD2	6.00	1.36	0.36
10RD3	0.70	0.46	0.10
20RD3	0.74	0.50	0.15
30RD3	1.17	1.08	0.23
10RD4	0.35	0.28	0.07
20RD4	0.62	0.43	0.09
30RD4	0.67	0.38	0.04
10RD5	0.44	0.48	0.11
20RD5	0.60	0.43	0.09
30RD5	1.00	0.79	0.08

3.1.4. Swelling properties

Swelling is an important parameter of polymer for their potential application in industry. Swelling experiments were carried out at room temperature (18 °C) to

evaluate the swelling capacity in polar and non-polar solvents of the photocross-linked polymers **Neat1** – **30RD5**. The swelling degree curves versus time of photocross-linked polymers with 30 mol.% of RDs in water, chloroform, and toluene are shown in Fig. 3.8. The swelling equilibrium was reached after 1.5-2.5 h in water and toluene, and after 1.5-2.0 h in chloroform. Swelling degree values in distilled water, chloroform, and toluene after 4 hours (swelling equilibrium) are listed in Table 3.6. Swelling degree values of polymer films in water and toluene were very low probably due to the poor polymer-solvent interaction. The highest swelling degree observed after 4 h in water was 6.6 % and that in toluene was 5.2 %. Much higher swelling degree values were observed in chloroform. The highest swelling degree obtained in chloroform was 41.8 %. Swelling degree values of the photocross-linked polymer films with the fragments of RDs estimated in water were in the range of 0.9-6.6 % while the swelling degree of polymer **Neat1** was 6.0 %. Only the polymer **10RD3** with the 10 mol.% of RD3 (DGEBA) exhibited the similar swelling degree in water to commercial SU8 2000 and SOMOS® brand materials based on ERs (0.35-0.75 %) [230, 231]. Polymer **Neat1** exhibited swelling degree of 39.6 % in chloroform, while swelling degree values of the polymers with the fragments of RDs ranged from 26.1 % to 41.8 %. The addition of RDs increased the swelling degree in toluene (1.2-5.2 %) as swelling degree of polymer **Neat1** was 1.1 %. Almost all polymers with the fragments of the saturated RDs swallowed up more due to more flexible macromolecular chains than the polymers with the fragments of aromatic RDs. The swelling degree increased with an increase of the amount of the fragments of RD in the polymer structure. This observation can be explained by the formation of the longer chains between the cross-linking points of the network when the higher amount of the RD was used.
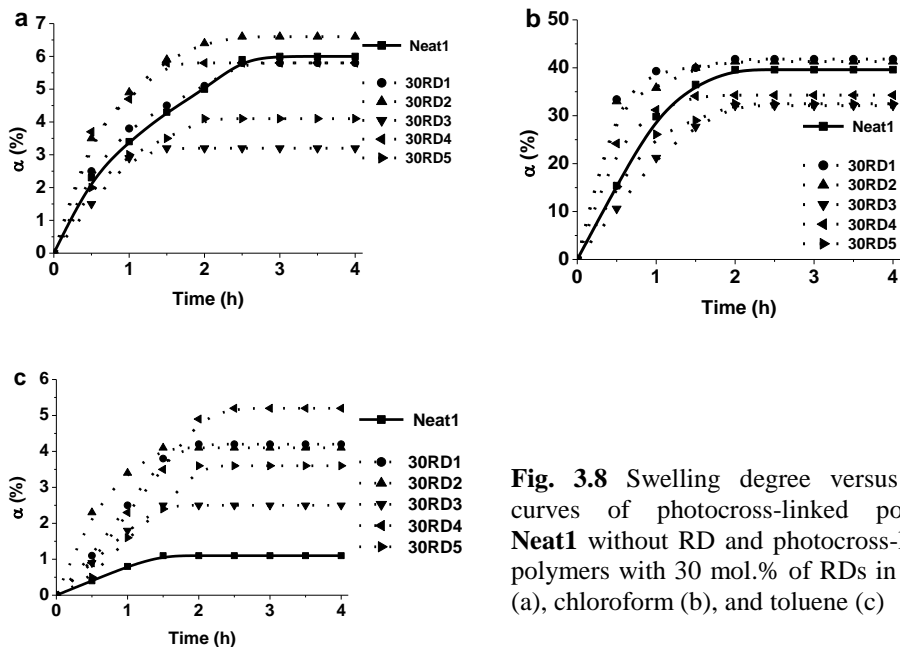
Fig. 3.8 Swelling degree versus time curves of photocross-linked polymer **Neat1** without RD and photocross-linked polymers with 30 mol.% of RDs in water (a), chloroform (b), and toluene (c)

Table 3.6 Swelling degree α of photocross-linked polymers **Neat1** – **30RT5** in distilled water, chloroform, and toluene at room temperature (18 °C) after 4 hours

Photocross-linked polymer	Swelling degree α (%) in		
	distilled water	chloroform	toluene
Neat1	6.0	39.6	1.1
10RD1	4.1	26.1	1.6
20RD1	5.0	31.4	4.1
30RD1	5.8	41.8	4.2
10RD2	4.5	35.7	2.5
20RD2	4.6	41.2	2.6
30RD2	6.6	41.3	4.1
10RD3	0.9	30.7	1.2
20RD3	1.4	31.8	2.0
30RD3	3.2	32.1	2.5
10RD4	4.4	31.2	2.8
20RD4	4.9	33.1	3.6
30RD4	5.8	34.3	5.2
10RD5	1.2	28.2	1.8
20RD5	2.6	30.9	2.4
30RD5	4.1	32.5	3.6

3.1.5. Biodegradability

In order to evaluate the biodegradability of the photocross-linked polymers **Neat1** – **30RD5**, the soil burial test was performed in a period of 3 months. Mass losses of the photocross-linked polymers observed in the period of 1-3 months are shown in Fig. 3.9. The most of the mass was lost during the first month compared to the other 2 months. Mass losses of the photocross-linked films with the fragments of RDs after 3 months ranged from 3.9 % to 8.3 % while the mass loss of polymer **Neat1** was 3.1 %. This observation showed that the fragments of RDs increased the biodegradability of GDGE. No clear dependence of RD amount on mass loss was observed. Mass losses of the polymers with the fragments of RDs and different amounts of them varies since the biodegradability in the burial tests depended not only on chemical structure of a specimen but also on the microorganisms present in the soil. The highest mass loss (8.3 %) was observed for the polymer **20RD1** containing the fragments of RD1 (CAE). Despite of the presence of two aromatic rings, the mass losses of the photocross-linked polymers containing fragments of aromatic RD3 and RD5 was higher in comparison with polymer **Neat1**. The previous studies showed that fungi species such as *Pycnoporus sanguineus* and *Trametes versicolor* can degrade bisphenol A [280]. Bisphenol F can be degraded by fungi species such as *Sphingobium yanoikuyae* [281].
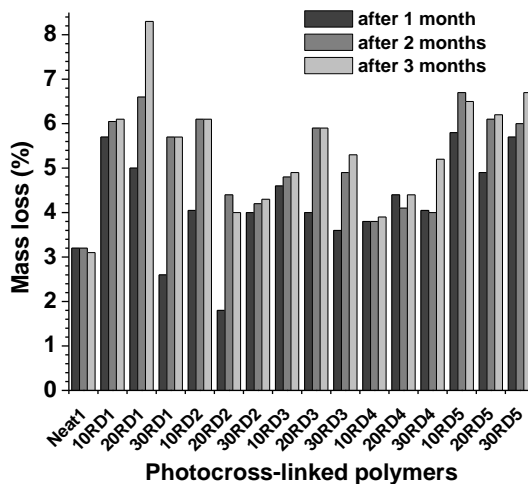
Fig. 3.9 Mass loss of the photocross-linked polymers **Neat1 – 30RD5** after 1-3 months exposition in soil

3.2. Biodegradable photocross-linked polymers of glycerol diglycidyl ether and di- or trihydroxyl compounds

The photocross-linked polymers **Neat2 – 30A4** were synthesized by the reaction of GDGE with different molar amount (10 mol.%, 20 mol.%, and 30 mol.%) of structurally different di- or trihydroxyl compounds under UV/Vis light, using 3 mol% of triarylsulfonium hexafluorophosphate salts as CPI (see Table 2.2) in order to evaluate the effect of their chemical structure and amount on the photocross-linking of GDGE and on the properties of the resulting polymers. The obtained photocross-linked polymeric films of GDGE and di- or trihydroxyl compounds (thickness of 300 ± 60 μm) were transparent and smooth.

The characteristic groups of the photocross-linked polymers were identified by FT-IR spectroscopy:

IR (cm^{-1}) of photocross-linked polymer **Neat2**: 3430 (ν O–H), 2919 (ν CH$_2$ aliph.), 2870 (ν C–H aliph.), 1074 (ν C–O–C).

IR (cm^{-1}) of photocross-linked polymers **10 – 30A1**: 3457–3421 (ν O–H), 2913–2911(ν CH$_2$ aliph.), 2867–28764 (ν C–H aliph.), 1085-1084 (ν C–O–C).

IR (cm^{-1}) of photocross-linked polymers **10 – 30A2**: 3439–3397 (ν O–H), 2913–2911 (ν CH$_2$ aliph.), 2870–2869 (ν C–H aliph.), 1086-1084 (ν C–O–C).

IR (cm^{-1}) of photocross-linked polymers **10 – 30A3**: 3398–3378 (ν O–H), 3041-3039 (ν CH$_2$ ar.), 2913–2911 (ν CH$_2$ aliph.), 2872–2869 (ν C–H aliph.), 1512–1511 (ν C=C ar.), 1085-1084 (ν C–O–C).

IR (cm^{-1}) of photocross-linked polymers **10 – 30A4**: 3426–3376 (ν O–H), 3042-3040 (ν CH$_2$ ar.), 2913–2911 (ν CH$_2$ aliph.), 2869–2868 (ν C–H aliph.), 1512 (ν C=C ar.), 1089-1086 (ν C–O–C).

Absorption band of OH groups at (3347-3258) cm^{-1} which was present in the FT-IR spectra of di- or trihydroxyl compounds and absorbtion band of epoxy group

which was present at 985 cm^{-1} in the FT-IR spectrum of GDGE decreased in the FT-IR spectra of all polymers **10A1** – **30A4**. The increase of intensity of C–O–C group in the FT-IR spectra of all photocross-linked polymers was determined. For the illustration of this statement, the FT-IR spectra of GDGE, A1, and the photocross-linked polymer **10A1** are presented in Fig. 3.10.
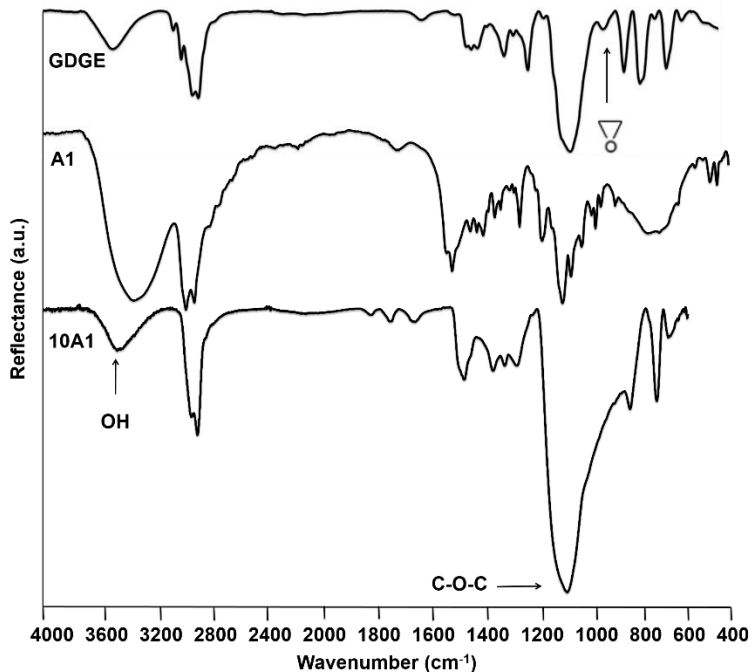
Fig. 3.10 FT-IR spectra of glycerol diglycidyl ether, 1,4-cyclohexanedimethanol, and the photocross-linked polymer **10A1**

The rheological changes of the compositions **Neat2** – **30A4** were monitored by real time photorheometry. The results showed that the addition of di- or trihydroxyl compounds into the compositions accelerated photocross-linking of GDGE as t$_{gel}$ was reached much more faster (Table 3.7). The lower amout of di- or trihydroxyl compound was used in the composition, the t$_{gel}$ was reached faster and the higher G', G", and ŋ* values (Table 3.7) were observed in all cases.

Table 3.7 Real time photorheometry data of photocross-linked polymers **Neat2** – **30A4**

Photocross-linked polymer	Storage modulus G' (MPa)	Loss modulus G'' (MPa)	Complex viscosity η* (MPa·s)	Gel point t_{gel} (min)
Neat2	6.04	0.11	0.96	3.84
10A1	8.21	0.30	1.31	1.50
20A1	7.26	0.20	1.16	1.80
30A1	4.46	0.05	0.71	1.88
10A2	7.01	0.12	1.12	1.60
20A2	5.18	0.04	0.82	1.90
30A2	4.74	0.039	0.76	2.30
10A3	15.40	10.20	2.94	2.29
20A3	7.39	0.32	1.18	2.45
30A3	5.56	0.14	0.89	2.60
10A4	6.45	1.45	1.04	2.10
20A4	5.53	1.18	0.90	2.70
30A4	3.63	0.05	0.58	3.00

The decrease of di- or trihydroxyl compound in the composition amount led to the increase of effective proton concentration, thus accelerated photocross-linking of GDGE and contributed to the formation of the more rigid network. The t_{gel} of the compositions with the diols A3 and A4 was reached later compared to the compositions with the diol A1 or triol A2 due to the lower reactivity. The most rigid photocross-linked polymer **10A3** with the highest G' modulus of 15.40 MPa was obtained due to the highest cross-linking density of 6258 mol/m³ (Table 3.8).

The photocross-linking of GDGE was the fastest (t_{gel} = 1.50 min) when 10 mol.% of A1 was used (Fig. 3.11a). After an induction period (1.49 min), G', G'', η* increased indicating growth of chains and network formation in the initial stage of photocross-linking (1.49-2.50 min). G' increased faster and exceeded G'' (1.50 min) while tanδ started to decrease in the intermediate stage. During the late stage, G', G'', and η* continued to increase with time due to gel aging and settled down into steady-state (plateau) indicating the end of the gelation process. All the photocross-linked polymers **Neat2** – **30A4** showed the same tendencies. As G' modulus characterizes the rigidity of polymer, the G' modulus curves versus irradiation time of the photocross-linked polymers with the diferent amount of A1 and same 10 mol.% amount of different di- or trihydroxyl compounds are presented in Fig. 3.11b and c. The induction period of photocross-linking of the composition **Neat2** was significantly longer and the reaction rate was lower in comparison with those of compositions containing di- or trihydroxyl compounds. This observation showed that the addition of di- or trihydroxyl compound into the composition can shorten the induction period and accelerate photocross-linking of GDGE due to the faster epoxy ring opening via AM mechanism in comparison to conventional epoxy ring opening via ACE mechanism [200].
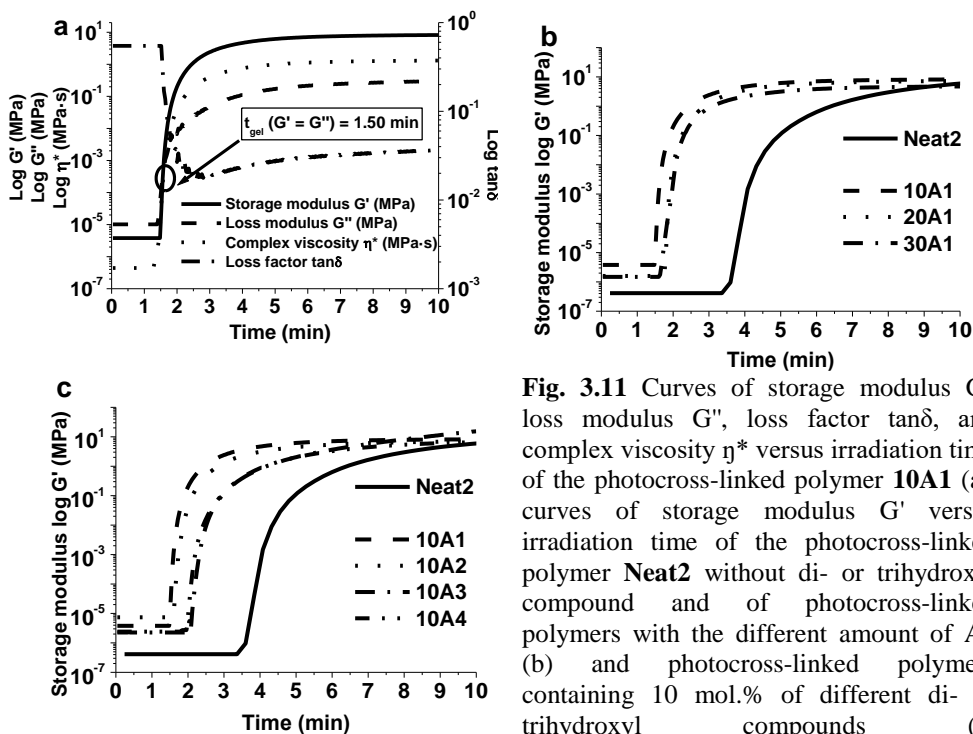
Fig. 3.11 Curves of storage modulus G', loss modulus G'', loss factor tanδ, and complex viscosity η* versus irradiation time of the photocross-linked polymer **10A1** (a), curves of storage modulus G' versus irradiation time of the photocross-linked polymer **Neat2** without di- or trihydroxyl compound and of photocross-linked polymers with the different amount of A1 (b) and photocross-linked polymers containing 10 mol.% of different di- or trihydroxyl compounds (c)

The photocross-linked polymers obtained from GDGE and di- or trihydroxyl compounds were insoluble in all common organic solvents. In order to evaluate the formation of cross-linked structure, Soxhlet extraction was performed and cross-linking densities were calculated according to the theory of rubber elasticity. The yields of insoluble fraction of the photocross-linked films with the fragments of di- or trihydroxyl compounds were in the range of 85-99 % after the extraction with chloroform for 24 h, while the yield of insoluble fraction of polymer **Neat2** was 99 % (Table 3.8), and were similar to those described for photocross-linked polymers of DGEBA (95-98 %) [207]. The cross-linking densities of the photocross-linked films with the fragments of di- or trihydroxyl compounds ranged from 1475 mol/m^3 to 6258 mol/m^3 while the cross-linkind density of polymer **Neat2** was 2454 mol/m^3. These values showed that both GDGE and di- or trihydroxyl compound participated in the formation of the cross-linked structure. The yield of insoluble fraction of polymer **Neat2** (99 %) in most cases was higher than that of photocross-linked polymers containing di- or trihydroxyl compound fragments, except for the polymers **10A1** and **10A2** with 10 mol.% of fragments of diol A1 and triol A2 (99 %). This can be explained by the plasticization effect due to the flexible structure of A1 and A2 resulting in an increase of the reactive species mobility [207]. The yields of insoluble fraction of the photocross-linked polymers **10A1** – **30A2** having fragments of diol A1 and triol A2 were slightly higher (96-99 %) than those of photocross-linked polymers **10A3** – **30A4** bearing rigid aromatic fragments of diols A3 and A4 (85-94 %). Aromatic hydroxyl compounds have lower pK$_a$ (are acidic)

and are less nucleophilic and less reactive, therefore produce lower conversion of epoxy groups [211] resulting to the lower insoluble fraction of obtained polymer. Bisphenol A (A4) with $pK_a = 9.6$ [282] decreased the yields of insoluble fraction of polymers (85-94 %) more in comparision to hydroquinone (A3) with $pK_a = 10.35$ [283] (91-94 %). The highest cross-linking density was observed for the photocross-linked polymer **30A3** when the 30 mol.% of A3 was used. Three hydroxyl groups of A2 had no influence on insoluble fraction and cross-linking as compared to the diol A1 with two hydroxyl groups. By increasing the amount of di- or trihydroxyl compound, the yield of insoluble fraction and cross-linking density decreased in all cases. This suggests that an AM mechanism took place during the propagation step of the ring opening polymerization of GDGE by di- or trihydroxyl compounds which resulted in a large amount of nucleophilic hydroxyl groups released and competing with protonation of epoxy ring, decreasing the amount of reactive oxirane cationic groups formed by photoacid addition [207]. The concentration of released protons was a limiting factor for photopolymerization [206].

Table 3.8 Yields of insoluble fraction and cross-linking densities of photocross-linked polymers **Neat2** – **30A4**

Photocross-linked polymer	Yield of insoluble fraction Y (%)	Cross-linking density N (mol/m^3)
Neat2	99	2454
10A1	99	3336
20A1	97	2950
30A1	96	1812
10A2	99	2849
20A2	97	2105
30A2	96	1926
10A3	94	6258
20A3	92	3003
30A3	91	2259
10A4	94	2621
20A4	88	2247
30A4	85	1475

3.2.1. Thermal properties

Thermal characteristics of the photocross-linked polymers **Neat2** – **30A4** investigated by DSC, DMTA, and TGA are summarized in Table 3.9. DSC and DMTA analysis were performed to determine T_g of photocross-linked polymers. The T_g values of the photocross-linked films with the fragments of di- or trihydroxyl compounds estimated by DSC were in the range of 6-22 °C while the T_g of polymer **Neat2** was 8 °C. These T_g values were determined as the middle point of the transitions which appeared as a small step in DSC curves (Fig. 3.12a), the more appropriate DMTA method to define T_g with a clearly visible maximum peak of tanδ curves (Fig 3.12b) was also applied. The T_g values of the photocross-linked films with the fragments of di- or trihydroxyl compounds estimated by DMTA were in the range of 0-18 °C while the T_g of polymer **Neat2** was 13 °C. The obtained T_g

values were lower compared with SL5170, SU8 2000 and SOMOS® brand materials based on ERs printed by SLA (43-210 °C) [229-233]. The T_g values lower than 13 °C were observed for the polymers **10 – 30A1** and **10 – 30A2** with the the fragments of diol A1 and triol A2 which acted as plasticizers [201] and increased free volume between chains resulting in easy movement and rotation of chain segments resulting in decreased T_g values. The higher than 13 °C T_g values were observed for the polymers **10 – 20A3** and **10 – 30A4** with the aromatic fragments of diols A3 and A4 which restricted rotational motions and raised the T_g. The photocross-linked polymers **10A3** and **10A4** with the 10 mol.% of A3 and A4 exhibited the highest T_g = 18 °C. By increasing the amount of di- or trihydroxyl compound, the T_g was shifted towards lower values due to obtained lower cross-linking density.

TGA was used to study thermal stability of the photocross-linked polymers. The $T_{dec-10\%}$ values of the photocross-linked polymers **Neat2 – 30A4** with the fragments of di- or trihydroxyl compounds ranged from 270 °C to 343 °C while the $T_{dec-10\%}$ of polymer **Neat2** was 338 °C (Table 3.9). The photocross-linked polymer **10A1** with the 10 mol.% of diol A1 exhibited the highest $T_{dec-10\%}$ = 343 °C. The termal stability of polymers increased with a decrease of di- or trihydroxyl compound amount in the composition due to higher T_g and better cross-linking by AM mechanism. Thermal decomposition of all polymers proceeded in one step. As an example, thermogravimetric curves of photocross-linked polymers with the fragments of A1 are shown in Fig 3.12c. The residue yield after thermal degradation of the photocross-linked films ranged from 2.4 % to 7.9 % while the residue yield of polymer **Neat2** was 5.6 % (Table 3.9). The residue yield of above 5.6 % were observed for the polymers **10 – 30A3** and **10 – 30A4** having rigid fragments of the diols A3 and A4. The lower residue yield of 5.6 % were observed for the polymers **10 – 30A1** and **10 – 30A2** due to the aliphatic structure of the diol A1 and triol A2.

Table 3.9 DSC, DMTA and TGA data of photocross-linked polymers **Neat2 – 30A4**

Photocross-linked polymer	Glass transition temperature T_g (°C)		Temperature at the weight loss of 10 % $T_{dec.-10\%}$ (°C)	Residue yield after thermal degradation Res. (%)
	estimated by DSC	estimated by DMTA		
Neat2	8	13	338	5.6
10A1	17	11	343	4.3
20A1	7	8	336	2.4
30A1	6	7	335	3.8
10A2	13	10	342	4.1
20A2	11	5	336	4.3
30A2	9	0	328	4.0
10A3	18	18	312	7.2
20A3	12	16	306	7.3
30A3	10	12	270	7.3
10A4	22	18	305	7.6
20A4	20	17	279	7.9
30A4	18	15	274	7.0
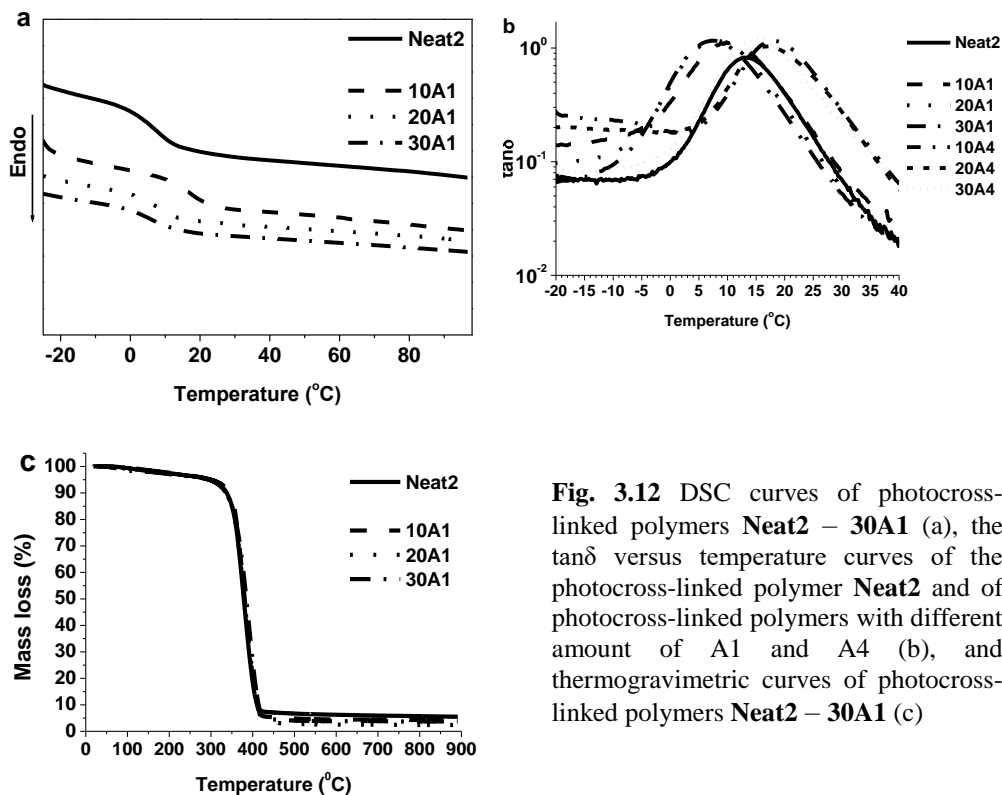
Fig. 3.12 DSC curves of photocross-linked polymers **Neat2** – **30A1** (a), the tanδ versus temperature curves of the photocross-linked polymer **Neat2** and of photocross-linked polymers with different amount of A1 and A4 (b), and thermogravimetric curves of photocross-linked polymers **Neat2** – **30A1** (c)

3.2.2. Mechanical properties

Mechanical characteristics estimated by tensile test of the photocross-linked films **Neat2** – **30A4** are summarized in Fig. 3.13. The addition of di- or trihydroxyl compounds in the most compositions decreased the elongation at break which ranged from 9.2 % to 78.6 % while the elongation at break of polymer **Neat2** was 64.7 %. The polymers **Neat2** – **30A4** have better ductility than commercial acrylate material PR48 (3-5 %) [228], SL5170, SU8 2000, and SOMOS® brand materials based on ERs (1.4-25.0 %) [229-233] printed by SLA. The tensile strength of the photocross-linked films **10A1** – **30A3** were from 6.8 MPa to 12.8 MPa and were lower than those observed for polymer **Neat2** (14.9 MPa). The di- or trihydroxyl compounds acted as plasticizers and decreased the tensile strength [203]. The polymers **10** – **30A4** reached the higher tensile strength of 15.7-22.7 MPa due to the higher amount of cross-linked moieties which restricted the motion of the chains and increased the strength of the polymer. Commercial acrylate material PR8 and SL5170, SU8 2000, and SOMOS® brand materials have higher tensile strength (16-28 MPa, (30.0-68.1 MPa) [228-233], respectively). The Young's modulus of the photocross-linked films with the fragments of di- or trihydroxyl compounds were in the range of 127-468 MPa, while polymer **Neat2** exhibited Young's modulus of 233 MPa, and was lower than Young's modulus of commercial acrylate material PR8 (600-1400 MPa), commercial SL5170, SU8 2000, and SOMOS® brand materials (1227-11700 MPa) [229-233]. The highest Young's modulus were observed for the

71

polymer **10A4** (468 MPa) with the aromatic fragments of the diol A4. By increasing the amount of di- or trihydroxyl compound in the composition, Young's modulus and elongation at break increased in all cases due to higher cross-linking density. However, no dependence of tensile strength on the cross-linking density was observed.
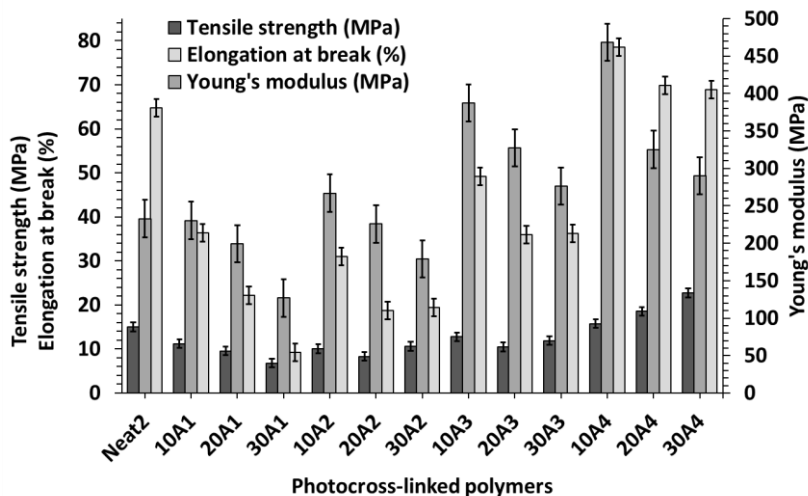
Fig. 3.13 Mechanical characteristics of the photocross-linked polymers **Neat2** – **30A4**

3.2.3. Thermomechanical properties

The changes of rigidity (G' modulus) by raising the temperature are summarized in Fig. 3.14. At lower temperatures below the T_g (0-5 ℃), the movement of molecular chains was restricted [277] and polymers were in the glassy or elastic state and remained rigid and brittle (Fig. 3.14a). When the temperature increased (5-23 ℃), the molecules gained more free volume and G' modulus started to decrease [278]. The polymers transited to the rubbery/viscoelastic state (23-40 ℃) and were soft and rubbery. This region had a clearly visible rubbery plateau with relatively stable G' modulus. The photocross-linked polymers **10A1** and **10A2** with aliphatic fragments exhibited a rubbery plateau at about 20 ℃ while the polymers **10A3** and **10A4** with aromatic fragments exhibited a rubbery plateau at about 30 ℃ depending on cross-linking density (Fig. 3.14b).

The G' modulus values of the photocross-linked polymers **Neat2** – **30A4** at different temperatures are summarized in Table 3.10. The G' modulus in the glassy state (at 0 ℃) of the polymers with the fragments of di- or trihydroxyl compounds were in the range of 0.32-17.92 MPa while the G' modulus of **Neat2** polymer was 5.59 MPa. The G' modulus of polymers increased with decreased amount of the fragments of di- or trihydroxyl compounds which is due to the restrictions in the chain mobility. At room temperature (20 ℃), the G' modulus decreased greatly. Polymer **Neat2** had G' modulus of 0.25 MPa and polymers with the fragments of di- or trihydroxyl compounds had G' modulus of (0.06-0.86) MPa. In the rubbery (viscoelastic) state (at 40 ℃) polymers with the fragments of di- or trihydroxyl compounds were soft and rubbery with G' modulus of (0.06-0.26) MPa while the G'

72

modulus of polymer **Neat2** was 0.18 MPa. At 40 ºC, the polymer **10A4** containing the fragments of A4 had the highest G' modulus (0.26 MPa) due to the high amount of cross-linked moieties.
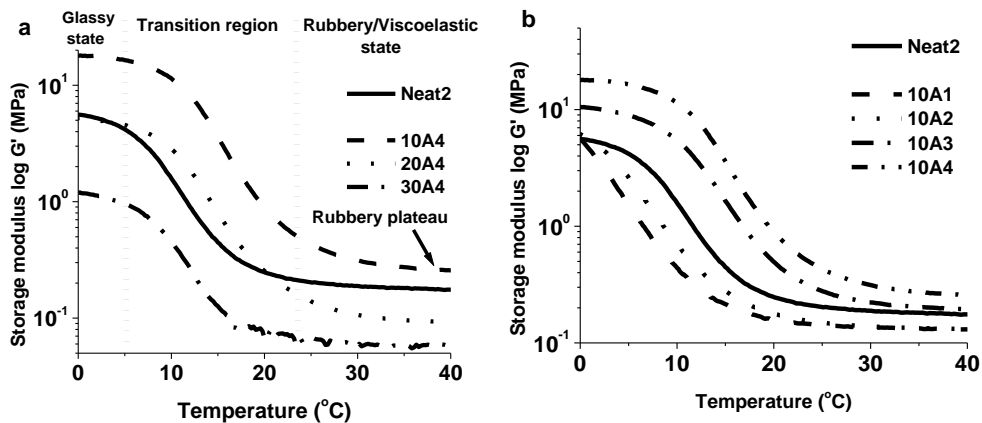
Fig. 3.14 Curves of storage modulus G' versus temperature of the photocross-linked polymer **Neat2** without di- or trihydroxyl compound and of photocross-linked polymers **10 − 30A4** with the different concentrations of A4 (a), and photocross-linked polymers containing 10 mol.% of different di- or trihydroxyl compounds (b)

Table 3.10 Storage modulus G' of the photocross-linked polymers **Neat2** – **30A4** in the glassy state (at 0 ºC), at 20 ºC, and rubbery (viscoelastic) state (at 40 ºC)

Photocross-linked polymer	Storage modulus G' (MPa) at temperature of		
	0 ºC (glassy state)	20 ºC	40 ºC (rubbery (viscoelastic) state)
Neat2	5.59	0.25	0.18
10A1	5.48	0.16	0.13
20A1	4.78	0.16	0.13
30A1	2.79	0.18	0.07
10A2	6.05	0.18	0.13
20A2	3.33	0.17	0.16
30A2	0.32	0.06	0.06
10A3	10.51	0.49	0.19
20A3	6.08	0.26	0.13
30A3	5.90	0.35	0.26
10A4	17.92	0.86	0.26
20A4	5.22	0.26	0.09
30A4	1.20	0.07	0.06

3.2.4. Swelling properties

Polymer swelling is important due to the polymer-solvent compatibility during polymer applications. The swelling degree curves versus time of photocross-linked polymers **10 – 30A1** with different amount of the the fragments of diol A1 (Fig. 3.15a and b) and of polymers with 30 mol.% of different di- or trihydroxyl compounds (Fig. 3.15c and d) in water and chloroform are presented.
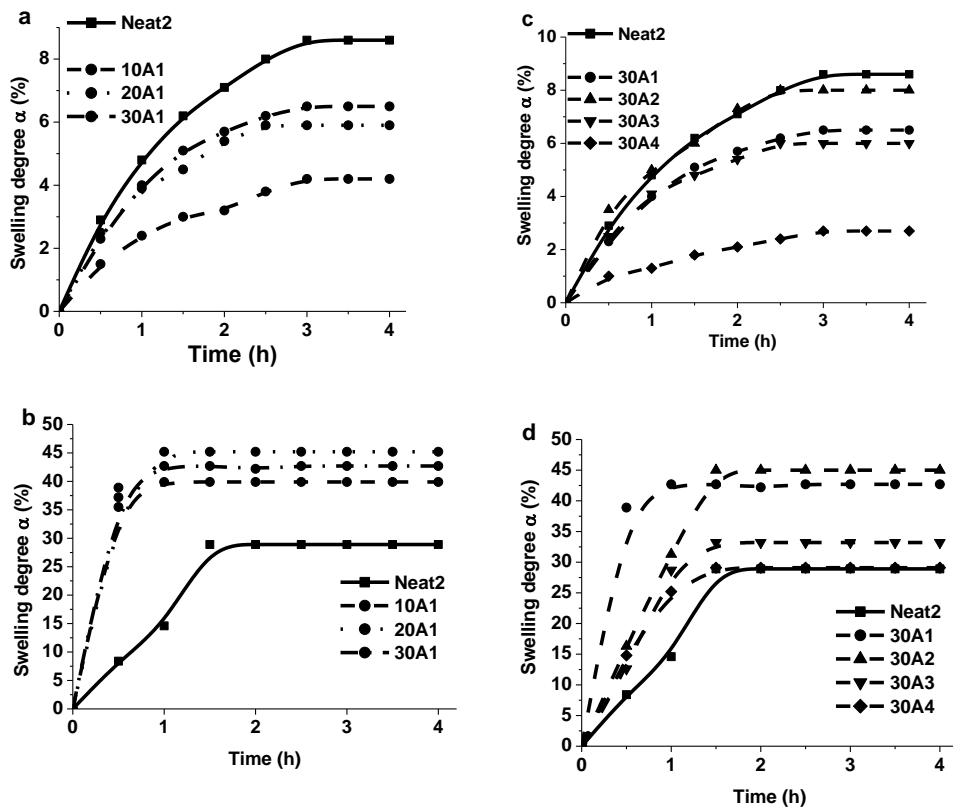
Fig. 3.15 Swelling degree α versus time curves of the photocross-linked polymer **Neat2** without di- or trihydroxyl compound and of photocross-linked polymers **10 − 30A1** with the different concentrations of A1 in water (a), in chloroform (b), and photocross-linked polymers containing 30 mol.% of different di- or trihydroxyl compounds in water (c), in chloroform (d)

The swelling equilibrium was reached after 3.5 h in water and after 2.5 h in chloroform. Swelling degree values in distilled water and chloroform after 4 h (swelling equilibrium) are listed in Table 3.11. The polymers did not swell in toluene for the duration of 4 h probably due to the poor polymer–solvent interaction. Swelling degree values of polymer films in water were very low. The highest swelling degree observed after 4 h in water was 8.6 % for polymer **Neat2**. The addition of di- or trihydroxyl compounds into the compositions lowered the swelling degree, as a result of this the photocross-linked polymers **10A1** – **30A4** exhibited swelling degree values in the range of 1.8-8.0 %. Nevertheless, SU8 2000 and SOMOS® brand materials have lower swelling degree (0.35-0.75 %) [230, 231]. Much higher values were observed in chloroform. The highest swelling degree reached in chloroform was 45.2 % for the polymer **20A1**. The addition of di- or trihydroxyl compounds increased the swelling degree as photocross-linked polymers exhibited values of 23.3-45.2 % while the swelling degree of polymer **Neat2** was 28.9 %. All polymers with the aliphatic fragments swallowed up more due to more

74

flexible macromolecular chains than the polymers with the aromatic fragments. The swelling degree increased with the increase of amount of the fragments of di- or trihydroxyl compound in the polymer structure. This is because polymers which had lower cross-linking density and longer chain length were easy to expand. The swelling degree curves versus time of photocross-linked polymers **10** – **30A1** with different amount of the the fragments of diol A1 (Fig. 3.15a and b) and of polymers with 30 mol.% of different di- or trihydroxyl compounds (Fig. 3.15c and d) in water and chloroform are presented. The swelling equilibrium was reached after 3.5 h in water and after 2.5 h in chloroform.

Table 3.11 Swelling degree α values of photocross-linked polymers **Neat2** – **30A4** in distilled water and chloroform at room temperature (18 $^{\circ}$C) after 4 hours

Photocross-linked polymer	Swelling degree α (%) in	
	distilled water	chloroform
Neat2	8.6	28.9
10A1	4.2	39.9
20A1	5.9	45.2
30A1	6.5	42.7
10A2	6.9	32.9
20A2	7.5	42.8
30A2	8.0	45.0
10A3	3.9	26.9
20A3	5.1	39.9
30A3	6.0	33.2
10A4	1.8	23.3
20A4	2.0	32.2
30A4	2.7	29.1

3.2.5. Biodegradability

Biodegradability of the photocross-linked polymers **Neat2** – **30A4** was determined by soil burial test in 3 months. Mass losses of the photocross-linked polymers observed in the period of 1-3 months are shown in Fig. 3.16. Mass losses of the photocross-linked films with the fragments of di- or trihydroxyl compounds ranged from 3.1 % to 11.0 % after 3 months while the mass loss of polymer **Neat2** was 3.4 %. This observation showed that the addition of di- or trihydroxyl compounds in the most compositions increased the biodegradability of GDGE resin. By increasing the amount of di- or trihydroxyl compound, the mass loss increased in all cases due to lower cross-linking density. Despite of the presence of aromatic rings, the mass loss of the photocross-linked polymers containing fragments of diols A3 (hydroquinone) and A4 (bisphenol A) was higher in comparison with polymer **Neat2**. The highest mass loss (11 %) was observed for the polymer **30A3** containing the fragments of A3 (hydroquinone). Previous studies showed that there are fungi species able to degrade hydroquinone: *Candida parapsilosis*, *Tyromyces palustris*, *Gloeophyllum trabeum*, *Penicillium chrysogenum*, and *Phanerochaete chrysosporium* [284-287]. Bisphenol A can be degradable by fungi species such as *Pycnoporus sanguineus* and *Trametes versicolor* [280].
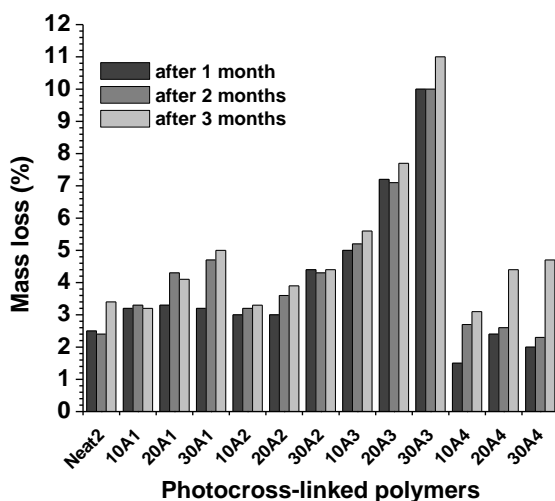
Fig. 3.16 Mass loss of the photocross-linked polymers **Neat2** – **30A4** after 1-3 months exposition in soil

3.3. Application of glycerol diglycidyl ether based compositions in optical 3D printing

Before selecting the composition based on glycerol diglycidyl ether for optical 3D printing experiments, the time when t_{gel} was reached, the rigidity of obtained polymers and their T_g were evaluated. The compositions based on glycerol diglycidyl ether and epoxy reactive diluents reached t_{gel} faster (after 0.50-2.25 min) compared to compositions with di- or trihydroxyl compounds (after 1.50-3.00 min), the obtained polymers had higher rigidity (3.15-154.00 MPa compared with 3.63-15.40 MPa) and higher T_g values (20-45 °C compared with 0-18 °C). The composition **30RD1** was chosen for the LA and selective LA as RD1 (CAE) is known as very reactive compound and displays higher rates of polymerization [186]. Also, the photocross-linked polymer **30RD1** with the fragments of RD1 (CAE) reached high yield of insoluble fraction, cross-linking density, G' modulus (rigidity), T_g, Young's modulus, and biodegradability compared to the polymers with other RDs and some of these values were comparable with the commercial ERs used for stereolithography (SLA). The suitability of the composition **30RD1** containing 30 mol.% of RD1 and 3 mol. % of triarylsulfonium hexafluorophosphate salts as CPI for the 3D printing was investigated by photolithography (LA) and selective LA.

By using LA technology, the commercial resin PR48 was completely polymerized after 2 s of irradiation with UV/Vis light and absorbed 6 mJ·cm^{-2} of irradiance energy dose (E), while the composition **30RD1** hardened after 150 s and absorbed 270 mJ·cm^{-2} of E. The composition **30RD1** required higher energy doses, resulting in prolonged irradiation time. In the selective LA, as the mask formed additional glass layer, more UV/Vis light was absorbed before affecting the compositions resulting in even longer hardening time. For composition **30RD1** hardening time increased to 260 s (396 mJ·cm^{-2}). Despite this, the selectively

polymerized structures were obtained. The experiment showed that the composition **30RD1** can be used in LA technology.

The suitability of the compositions **1BAPO** – **5TPO** containing 30 mol.% of RD1 and different amout of BAPO or TPO as PI for the 3D printing was determined by dynamic projection lithography (DPL). To cross-link the compositions **1BAPO** – **5TPO** with optical printer Ember an increased E and irradation time were required. The best results were obtained when the composition **3BAPO** was used for the photocross-linking. In this case, the composition was cured after $E \approx 16$ $J \cdot cm^{-2}$ and the formed layers were well-defined, continuous, and straight. Using compositions **1BAPO** and **2BAPO** for the photocross-linking, resulted in E dose exceeding 24 $J \cdot cm^{-2}$. Using compositions **4BAPO** and **5BAPO** for the photocross-linking did not make any significant changes in curing time, showing that inhibition of polymerization started using high concentrations of PI. When TPO was used instead of BAPO, no samples were photocross-linked in the range of 16-32 $J \cdot cm^{-2}$ of E dose. After irradation, affected areas looked more transparent than unaffected. All obtained samples were sputtered with a 20-nm gold layer. The quality of photocross-linked layers of various width after different E dose is summarized in Table 3.12. When the lower E of 16-18 $J \cdot cm^{-2}$ was used and the irradation time was 11 min, the layers with width of 50-200 μm were poorly formed and barely adhered to the substrate (Fig. 3.17a). Green rectangles show features, formed perpendicularly to the main layers. By increasing the width until or more than 200 μm, the formed layers were well-defined, continuous, and straight during the whole E range of 16-24 $J \cdot cm^{-2}$ (Fig. 3.17b). By increasing the E until 20-24 $J \cdot cm^{-2}$, the curing time reached 15 min and the formed layers were well-defined, continuous, and straight (Fig. 3.17c, d). Red nets represent pixel arrangement on the polydimethylsiloxane window. In all cases, fully separated layers were obtained when a slit in between them was >200 μm. The experiment showed that the compositions **1** – **5BAPO** can be used in DPL technology.

Table 3.12 Quality of photocross-linked layers of various width after different energy dose irradation [261]

Layers width (μm)	Irradiation dose E ($J \cdot cm^{-2}$)		
	16 to 18	**20**	**24**
50, 100 to 200	Poorly formed layers, barely adhered to the substrate	Well-defined, continuous, and straight layers	
>200	Well-defined, continuous, and straight layers		
Typical height (μm)	100 to 130	190 to 220	250 to 280
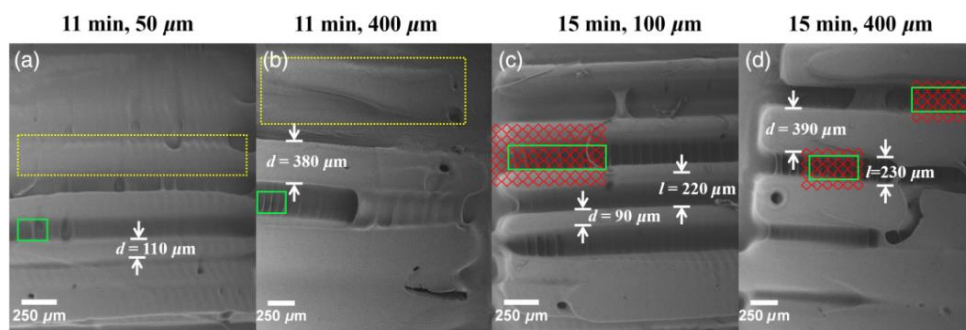
Fig. 3.17 SEM images of the photocross-linked composition **3BAPO** obtained with 3D optical printer by varying irradiation dose: 50 μm, 18 J·cm^{-2} (a); 400 μm, 18 J·cm^{-2} (b); 100 μm, 24 J·cm^{-2} (c); 400 μm, 24 J·cm^{-2} (d) [261]

The suitability of the composition **3BAPO** for the 3D printing was investigated by 3D laser lithography (3DLL). 3D hexagonal structure was formed (Fig. 3.18). The structures exhibited rounded edges and the top of the 3D hexagon was deformed, hinting at shrinkage (indicated with black arrows). After measurement of base of the structure (that should not be deformed, as it is permanently attached to the glass substrate) and the top (that could change its shape easily) it was determined that the sizes are ~200 μm and ~178 μm, respectively resulting in a yielding shrinkage of at least 11%. The experiment showed that the composition **3BAPO** can be used in 3DLL technology.
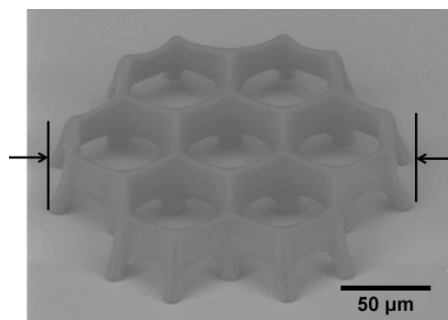
Fig. 3.18 SEM image of 3D structure produced out of composition **3BAPO**

3.4. Biodegradable photocross-linked polymer composites of glycerol diglycidyl ether and industrial waste materials

Three different biobased industrial waste materials (rapeseed cake (RC), phosphogypsum (PG), and horn meal (HM)) were selected for the investigation of the effect of their nature and amount on the photocross-linking of GDGE and on properties of the resulting composites. The photocross-linked polymer composites **5RC** – **20HM** were formed by the mixing of GDGE with different amount (5 wt.%, 10 wt.%, 15 wt.%, and 20 wt.%) of different fillers and curing under UV/Vis light, using 3 mol.% of triarylsulfonium hexafluorophosphate salts (see Table 2.2). Such concentrations of the fillers were chosen taking care not to deteriorate the curing

process and the properties of the UV/Vis cured films and were increased gradually in the compositions. The polymer composite films of GDGE and various biobased industrial waste fillers (thickness 445 ± 85 µm) were obtained. The color of the polymeric composite films depended on the filler used.

Chemical composition of the cross-linked polymer composites was confirmed by FT-IR spectroscopy:

IR (cm^{-1}) of photocross-linked polymer **Neat3**: 3430 (ν O–H), 2919 (ν CH$_2$ aliph.), 2870 (ν C–H aliph.), 1074 (ν C–O–C).

IR (cm^{-1}) of photocross-linked polymer composites **5 – 20RC**: 3443–3419 (ν O–H), 2946–2917 (ν CH$_2$ aliph.), 2874–2870 (ν C–H aliph.), 1729–1725 (ν C=O aliph.), 1078-1071 (ν C–O–C).

IR (cm^{-1}) of photocross-linked polymer composites **5 – 20PG**: 3433–3378 (ν O–H), 2922–2919 (ν CH$_2$ aliph.), 2870–2867 (ν C–H aliph.), 1739–1726 (ν C=O aliph.), 1074-1071 (ν C–O–C).

IR (cm^{-1}) of photocross-linked polymer composites **5 – 20HM**: 3445–3435 (ν O–H), 2917–2915 (ν CH$_2$ aliph.), 2873–2869 (ν C–H aliph.), 1735–1725 (ν C=O aliph.), 1075-1074 (ν C–O–C).

The intensity of the signals of hydroxyl groups, which are present in the FT-IR spectrum of GDGE at 3492 cm^{-1} and in the FT-IR spectra of the fillers at (3405–3293) cm^{-1} decreased considerably in the FT-IR spectra of the cross-linked polymer composites. The spectral range of the epoxy group which was present at 985 cm^{-1} in the FT-IR spectrum of GDGE is absent in the FT-IR spectra of the photocross-linked polymer composites. Also, the intensity of C–O–C group increased in the FT-IR spectra of all photocross-linked polymers. As an example, the FT-IR spectra of GDGE, RC, and the photocross-linked polymer composite **20RC** are presented in Fig. 3.19.
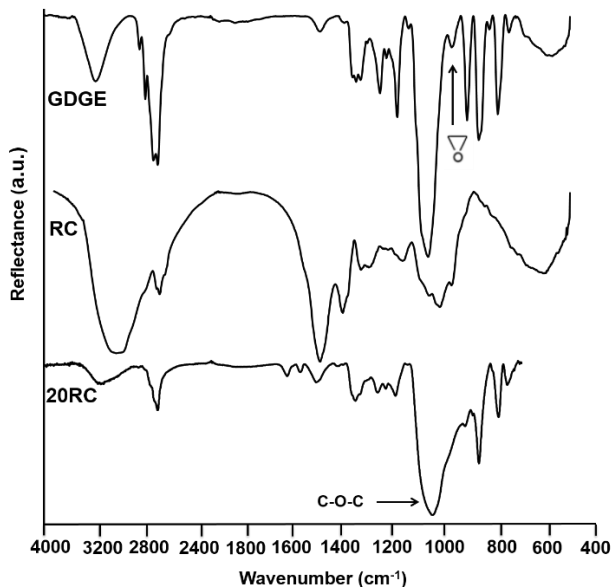
Fig. 3.19 FT-IR spectra of glycerol diglycidyl ether, rapeseed cake, and the photocross-linked polymer composite **20RC**

The rheological changes of the compositions **Neat3** – **20HM** were monitored by real time photorheometry. Photocross-linking was faster and the higher G', G", and η* (Table 3.13) were observed when the higher amount of GDGE was present in the composition. The lower amount of filler was used in the composition, the faster t_{gel} was reached. The most rigid photocross-linked polymer composite **5HM** with the highest G' modulus of 54.80 MPa was obtained due to the highest cross-linking density of 34336 mol/m^3 (Table 3.14). The G' and G" modulus, tanδ, and η* versus irradiation time curves of the photocross-linked polymer composite **5RC** are shown in Fig. 3.20a. After an induction period (1 min) G', G", η* increased indicating growth of chains and network formation in the initial stage of photocross-linking (1-2.5 min). G' increased faster and exceeded G" (1.44 min) while tanδ started to decrease in the intermediate stage. During the late stage, G', G", and η* continued to increase with time due to gel aging and settled down into steady-state (plateau) indicating the end of the gelation process. All the photocross-linked polymer composites **5RC** – **20HM** showed the same behaviour. As G' modulus characterizes the rigidity of the polymer, the G' modulus curves versus irradiation time of the photocross-linked polymer composites with the diferent amount of rapeseed cake and the same amount of 5 wt.% of different fillers are presented in Fig. 3.20b and c. The induction period of photocross-linking of composition **Neat3** was shorter, and the reaction rate was higher in comparison with those of compositions containing fillers. This suggests that the filler particles slowed down the chain mobility of polymeric composite [288]. Incorporation of the different industrial waste fillers into the GDGE based polymer does not have any significant effect on the rate of photocross-linking and the rheological properties of the resulted polymeric composites.

Table 3.13 Real time photorheometry data of photocross-linked polymer **Neat3** and of photocross-linked polymer composites **5RC** – **20HM**

Photocross-linked polymer composite	Storage modulus G' (MPa)	Loss modulus G'' (MPa)	Complex viscosity η* (MPa·s)	Gel point t_{gel} (min)
Neat3	58.30	19.10	9.77	0.92
5RC	21.10	15.08	4.20	1.44
10RC	7.18	0.59	1.15	1.92
15RC	6.65	2.43	1.13	2.40
20RC	0.02	0.01	0.01	3.12
5PG	39.70	15.10	6.76	1.20
10PG	32.60	13.00	5.59	1.44
15PG	17.30	11.20	3.28	1.20
20PG	14.40	4.96	2.42	1.44
5HM	54.80	14.30	9.02	1.44
10HM	48.40	14.00	8.02	1.44
15HM	40.70	13.00	6.81	1.92
20HM	24.90	9.54	4.24	2.15
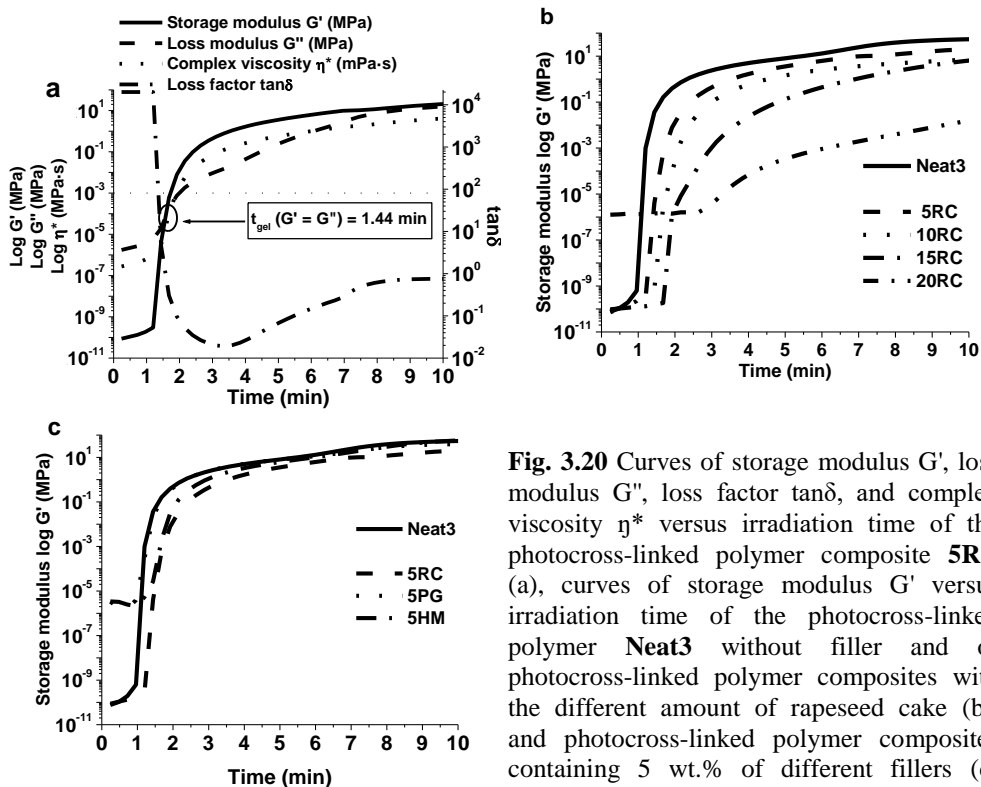
Fig. 3.20 Curves of storage modulus G', loss modulus G", loss factor tanδ, and complex viscosity η* versus irradiation time of the photocross-linked polymer composite **5RC** (a), curves of storage modulus G' versus irradiation time of the photocross-linked polymer **Neat3** without filler and of photocross-linked polymer composites with the different amount of rapeseed cake (b), and photocross-linked polymer composites containing 5 wt.% of different fillers (c)

The photocross-linked polymer composites obtained from GDGE and industrial waste materials as fillers were insoluble in all common organic solvents. The yields of insoluble fraction of the photocross-linked films with the fillers were in the range of 88.8-99.9 % after the extraction with chloroform for 24 h, while the yield of insoluble fraction of polymer **Neat3** was 96.9 % (Table 3.14). The yields of insoluble fraction of the composites containing phosphogypsum **5 – 20PG** were slightly higher than those of composites containing rapeseed cake **5 – 20RC** or horn meal **5 – 20HM**. The higher yield of insoluble fraction was obtained when the lower amount of the waste filler was used in the composition. The cross-linking densities of the photocross-linked polymer films with the fillers ranged from 15685 mol/m^3 to 34336 mol/m^3 while the cross-linking density of polymer **Neat3** was 35596 mol/m^3. By increasing the amount of filler, the cross-linking density decreased in all cases. This suggests that the filler particles may slow down the chain mobility of polymer composite [288]. The highest cross-linking density was obseved for the photocross-linked polymer composite **5HM** when the 5 wt.% of horn meal was used.

Table 3.14 Yields of insoluble fraction and cross-linking densities of the photocross-linked polymer **Neat3** and of photocross-linked polymer composites **5RC** – **20HM**

Photocross-linked polymer composite	Yield of insoluble fraction Y (%)	Cross-linking density N (mol/m^3)
Neat3	96.9	35596
5RC	98.5	26941
10RC	96.9	23081
15RC	90.2	21211
20RC	88.8	15685
5PG	99.9	29420
10PG	99.8	22837
15PG	99.7	22512
20PG	99.6	21293
5HM	98.9	34336
10HM	96.9	26209
15HM	96.1	25234
20HM	95.0	24096

3.4.1. Thermal properties

DSC and DMA data revealed that all the photocross-linked polymer composites were amorphous materials. Only glass transitions were observed in the DSC curves (Fig. 3.21a). The T_g values of the photocross-linked films with fillers estimated by DSC were in the range of 21-38 °C while the T_g of polymer **Neat3** was 36 °C (Table 3.15). The T_g depended on the cross-linking density. The higher T_g was obtained when the lower amount of the waste filler was used in the composition. The T_g values estimated by DMA were found to be slightly diferent relative to those obtained by DSC. The T_g values of the photocross-linked films with fillers estimated by DMA were in the range of 30-44 °C while the T_g of polymer **Neat3** was 40 °C. The higher than 40 °C T_g values were observed for the polymeric composite **20RC** with 20 wt.% of rapeseed cake, **15 – 20PG** with 15 wt.% and 20 wt.% of phosphogypsum, and **20HM** with 20 wt.% of horn meal. Apparently, the filler particles hindered the motion of the polymer chains and increased the T_g values.The DMA curves of composites with rapeseed cake are presented in Fig. 3.21b.

The thermal stability of the photocross-linked polymer composites was investigated by TGA. The $T_{dec.-10\%}$ values of the photocross-linked films with fillers ranged from 302 ºC to 331 ºC while the $T_{dec.-10\%}$ of polymer **Neat3** was 337 °C (Table 3.15) and increased with the increase of yield of insoluble fraction and higher T_g. Thermal decomposition of all polymer composites proceeded in one step (Fig. 3.21c). The residue yield after thermal degradation of the photocross-linked films with fillers ranged from 4.4 % to 15.8 % while the residue yield of polymer **Neat3** was 5.5 % (Table 3.15) and almost in all cases increased with the increase of the filler amount in the composite.

Table 3.15 DSC, DMA, and TGA data of photocross-linked polymer **Neat3** and of photocross-linked polymer composites **5RC** – **20HM**

Photocross-linked polymer composite	Glass transition temperature T_g (°C)		Temperature at the weight loss of 10 % $T_{dec.-10\%}$ (°C)	Residue yield after thermal degradation Res. (%)
	estimated by DSC	estimated by DMA		
Neat3	36	40	337	5.5
5RC	33	41	322	8.5
10RC	28	36	310	10.9
15RC	27	37	306	13.1
20RC	23	36	300	13.4
5PG	38	42	331	6.4
10PG	37	44	324	4.4
15PG	36	35	322	10.8
20PG	35	34	315	10.1
5HM	25	42	317	9.6
10HM	23	32	309	12.5
15HM	22	35	305	14.9
20HM	21	30	302	15.8
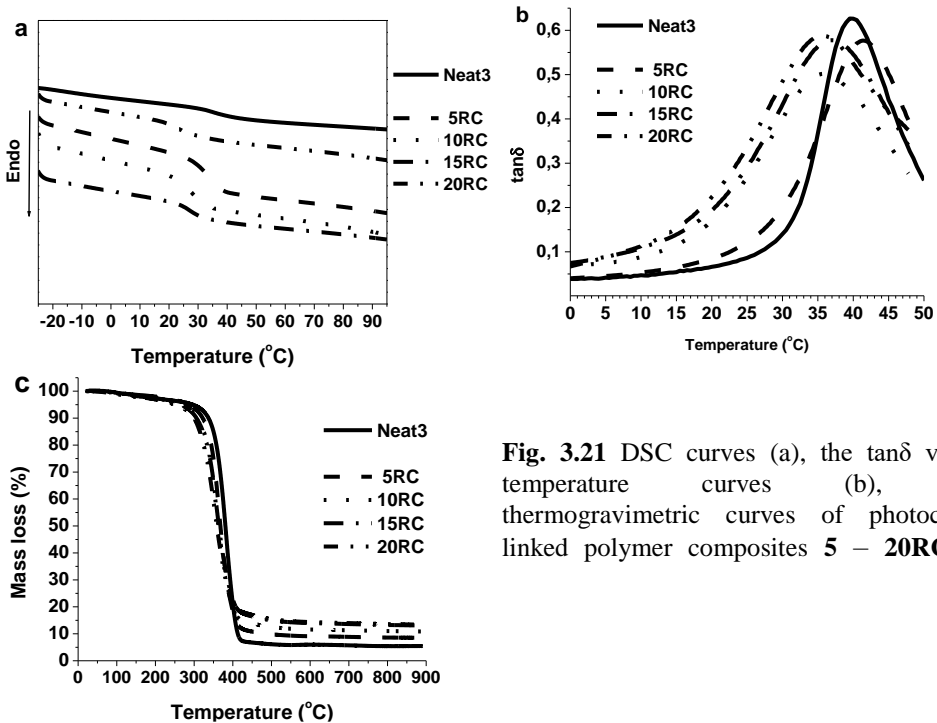
Fig. 3.21 DSC curves (a), the tanδ versus temperature curves (b), and thermogravimetric curves of photocross-linked polymer composites **5 – 20RC** (c)

3.4.2. Mechanical properties

Mechanical characteristics of the photocross-linked polymer composite films **Neat3** – **20HM** determined by the tensile test are summarized in Fig. 3.22a. The images of the dogbone shaped samples before the tensile test are shown in Fig. 3.22b.
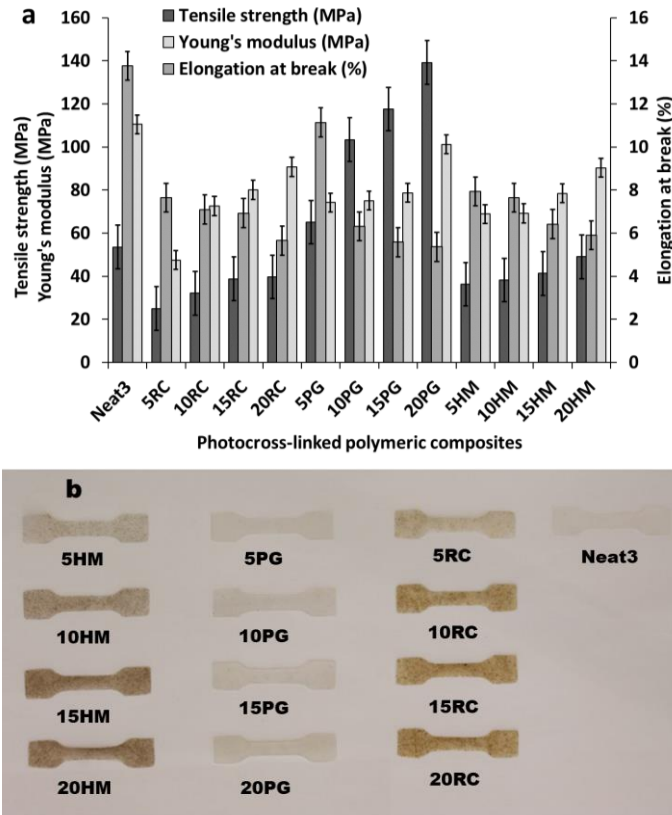
Fig. 3.22 Mechanical characteristics of the photocross-linked polymer **Neat3**, photocross-linked polymer composites **5RC** – **20HM** (a), and images of the dogbone shaped samples of composites before the tensile test (b)

The incorporation of fillers into the GDGE based polymer in most cases decreased elongation at break and Young's modulus. The elongation at break of photocross-linked polymer composites ranged from 4.5 % to 11.1 % while the elongation at break of polymer **Neat3** was 13.8 %. These values were similar to those of PVA and CG composites filled with RC and HM tested by the same tensile test method (3.45-4.62 %) [260]. The Young's modulus of the photocross-linked films with fillers were in the range of 48-101 MPa, while polymer **Neat3** exhibited Young's modulus of 111 MPa, and were lower than those of PVA and CG composites filled with RC, PG and HM tested by the same tensile test method (152-539 MPa) [260]. The tensile strength of the photocross-linked composites were from 25.0 MPa to 139.2MPa while polymer **Neat3** exhibited the tensile strength of 53.6

84

MPa. The addition of phosphogypsum into the compositions enchanced the tensile strength. The composites **5 – 20PG** reached tensile strength of 74.2-101.2 MPa which was higher than that of polymer **Neat3** (53.6 MPa). These values were higher compared to those of the PVA and CG composites filled with RC, PG and HM tested by the same tensile test method (4.95-35.40 MPa) [260] and higher than that of LDPE which is used as biodegradable plastic mulching film (15.37 MPa) [241]. The photocross-linked films with the higher cross-linking density demonstrated the higher elongation at break. Tensile strength and Young's modulus increased with the increase of the filler amount in the composite. After evaluating the mechanical properties, the photocross-linked polymer composites could be used as potential mulching coatings.

3.4.3. Thermomechanical properties

Viscoelastic properties of the photocross-linked polymer composites were investigated by DMA. The E' modulus of the photocross-linked polymer **Neat3** and polymer composites **5RC – 20HM** at different temperatures are listed in Table 3.16. The E' modulus in the glassy state (at 0 ºC) of the polymers with fillers were in the range of 1326-3247 MPa while the E' modulus of polymer **Neat3** was 1942 MPa. The E' modulus increased in most of composites with the increase of the filler amount due to the restrictions in the chain mobility. At room temperature (20 ºC), the E' modulus decreased slightly. Polymer **Neat3** had E' modulus of 1700 MPa and polymer composites with fillers had E' modulus of 1079-1759 MPa. In the rubbery (viscoelastic) state (at 45 ºC) polymers with fillers were soft and rubbery with E' modulus of 52-255 MPa while the E' modulus of polymer **Neat3** was 90 MPa. At 45 ºC, the composite **10PG** containing 10 wt.% of phosphogypsum had the highest E' modulus (255 MPa).

Table 3.16 Storage modulus E' values of the photocross-linked polymer **Neat3** and photocross-linked polymer composites **5RC – 20HM** in the glassy state (at 0 ºC), at 20 ºC, and rubbery (viscoelastic) state (at 45 ºC)

Photocross-linked polymer composite	Storage modulus E' (MPa) at temperature of		
	0 ºC (glassy state)	20 ºC	45 ºC (rubbery (viscoelastic) state)
Neat3	1942	1700	90
5RC	1326	1129	59
10RC	1755	1270	73
15RC	3247	1946	143
20RC	2934	1540	101
5PG	1920	1596	135
10PG	1867	1603	255
15PG	2100	1620	81
20PG	2657	1992	52
5HM	2211	1759	135
10HM	2125	1195	81
15HM	2610	1424	135
20HM	2750	1079	112

The E' modulus versus temperature curves of the photocross-linked polymer **Neat3** without filler and of photocross-linked polymer composites with the different industrial waste fillers are shown in Fig. 3.23. The E' modulus of the polymeric composites **15 – 20RC** containing rapeseed cake started to derease immediately with the increase of the temperature (Fig. 3.23a) but the E' modulus of the other polymeric composites started to decrease at ca. (10-25) ºC (Fig. 3.23b, c). The E' modulus of the polymeric composites **15 – 20RC** with rapeseed cake, **5 – 10PG** with phosphogypsum, and **5 – 20HM** with horn meal were higher up to 25 ºC compared to E' modulus of polymer **Neat3** without filler. The photocross-linked polymer composites with rapeseed cake and horn meal exhibited a rubbery plateau at about 40 ºC while composites with phosphogypsum exhibited a rubbery plateau later at about 45 ºC due to the reinforcement effect and restrictions of the chain mobility.
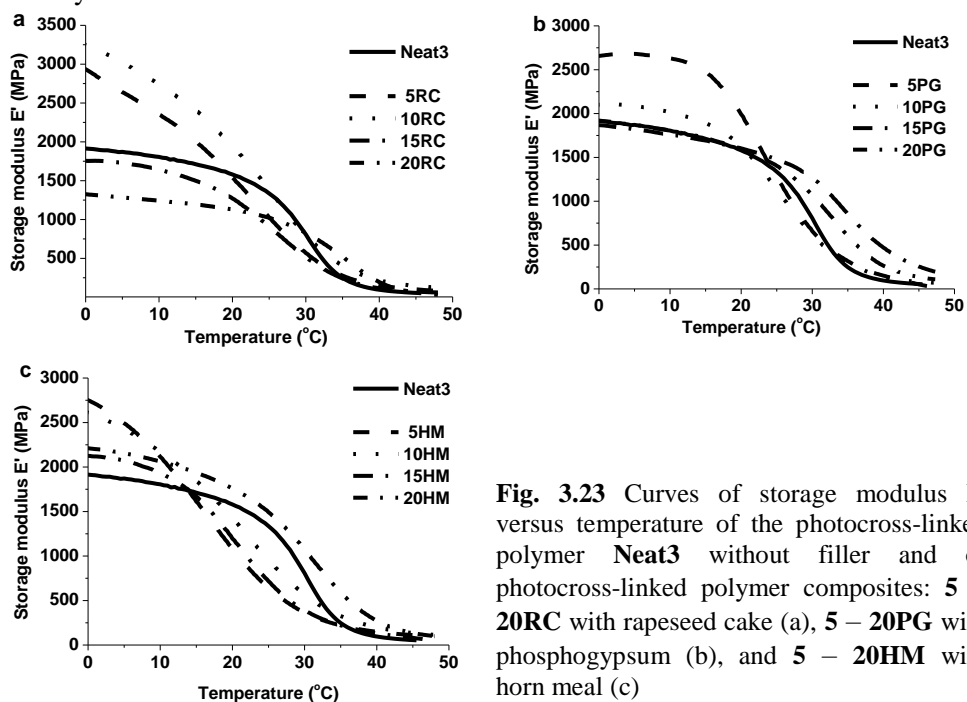
Fig. 3.23 Curves of storage modulus E' versus temperature of the photocross-linked polymer **Neat3** without filler and of photocross-linked polymer composites: **5 – 20RC** with rapeseed cake (a), **5 – 20PG** with phosphogypsum (b), and **5 – 20HM** with horn meal (c)

3.4.4. Swelling properties

Swelling capacity is related to the cross-linking density and therefore swelling test is one of the methods to characterize the structure of cross-linked polymer. Also, swelling properties in water of composites which could be used as plastic mulching films in agriculture are relevant. The swelling degree in distilled water versus time curves of the photocross-linked polymer **Neat3** without filler and photocross-linked polymer composites **5RC – 20HM** with the different industrial waste fillers estimated at room temperature (18 °C) for 2 h are shown in Fig. 3.24. The swelling equilibrium was reached after 1.25 h for the composites with rapeseed cake and horn

meal and after 1.75 h for the composites with phosphogypsum. Swelling degree values of the composite films in water were very low. The hydrophobic fragments of the cross-linked polymer tend to repel water. The incorporation of waste materials into the GDGE based polymer increased the swelling degree, as a result of this the photocross-linked composites **5RC** – **20HM** exhibited values of 2.8-7.2 % while polymer **Neat3** exhibited swelling degree of 1.7 %. Swelling degree values of polymeric composites were higher by (1.1-5.5) % in comparison with polymer **Neat3** without filler. The highest swelling degree observed after 2 h in water was 7.2 % for the polymeric composite **20PG** containing 20 wt.% of phosphogypsum. The swelling degree increased with the increase of filler amount in the composite. This is because polymer composites which had lower cross-linking densities and longer chain length were easy to expand.
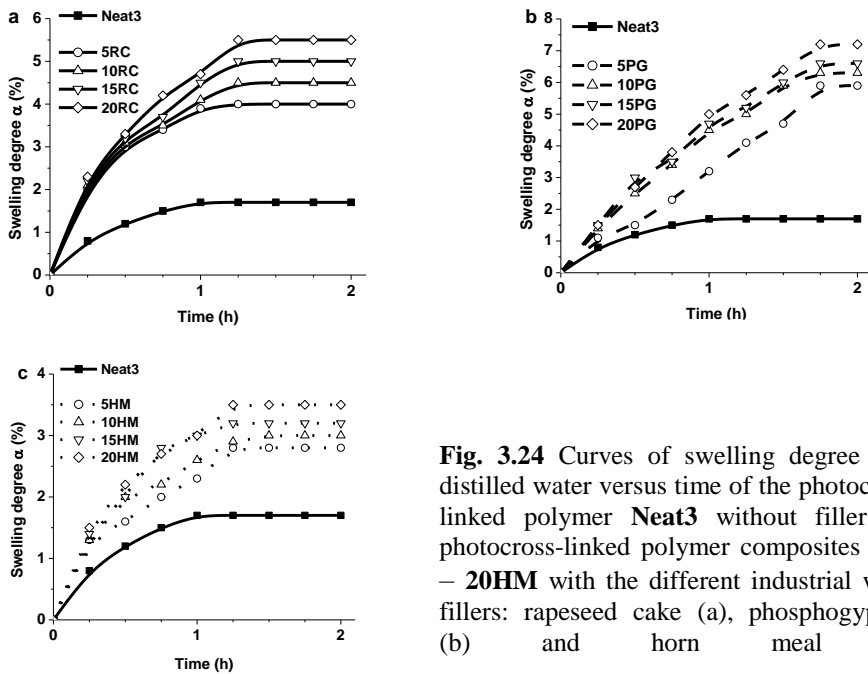
Fig. 3.24 Curves of swelling degree α in distilled water versus time of the photocross-linked polymer **Neat3** without filler and photocross-linked polymer composites **5RC** – **20HM** with the different industrial waste fillers: rapeseed cake (a), phosphogypsum (b) and horn meal (c)

3.4.5. Wettability properties

Measurement of contact angle on polymers is the method which characterizes liquid/solid interaction and the wettability of polymers [289]. Calculations based on these measurements produce parameters such as surface free energy (SFE) which characterizes the disruption of intermolecular bonds that occur when a surface is created and also the wettability of polymers [289]. The data of contact angle and surface free energy based on different methods of the photocross-linked polymer **Neat3** and photocross-linked polymer composites **5RC** – **20HM** are summarized in the Table 3.17. Three different methods were chosen for the measurement of contact angle and calculation of surface free energy. The Equation of State is the universal

method for the measurement of contact angle of polymers, coatings, and varnishes which requires only one liquid for the measurements [289]. Contact angle values of water of the photocross-linked polymer composite films with fillers were in the range of 31.31-70.19 ° and were lower than of polymer **Neat3** (73.51 °) (Table 3.17). Surface free energy values of composites calculated according to Equation of State method ranged from 40.15 mN/m to 53.55 mN/m and were higher than of polymer **Neat3** (34.36 mN/m). This method has one demerit as it does not estimate the molecular origins of surface tension and takes no statistical mechanical insight [289]. The Owens-Wendt-Rabel-Kaelble (OWRK) method is also the universal method for the measurement of contact angle of polymers, coatings, and varnishes and has one merit compared to the Equation of State method. OWRK method requires two liquids for the measurement of contact angle and provides information about the polar and disperse parts of surface free energy [289]. This method includes interactions of two substances molecules as the geometric mean of intermolecular interactions within the substance [289]. Contact angle values of diiodomethane of the photocross-linked polymeric composite films with fillers were in the range of 28.21-51.44 ° and were lower than of polymer **Neat3** (62.66 °). Surface free energy values of composites calculated according to OWRK method ranged from 42.72 mN/m to 68.15 mN/m and were higher than of polymer **Neat3** (36.93 mN/m). Disperse part of composites were in the range of 33.46-44.94 mN/m and polar part ranged from 8.99 mN/m to 28.41 mN/m. The Wu method is created for the contact angle measurements of low energetic systems as polymers, organic solutions, and organic pigments [289]. It also requires two liquids for the measurement as it provides information about disperse and polar parts. This method includes harmonic mean to combine the polar and dispersion components of the solid and liquid surface energies [289]. Surface free energy values calculated according to Wu method of composites ranged from 48.69 mN/m to 72.13 mN/m and were higher than of polymer **Neat3** (43.02 mN/m). Disperse part of composites were in the range of 34.70-45.10 mN/m, polar part ranged from 13.99 mN/m to 31.85 mN/m and were higher than of disperse and polar part of polymer **Neat3** (29.18 mN/m and 13.84 mN/m, respectively). The selected methods for the calculation of surface free energy of the photocross-linked polymer composite films did not show any significant differences as calculated values of surface free energy were in the same range. The dependence of the contact angle, surface free energy, disperse, and polar part on the cross-linking density was observed. The lower contact angle and the higher surface free energy, dispersive part, and polar part were recorded when a higher amount of the waste filler was used in the composition. The used methods showed that the incorporation of the fillers into GDGE based polymer incresed wettability of composites as contact angle was decreased and surface free energy was increased compared to the polymer without the fillers. Surface free energy values obtained with three methods differ due to errors of the contact angle measurements and different mathematical expression between contact angle and surface free energy in formulas used.

Table 3.17 Contact angle and surface free energy based on different methods of the photocross-linked polymer **Neat3** and the photocross-linked polymer composites **5RC** – **20HM**

Photocross-linked polymer composite	Contact angle of water (º) ± SD	Contact angle of diiodo-methane (º) ± SD	Surface free energy (mN/m)						
			Equation of State	OWRK			Wu		
			Total	Total	Disperse part	Polar part	Total	Disperse part	Polar part
Neat3	73.51 ± 0.23	62.66 ± 0.27	34.36	36.93	27.05	9.88	43.02	29.18	13.84
5RC	63.09 ± 0.30	37.57 ± 0.02	43.93	51.23	40.81	10.42	57.25	41.26	15.99
10RC	60.29 ± 0.00	34.54 ± 0.16	44.20	53.63	42.24	11.39	59.66	42.57	17.10
15RC	57.67 ± 0.39	31.79 ± 0.08	46.87	55.82	43.47	12.35	61.87	43.71	18.16
20RC	55.34 ± 0.46	28.21 ± 0.20	48.28	57.99	44.94	13.05	64.12	45.10	19.02
5PG	68.82 ± 1.77	46.26 ± 0.04	40.15	45.32	36.33	8.99	51.29	37.22	14.07
10PG	64.24 ± 0.08	44.13 ± 0.03	42.10	48.44	37.48	10.96	54.32	38.24	16.08
15PG	48.13 ± 0.02	41.82 ± 0.07	47.83	58.33	38.68	19.65	63.33	39.32	24.01
20PG	31.31 ± 0.04	39.74 ± 0.01	53.55	68.15	39.74	28.41	72.13	40.28	31.85
5HM	70.19 ± 0.06	51.44 ± 0.42	38.43	42.72	33.46	9.26	48.69	34.70	13.99
10HM	67.11 ± 0.01	47.90 ± 0.02	40.28	45.60	35.46	10.16	51.51	36.42	15.09
15HM	63.03 ± 0.31	42.88 ± 0.06	42.78	49.51	38.14	11.37	55.38	38.83	16.55
20HM	60.17 ± 1.05	39.29 ± 0.22	44.29	51.85	39.96	11.89	57.75	40.48	17.26

3.4.6. Biodegradability

Mass losses of the photocross-linked polymer composites observed in the period of 3 months are shown in Fig. 3.25. Mass losses of the photocross-linked polymer films with fillers after 3 months ranged from 3.3 % to 22.2 % while the mass loss of polymer **Neat3** was 3.6 %. This observation showed that the incorporation of waste materials in most cases increased the biodegradability of GDGE resin. By increasing the amount of the filler in the composite, the mass loss increased in all cases. The highest mass loss (12.3-22.2 %) was observed for the composites **10 – 20RC** because rapeseed cake contains of lysine amino acid [257], which is important for the growth and metabolic processes of microorganisms. The incorporation of phosphogypsum into composites increased the biodegradability because sulfate-reducing bacteria present in the soil apparently converted gypsum into hydrogen sulfide gas [256]. The low mass loss of horn meal can be explained by the presence of cistein amino acid, which has sulphur and forms intramolecular and intermolecular physical bonds [255].
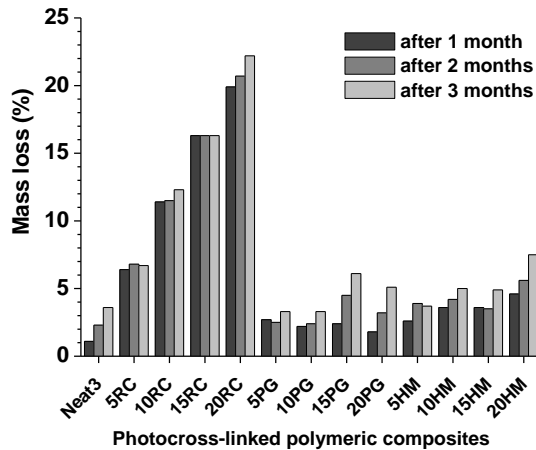
Fig. 3.25 Mass loss of the photocross-linked polymer **Neat3** and of polymeric composites **5RC – 20HM** after 1-3 months exposition in soil

CONCLUSIONS

1. Novel biodegradable photocross-linked polymers of glycerol diglycidyl ether and epoxy reactive diluents were synthesized and their properties were studied. The addition of reactive diluents into the compositions reduced reaction duration and improved the rheological, thermal, and mechanical properties of the resulting polymers due to the increased cross-linking density. Biodegradability of photocross-linked polymers was increased by the introduction of reactive diluents fragments.

2. Novel biodegradable photocross-linked polymers of glycerol diglycidyl ether and di- or trihydroxyl compounds were synthesized and their properties were studied. The addition of di- or trihydroxyl compounds into the compositions reduced reaction duration. The thermal and mechanical properties of the resulting polymers were improved by decreasing the amount of di- or trihydroxyl compound. By increasing the amount of di- or trihydroxyl compound in the compositions the biodegradability of resulting polymers was increased.

3. The suitability of the composition of glycerol diglycidyl ether and 3',4'-epoxycyclohexylmethyl-3,4-epoxycyclohexanecarboxylate for the formation of 3D structures by optical 3D printing was confirmed. 3D hexagonal structure was formed by 3D laser lithography.

4. Novel biodegradable composites of glycerol diglycidyl ether-based photocross-linked polymer and biobased industrial waste materials (rapeseed cake, phosphogypsum, horn meal) were produced and their properties were studied. The incorporation of various industrial waste fillers did not have any significant effect on the reaction duration. The swelling capacity, wettability, and biodegradability were improved by incorporating the selected industrial waste fillers. The mechanical properties of biocomposites were similar to biodegradable plastic mulching films. The obtained biocomposites could be used as mulching coatings.

REFERENCES

1. QUALMAN, D. (2017). *Global plastics production, 1917 to 2050* [seen on 2018-05-12]. Access via: https://www.darrinqualman.com/global-plastics-production/

2. REDDY, M. M., S. VIVEKANANDHAN, M. MISRA, S. K. BHATIA, A. K. MOHANTY. Biobased plastics and bionanocomposites: Current status and future opportunities. *Progress in Polymer Science*. 2013, 38(10-11), 1653-1689. ISSN: 0079-6700.

3. EUROPEAN BIOPLASTICS, NOVA-INSTITUTE. (2017). *Bioplastics facts and figures*. [seen on 2018-05-17]. Access via: http://docs.european-bioplastics.org/publications/EUBP_Facts_and_figures.pdf

4. *EUROPE 2020*. (no year given). [seen on 2018-05-17]. Access via: https://www.european-bioplastics.org/policy/europe-2020/

5. MONTEIRO, M. R., C. L. KUGELMEIER, R. S. PINHEIRO, M. O. BATALHA, A. DA SILVA CESAR. Glycerol from biodiesel production: Technological paths for sustainability. *Renewable and Sustainable Energy Reviews*. 2018, 88, 109-122. ISSN: 1364-0321.

6. *GLOBAL Plastic Products Manufacturing Market Briefing* 2018-2023. (2018). [seen on 2018-05-12]. Access via: https://www.businesswire.com/news/home/20180130006255/en/Global-Plastic-Products-Manufacturing-Market-Briefing-2018-2023

7. HERAEUS NOBLELIGHT AMERICA LLC UV LEARNING CENTER. (no year given). [seen on 2018-05-12]. Access via: http://www.fusionuv.com/uvlearningcenter.aspx?id=206

8. VOX, G., G. SANTAGATA, M. MALINCONICO, B. IMMIRZI, G. SCARASCIA MUGNOZZA, E. SCHETTINI. Biodegradable films and spray coatings as eco-friendly alternative to petro-chemical derived mulching films. *Journal of Agricultural Engineering*. 2013, 44, 221-225. ISSN: 1974-7071.

9. TREINYTE, J., V. GRAZULEVICIENE, R. PALECKIENE, J. OSTRAUSKAITE, L. CESONIENE. Biodegradable Polymer Composites as Coating Materials for Granular Fertilizers. *Journal of Polymers and the Environment*. 2018, 26(2), 543-554. ISSN: 1566-2543.

10. PERRY, Robert H., Don W. GREEN, James O. MALONEY. *Perry's chemicalengineers' handbook*. 7th ed. USA: McGraw-Hill, 1997. ISBN: 9780071422949.

11. RAHMAT, N., A. A. ZUHAIRI, A. R. MOHAMED. Recent progress on innovative and potential technologies for glycerol transformation into fuel additives: a critical review. *Renewable and Sustainable Energy Reviews*. 2010, 14, 987-1000. ISSN: 1364-0321.

12. QUISPE, C. A. G., C. J. R. CORONADO, J. A. CARVALHOJR. Glycerol: Production, consumption, prices, characterization and new trends in combustion. *Renewable and Sustainable Energy Reviews*. 2013, 27, 475-493. ISSN: 1364-0321.

13. *BIODIESEL barriers, potentials, and impacts. Glycerine*. (no year given). [seen on 2018-05-14]. Access via: http://www.esru.strath.ac.uk/EandE/Web_sites/06-07/Biodiesel/glycerine.htm

14. TREMBLAY, S. (2017). *Sources of Glycerine* [seen on 2018-05-14]. Access via: https://www.livestrong.com/article/327146-sources-of-glycerine/

15. CHRISTOPH, R., B. SCHMIDT, U. STEINBERNER, W. DILLA, R. KARINEN. Glycerol. In *Ullmann's Encyclopedia of Industrial Chemistry*, (pp. 61-81). Weinheim: Wiley-VCH Verlag GmbH & Co. KgaA, 2012. Access via doi:10.1002/14356007.a12_477.pub2.

16. ALICKE, A. A., B. C. LEOPERCIO, F. H. MARCHESINI, P. R. DE SOUZA MENDES. Guidelines for the rheological characterization of biodiesel. *Fuel*. 2015, 140, 446-452. ISSN: 0016-2361.

17. OMIDVARBORNA, H., A. KUMAR, D. S. KIM. Characterization of particulate matter emitted from transit buses fueled with B20 in idle modes. *Journal of Environmental Chemical Engineering*. 2014, 2(4), 2335-2342. ISSN: 2213-3437.

18. OKOYE, P. U., B. H. HAMEED. Review on recent progress in catalytic carboxylation and acetylation of glycerol as a byproduct of biodiesel production. *Renewable and Sustainable Energy Reviews*. 2016, 53, 558-574. ISSN: 1364-0321.

19. SALEH, J., A. Y. TREMBLAY, M. A. DUBE. Glycerol removal from biodiesel using membrane separation technology. *Fuel*. 2010, 89, 2260-2266. ISSN: 0016-2361.

20. BINHAYEEDING, N., S. KLOMKLAO, K. SANGKHARAK. Utilization of Waste Glycerol from Biodiesel Process as a Substrate for Mono-, Di-, and Triacylglycerol Production. *Energy Procedia*. 2017, 138, 895-900. ISSN: 1876-6102.

21. SHEHATA, M. S. Emissions, performance and cylinder pressure of diesel engine fuelled by biodiesel fuel. *Fuel*. 2013, 112, 513-522. ISSN: 0016-2361.

22. ARANSIOLA, E. F., T. V. OJUMU, O. O. OYEKOLA, T. F. MADZIMBAMUTO, D. I. O. IKHU-OMOREGBE. A review of current technology for biodiesel production: state of the art. *Biomass and Bioenergy*. 2014, 61, 276-297. ISSN: 0961-9534.

23. KISS, A. A., A. C. DIMIAN, G. ROTHENBERG. Biodiesel by catalytic reactive distillation powered by metal oxides. *Energy Fuel*. 2008, 22(1), 598-604. ISSN: 0887-0624.

24. DA SILVA, G. P., M. MACK, J. CONTIERO. Glycerol: A promising and abundant carbon source for industrial microbiology. *Biotechnology Advances*. 2009, 27, 30-39. ISSN: 0734-9750.

25. HEJNA, A., P. KOSMELA, K. FORMELA, L. PISZCZYK, J. T. HAPONIUK. Potential applications of crude glycerol in polymer technology–Current state and perspectives. *Renewable and Sustainable Energy Reviews*. 2016, 449-475. ISSN: 1364-0321.

26. *OECD-FAO Agricultural Outlook 2013-2022: BIOFUEL - OECD-FAO Agricultural Outlook 2013-2022*. (2018). [seen on 2018-02-19]. Access via: http://stats.oecd.org/index.aspx?queryid=30104

27. *Leading biodiesel producers worldwide in 2016, by country (in billion liters*. (2018). [seen on 2018-02-21]. Access via: https://www.statista.com/statistics/271472/biodiesel-production-in-selected-countries/

28. YANG, F., M. A. HANNA, S. RUNCANG. Value-added uses for crude glycerol–a by product of biodiesel production. *Biotechnology for Biofuels*. 2012, 5(1), 13-23. E-ISSN: 1754-6834.

29. PRADIMA, J., M. RAJESWARI KULKARNI, ARCHNA. Review on enzymatic synthesis of value added products of glycerol, a by-product derived from biodiesel production. *Resource-Efficient Technologies*. 2017, 3, 394-405. ISSN: 2405-6537.

30. DING, X., H. LIU, Q. YANG, N. LI, X. DONG, S. WANG, X. ZHAO, Y. WANG. A novel route to synthesis of glycerol dimethyl ether from epichlorohydrin with high selectivity. *Biomass and Bioenergy*. 2014, 70, 400-406. ISSN: 0961-9534.

31. GONZALEZ-PAJUELO, M., J. C. ANDRADE, I. VASCONCELOS. Production of 1,3-propanediol by *Clostridium butyricum* VPI 3266 using a synthetic medium and raw glycerol. *Journal of Industrial Microbiology and Biotechnology*. 2004, 31(9), 442-446. ISSN: 1367-5435.

32. MELERO, J. A., G. VICENTE, G. MORALES, M. PANIAGUA, J. M. MORENO, R. ROLDAN, A. EZQUERRO, C. PEREZ. Acid-catalyzed etherification of bio-glycerol and isobutylene over sulfonic mesostructured silicas. *Applied Catalysis A: General*. 2008, 346 (1), 44-51. ISSN: 0926-860X.

33. AVHAD, M. R., J. M. MARCHETTI. Review on recent advancement in catalytic materials for biodiesel production. *Renewable and Sustainable Energy Reviews*. 2015, 50, 696-718. ISSN: 1364-0321.

34. TALEBIAN-KIAKALAIEH, A., N. A. S. AMIN, H. HEZAVEH. Glycerol for renewable acrolein production by catalytic dehydration. *Renewable and Sustainable Energy Reviews*. 2014, 40, 28-59. ISSN: 1364-0321.

35. AYOUB, M., A. Z. ABDULLAH. Critical review on the current scenario and significance of crude glycerol resulting from biodiesel industry towards more sustainable renewable energy industry. *Renewable and Sustainable Energy Reviews*. 2012, 16(5), 2671-2686. ISSN: 1364-0321.

36. BAGHERI, S., N. M. JULKAPLI, W. A. YEHYE. Catalytic conversion of biodiesel derived raw glycerol to value added products. *Renewable and Sustainable Energy Reviews*. 2015, 41, 113-127. ISSN: 1364-0321.

37. TENG, W. K., G. C. NGOH, R. YUSOFF, M. K. AROUA. A review on the performance of glycerol carbonate production via catalytic transesterification: effects of influencing parameters. *Energy Conversion and Management.* 2014, 88, 484-497. ISSN: 0196-8904.

38. GHOLAMI, Z., A. Z. ABDULLAH, K. T. LEE. Dealing with the surplus of glycerol production from biodiesel industry through catalytic upgrading to polyglycerols and other value-added products. *Renewable and Sustainable Energy Reviews*. 2014, 39, 327-341. ISSN: 1364-0321.

39. *Glycerin specifications*. (2013). [seen on 2018-02-21]. Access via: http://www.srsbiodiesel.com/technologies/glycerin-purification/glycerin-specifications/

40. YAZDANI, S. S., R. GONZALEZ. Anaerobic fermentation of glycerol: A path to economic viability for the biofuels industry. *Current opinion in biotechnology*. 2007, 18(3), 213-219. ISSN: 0958-1669.

41. SIRICHARNSAKUNCHAI, P., L. SIMASATITKUL, A. A. SOOTTITANTAWAT. Use of reactive distillation for triacetin production from crude glycerol: Simulation and performance analysis. In Proceedings of the 11th International Symposium on Process System Engineering, July 15-19, 2012, Singapore, Singapore. Amsterdam: Elsevier, 2012. pp. 165-169.

42. SDRULA, N. A study using classical or membrane separation in the biodiesel process. *Desalination*. 2010, 250(3), 1070-1072. ISSN: 0011-9164.

43. DHAR, B. R., K. KIRTANIA. Excess Methanol Recovery in Biodiesel Production Process using a Distillation Column: a Simulation Study. *Chemical Engineering Research Bulletin*. 2009, 13(2), 55-60. ISSN: 0379-7678.

44. WAN ISAHAK, W. N. R., Z. A. CHE RAMLI, M. ISMAIL, J. MOHD JAHIM, M. A. YARMO. Recovery and Purification of Crude Glycerol from Vegetable Oil Transesterification: A Review. *Separation & Purification Reviews*. 2015, 44, 250-267. ISSN: 1542-2119.

45. NOBLE, Richard D., Patricia A. TERRY. *Principles of chemical separations with environmental applications*. 1st Ed. Cambridge: Cambridge University Press, 2004. ISBN-10: 0521010144

46. VAN GERPEN, J. Biodiesel processing and production. *Fuel Processing Technology*. 2005, 86(10), 1097-1107. ISSN: 0378-3820.

47. HASHEMINEJAD, M., M. TABATABAEI, Y. MANSOURPANAH, M. K. FAR, A. JAVANI. Upstream and downstream strategies to economize biodiesel production. *Bioresource Technology*. 2011, 102(2), 461-468. ISSN: 0960-8524.

48. ATADASHI, I. M., M. K. AROUA, A. ABDUL AZIZ. Biodiesel separation and purification: A review. *Renewable Energy*, 2011, 36(2), 437-443. ISSN: 0960-1481.

49. GOMES, M. C. S., N. C. PEREIRA, S. T. D. BARROS. Separation of biodiesel and glycerol using ceramic membranes. *Journal of Membrane Science*. 2010, 352(1), 271-276, ISSN: 0376-7388.

50. DEMIRBAS, A. Biodiesel fuels from vegetable oils via catalytic and non-catalytic supercritical alcohol transesterifications and other methods: a survey. *Energy Conversion and Management*. 2003, 44(13), 2093-2109. ISSN: 0196-8904.

51. LEONETI, A. B., V. ARAGAO-LEONETI, S. V. W. B. DE OLIVEIRA. Glycerol as a by-product of biodiesel production in Brazil: Alternatives for the use of unrefined glycerol. *Renewable Energy*. 2012, 45, 138-145. ISSN: 0960-1481.

52. DONKIN, S. S., S. L. KOSER, H. M. WHITE, P. H. DOANE, M. J. CECAVA. Feeding value of glycerol as a replacement for corn grain in rations fed to lactating dairy cows. *Journal of Dairy Science*. 2009, 92(10), 5111-5119. ISSN: 0022-0302.

53. BODIK, I., A. BLŠTAKOVA, S. SEDLAČEK, M. HUTNAN. Biodiesel waste as source of organic carbon for municipal WWTP denitrification. *Bioresource Technology*. 2009, 100(8), 2452-2456. ISSN: 0960-8524.

54. AZENHA, M., C. LUCAS, J. L. GRANJA, I. CARLOS-ALVES, E. GUIMARAES. Glycerol resulting from biodiesel production as an admixture for cement-based materials: an experimental study. *European Journal of Environmental and Civil Engineering*. 2017, 21(12), 1522-1538. ISSN: 1964-8189.

55. PAGLIARO, M., R. CIRIMINNA, H. KIMURA, M. ROSSI, C. DELLA PINA. From glycerol to value-added products. *Angewandte Chemie International Edition*. 2007, 46(24), 4434-4440. ISSN: 1433-7851.

56. BALTRUSAITIS, J., M. VALTER, A. HELLMAN. Geometry and Electronic Properties of Glycerol Adsorbed on Bare and Transition-Metal Surface-Alloyed Au(111): A Density Functional Theory Study. *Journal of Physical Chemistry C*. 2016, 120(3), 1749-1757. ISSN: 1932-7447.

57. SILVA, C., F. FIGUEIREDO, R. RODRIGUES, M. SAIRRE, M. GONCALVES, I. MATOS, I. FONSECA, D. MANDELLI, W. CARVALHO. Enhancing the biodiesel manufacturing process by use of glycerin to produce hyacinth fragrance. *Clean Technologies and Environmental Policy*. 2016, 18(5), 1551-1563. ISSN: 1618-954X.

58. CECILIA, J. A., C. GARCIA-SANCHO, J. M. MERIDA-ROBLES, J. SANTAMARIA GONZALEZ, R. MORENO-TOST, P. MAIRELES-TORRES. WO3 supported on Zr doped mesoporous SBA-15 silica for glycerol dehydration to acrolein. *Applied Catalysis A: General*. 2016, 516, 30-41. ISSN: 0926860X.

59. KATRYNIOK, B., H. KIMURA, E. SKRZYSKA, J.-S. GIRARDON, P. FORGARLAND, M. CAPRON, R. DUCOULOMBIER, N. MIMURA, S. PAUL, F. DUMEIGNIL. Selective catalytic oxidation of glycerol: perspectives for high value chemicals. *Green Chemistry*. 2011, 13(8), 1960-1979. ISSN: 1463-9262.

60. SADHUKHAN, S., R. VILLA, U. SARKAR. Microbial production of succinic acid using crude and purified glycerol from a Crotalaria juncea based biorefinery. *Biotechnology Reports*. 2016, 10, 84-93. ISSN: 2215-017X.

61. MURAKAMI, N., M. OBA, M. IWAMOTO, Y. TASHIRO, T. NOGUCHI, K. BONKOHARA, M. A. ABDEL-RAHMAN, T. ZENDO, M. SHIMODA, K. SAKAI, K. SONOMOTO. L-Lactic acid production from glycerol coupled with acetic acid metabolism by *Enterococcus faecalis* without carbon loss. *Journal of Bioscience and Bioengineering*. 2016, 121(1), 89-95. ISSN: 1389-1723.

62. AYADI, I., O. KAMOUN, H. TRIGUI-LAHIANI, A. HDIJI, A. GARGOURI, H. BELGHITH, M. GUERFALI. Single cell oil production from a newly isolated *Candida viswanathii* Y-E4 and agro-industrial by-products valorization. *Journal of Industrial Microbiology & Biotechnology*. 2016, 43(7), 901-914. ISSN: 1367-5435.

63. LIU, H., Y. XU, Z. ZHENG, D. LIU. 1,3-Propanediol and its copolymers: Research, development and industrialization. *Biotechnology Journal*. 2010, 5, 1137-1148. ISSN: 1860-6768.

64. CELINSKA, E. Debottlenecking the 1,3-propanediol pathway by metabolic engineering. *Biotechnology Advances*. 2010, 28(4), 519-530. ISSN: 0734-9750.

65. BIEBL, H., K. MENZEL, A. P. ZENG, W. D. DECKWER. Microbial production of 1,3-propanediol. *Applied Microbiology and Biotechnology*. 1999, 52(3), 289-297. ISSN: 0175-7598.

66. JOHNSON, E. E., L. REHMANN. The role of 1,3-propanediol production in fermentation of glycerol by *Clostridium pasteurianum*. *Bioresource Technology*. 2016, 209, 1-7. ISSN: 0960-8524.

67. MARINAS, A., P. BRUIJNINCX, J. FTOUNI, F. J. URBANO, C. PINEL. Sustainability metrics for a fossil- and renewable-based route for 1,2-propanediol production: A comparison. *Catalysis Today*. 2015, 239, 31-37. ISSN: 0920-5861.

68. SAXENA, R. K., P. ANAND, S. SARAN, J. ISAR. Microbial production of 1,3-propanediol: Recent developments and emerging opportunities. *Biotechnology Advances*. 2009, 27(6), 895-913. ISSN: 0734-9750.

69. D'HONDT, E., S. VAN DE VYVER, B. F. SELS, P. A. JACOBS. Catalytic glycerol conversion into 1,2-propanediol in absence of added hydrogen. *Chemical Communications*. 2008, 45, 6011-6012. ISSN: 1359-7345.

70. PAPANIKOLAOU, S., S. FAKAS, M. FICK, I. CHEVALOT, M. GALIOTOU-PANAYOTOU, M. KOMAITIS, I. MARC, G. AGGELIS. Biotechnological valorisation of raw glycerol discharged after bio-diesel (fatty acid methyl esters) manufacturing process: Production of 1,3-propanediol, citric acid and single cell oil. *Biomass and Bioenergy*. 2008, 32(1), 60-71. ISSN: 0961-9534.

71. GARLAPATI, V. K., U. SHANKAR, A. BUDHIRAJA. Bioconversion technologies of crude glycerol to value added industrial products. *Biotechnology Reports*. 2016, 9, 9-14. ISSN: 2215-017X.

72. POSADA, J., C. CARDONA, R. GONZALEZ. Analysis of the Production Process of Optically Pure d -Lactic Acid from Raw Glycerol Using Engineered *Escherichia coli* Strains. *Applied Biochemistry and Biotechnology*. 2012, 166(3), 680-699. ISSN: 0273-2289.

73. NGUYEN, C. M, J. S. KIM, J. K. SONG, G. J. CHOI, Y. H. CHOI, K. S. JANG, J. C. KIM. D-lactic acid production from dry biomass of Hydrodictyon reticulatum by simultaneous saccharification and co-fermentation using *Lactobacillus coryniformis* subsp. torquens. *Biotechnology letters*. 2012, 34(12), 2235-2240. E-ISSN: 1573-6776.

74. BAUER, R., N. KATSIKIS, S. VARGA, D. HEKMAT. Study of the inhibitory effect of the product dihydroxyacetone on *Gluconobacter oxydans* in a semi-continuous two-stage repeated-fed-batch process. *Bioprocess and Biosystems Engineering*. 2005, 28(1), 37-43. ISSN: 1615-7591.

75. ZHOU, X., Y. XU, S. YU. Simultaneous Bioconversion of Xylose and Glycerol to Xylonic Acid and 1,3-Dihydroxyacetone from the Mixture of Pre-Hydrolysates and Ethanol-Fermented Waste Liquid by *Gluconobacter oxydans*. *Applied Biochemistry and Biotechnology*. 2016, 178(1), 1-8. ISSN: 0273-2289.

76. JITRWUNG, R., V. YARGEAU. Biohydrogen and Bioethanol Production from Biodiesel-Based Glycerol by *Enterobacter aerogenes* in a Continuous Stir Tank Reactor. *International Journal of Molecular Sciences*. 2015, 16 (5), 10650-10667. ISSN: 14220067.

77. KATA, I., M. V. SEMKIV, J. RUCHALA, K. V. DMYTRUK, A. A. SIBIRNY. Overexpression of the genes PDC1 and ADH1 activates glycerol conversion to ethanol in the thermotolerant yeast *Ogataea* (Hansenula) *polymorpha*. *Yeast*. 2016, 33(8), 471-478. ISSN: 0749-503X.

78. TACONI, K. A., K. P. VENKATARAMANAN, D. T. JOHNSON. Growth and solvent production by *Clostridium pasteurianum* ATCC® 6013™ utilizing biodiesel-derived crude glycerol as the sole carbon source. *Environmental Progress & Sustainable Energy*. 2009, 28(1), 100-110. ISSN: 1944-7442.

79. ATSUMI, S., T. HANAI, J. C. LIAO. Non-fermentative pathways for synthesis of branched-chain higher alcohols as biofuels. *Nature*. 2008, 451(7174), 86-90. ISSN: 0028-0836.

80. KHAN, A., A. BHIDE, R. GADRE. Mannitol production from glycerol by resting cells of *Candida magnolia*. *Bioresource Technology*. 2009, 100(20), 4911-4913. ISSN: 0960-8524.

81. ANDRE, A., A. CHATZIFRAGKOU, P. DIAMANTOPOULOU, D. SARRIS, A. PHILIPPOUSSIS, M.GALIOTOU-PANAYOTOU, M. KOMAITIS, S. PAPANIKOLAOU. Biotechnological conversions of bio-diesel-derived crude glycerol by *Yarrowia lipolytica* strains. *Engineering in Life Sciences*. 2009, 9(6), 468-478. ISSN: 1618-0240.

82. GRENBY, Trevor H. Advances in Swetners. New York: Springer, 2011. ISBN 978-1-4613-1229-1

83. SONSECA, A., S. CAMARERO-ESPINOSA, L. PEPONI, C. WEDER, E. J. FOSTER, J. M. KENNY, E. GIMENEZ. Mechanical and shape-memory properties of poly(mannitol sebacate)/cellulose nanocrystal nanocomposites. *Journal of Polymer Science Part A: Polymer Chemistry*. 2014, 52(21), 3123-3133. ISSN: 0887-624X.

84. TANADCHANGSAENG, N., J. YU. Microbial synthesis of polyhydroxybutyrate from glycerol: Gluconeogenesis, molecular weight and material properties of biopolyester. *Biotechnology and Bioengineering*. 2012, 109(11), 2808-2818. ISSN: 0006-3592.

85. ASHBY, R. D., D. K. Y. SOLAIMAN, G. D. STRAHAN. Efficient Utilization of Crude Glycerol as Fermentation Substrate in the Synthesis of Poly(3-hydroxybutyrate) Biopolymers. *Journal of the American Oil Chemists' Society*. 2011, 88(7), 949-959. ISSN: 0003-021X.

86. ZHU, C., S. CHIU, J. P. NAKAS, C. T. NOMURA. Bioplastics from waste glycerol derived from biodiesel industry. *Journal of Applied Polymer Science*. 2013, 130(1), 1–13. ISSN: 0021-8995.

87. POLETO, L., P. SOUZA, F. E. MAGRINI, L. L. BEAL, A. P. RODRIGUES TORRES, M. PAULA DE SOUSA, J. PEREIRA LAURINO, S. PAESI. Selection and identification of microorganisms present in the treatment of wastewater and activated sludge to produce biohydrogen from glycerol. *International Journal of Hydrogen Energy*. 2016, 41(7), 4374-4381. ISSN: 0360-3199.

88. KONG, P. S., M. K. AROUA, W. M. A. W. DAUD. Conversion of crude and pure glycerol into derivatives: A feasibility evaluation. *Renewable and Sustainable Energy Reviews*. 2016, 63, 533-555. ISSN: 1364-0321.

89. LUO, X., X. GE, S. CUI, Y. LI. Value-added processing of crude glycerol into chemicals and polymers. Bioresource Technology, 2016, 215, 144-154. ISSN: 0960-8524.

90. ZAWANEH, P. N., A. M. DOODY, A. N. ZELIKIN, D. PUTNAM. Diblock copolymers based on dihydroxyacetone and ethylene glycol: synthesis, characterization, and nanoparticle formulation. *Biomacromolecules*. 2006, 7(11), 3245-3251. ISSN: 1525-7797.

91. WEISER, J. R., P. N. ZAWANEH, D. PUTNAM. Poly(carbonate-ester)s of dihydroxyacetone and lactic acid as potential biomaterials. *Biomacromolecules*. 2011, 12(4), 977-986. E-ISSN: 1526-4602.

92. SINGH, D., B. REDDY, A. GANESH, S. MAHAJANI. Zinc/Lanthanum Mixed-Oxide Catalyst for the Synthesis of Glycerol Carbonate by Transesterification of Glycerol. *Industrial & Engineering Chemistry Research*. 2014, 53(49), 18786-18795. ISSN: 0888-5885.

93. WANG, X., P. ZHANG, P. CUI, W. CHENG, S. ZHANG. Glycerol carbonate synthesis from glycerol and dimethyl carbonate using guanidine ionic liquids. *Chinese Journal of Chemical Engineering*. 2017, 25(9), 1182-1186. ISSN: 1004-9541.

94. ANITHA, M., S. K. KAMARUDIN, N. T. KOFLI. The potential of glycerol as a value-added commodity. *Chemical Engineering Journal*. 2016, 295, 119-130. ISSN: 1385-8947.

95. GEORGE, J., Y. PATEL, S. M. PILLAI, P. MUNSHI. Methanol assisted selective formation of 1,2-glycerol carbonate from glycerol and carbon dioxide using $^{n}Bu_2SnO$ as a catalyst. *Journal of Molecular Catalysis A: Chemical*. 2009, 304(1), 1-7. ISSN: 1381-1169.

96. PARK, J. H., J. S. CHOI, S. K. WOO, S. D. LEE, M. CHEONG, H. S. KIM, H. LEE. Isolation and characterization of intermediate catalytic species in the Zn-catalyzed glycerolysis of urea. *Applied Catalysis A: General*. 2012, 433-434, 35-40. ISSN: 0926-860X .

97. TENG, W. K., G. C. NGOH, R. YUSOFF, M. K. AROUA. A review on the performance of glycerol carbonate production via catalytic transesterification: Effects of influencing parameters. *Energy Conversion and Management*. 2014, 88, 484-497. ISSN: 0196-8904.

98. BAI, R., Y. WANG, S. WANG, F. MEI, T. LI, G. LI. Synthesis of glycerol carbonate from glycerol and dimethyl carbonate catalyzed by $NaOH/\gamma-Al_2O_3$. *Fuel Processing Technology*. 2013, 106, 209-214. ISSN: 0378-3820.

99. DU, M., Q. LI, W. DONG, T. GENG, Y. JIANG. Synthesis of glycerol carbonate from glycerol and dimethyl carbonate catalyzed by K_2CO_3 /MgO. *Research on Chemical Intermediates*. 2012, 38(3), 1069-1077. ISSN: 0922-6168.

100. GOMEZ-JIMENEZ-ABERASTURI, O., J. R. OCHOA-GOMEZ, A. PESQUERA-RODRIGUEZ, C. RAMIREZ-LOPEZ, A. ALONSO-VICARIO, J. TORRECILLA-SORIA. Solvent-free synthesis of glycerol carbonate and glycidol from 3-chloro-1,2-propanediol and potassium (hydrogen) carbonate. *Journal of Chemical Technology & Biotechnology*. 2010, 85(12), 1663-1670. ISSN: 0268-2575.

101. MOTA, Claudio J. A., Bianca P. PINTO, Ana L. DE LIMA. *Glycerol: A Versatile Renewable Feedstock for the Chemical Industry*. Springer International Publishing AG, 2017. ISBN: 9783319593746.

102. ZHOU, C. H. C., J. N. BELTRAMINI, Y. X. FAN, G. Q. M. LU. Chemoselective catalytic conversion of glycerol as a biorenewable source to valuable commodity chemicals. *Chemical Society Reviews*. 2008, 37(3), 527-549. ISSN: 0306-0012.

103. LUQUE, R., J. CAMPELO, J. CLARK. *Handbook of biofuels production: processes and technologies*. Burlington: Woodhead Publishing, 2010. ISBN: 1845696794.

104. TESTA, M. L., V. LA PAROLA, L. F. LIOTTA, A. M. VENEZIA. Screening of different solid acid catalysts for glycerol acetylation. *Journal of Molecular Catalysis A: Chemical*. 2013, 367, 69-76. ISSN: 1381-1169.

105. TALEBIAN-KIAKALAIEH, A., N. A. S. AMIN. Supported silicotungstic acid on zirconia catalyst for gas phase dehydration of glycerol to acrolein. *Catalysis Today*. 2015, 256, 315-324. ISSN: 0920-5861.

106. Process for producing biodiesel fuel with reduced viscosity and a cloud point below thirty-two (32) degrees Fahrenheit. Inventor: Hossein Noureddini. IPC: C10L 1/18. US patent 6015440. 2000-01-18. United States Patent and Trademark Office [seen on 2018-02-26]. Access via: https://patents.google.com/patent/US6015440A

107. MITTA, H., P. K. SEELAM, S. OJALA, R. L. KEISKI, P. BALLA. Tuning Y-zeolite based catalyst with copper for enhanced activity and selectivity in vapor phase hydrogenolysis of glycerol to 1,2-propanediol. *Applied Catalysis A: General*. 2018, 550, 308-319. ISSN: 0926-860X.

108. SUN, D., Y. YAMADA, S. SATO, W. UEDA. Glycerol hydrogenolysis into useful C3 chemicals. *Applied Catalysis B: Environmental*. 2016, 193, 75-92. ISSN: 0926-3373.

109. CLIMENT, M. J., A. CORMA, A. VELTY. Synthesis of hyacinth, vanilla, and blossom orange fragrances: the benefit of using zeolites and delaminated zeolites as catalysts. *Applied Catalysis A: General*. 2004, 263(2), 155-161. ISSN: 0926-860X.

110. ZHOU, L., E. AL-ZAINI, A. A. ADESINA. Catalytic characteristics and parameters optimization of the glycerol acetylation over solid acid catalysts. *Fuel*. 2013, 103, 617-625. ISSN: 0016-2361.

111. SUDARSANAM, P., B. MALLESHAM, A. N. PRASAD, P. S. REDDY, B. M. REDDY. Synthesis of bio–additive fuels from acetalization of glycerol with benzaldehyde over molybdenum promoted green solid acid catalysts. *Fuel Processing Technology*. 2013, 106, 539-545. ISSN: 0378-3820.

112. SILVA, P. H. R., V. L. C. GONCALVES, C. J. A. MOTA. Glycerol acetals as anti-freezing additives for biodiesel. *Bioresource Technology*. 2010, 101(15), 6225-6229. ISSN: 0960-8524.

113. SARI, P., M. RAZZAK, I. G. TUCKER. Isotropic Systems of Medium-Chain Mono- and Diglycerides for Solubilization of Lipophilic and Hydrophilic Drugs. *Pharmaceutical Development and Technology*. 2004, 9(1), 97-106. ISSN: 1083-7450.

114. NOR SHAHIRAH, M. N., S. ABDULLAH, J. GIMBUN, Y. H. NG, C. K. CHENG. A study on the kinetics of syngas production from glycerol over alumina-supported samarium–nickel catalyst. *International Journal of Hydrogen Energy*. 2016, 41(25), 10568-10577. ISSN: 0360-3199.

115. ADHIKARI, S., S. D. FERNANDO, A. HARYANTO. Hydrogen production from glycerin by steam reforming over nickel catalysts. *Renewable Energy*. 2008, 33(5), 1097-1100. ISSN: 0960-1481.

116. GO, Y. J., G. S. GO, H. J. LEE, D. J. MOON, N. C. PARK, Y. C. KIM. The relation between carbon deposition and hydrogen production in glycerol steam reforming. *International Journal of Hydrogen Energy*. 2015, 40(35), 11840-11847. ISSN: 0360-3199.

117. SILVA, J. M., M. A. SORIA, L. M. MADEIRA. Challenges and strategies for optimization of glycerol steam reforming process. *Renewable and Sustainable Energy Reviews*. 2015, 42, 1187-1213. ISSN: 1364-0321.

118. SCHWENGBER, C. A., H. J. ALVES, R. A. SCHAFFNER, F. A. DA SILVA, R. SEQUINEL, V. R. BACH, R. J. FERRACIN. Overview of glycerol reforming for hydrogen production. *Renewable and Sustainable Energy Reviews*. 2016, 58, 259-266. ISSN: 1364-0321.

119. GUTIERREZ ORTIZ, F.J., A. SERRERA, S. GALERA, P. OLLERO. Methanol synthesis from syngas obtained by supercritical water reforming of glycerol. *Fuel*. 2013, 105, 739-751. ISSN: 0016-2361.

120. Process for the preparation of polyglycerol. Inventor: H. Stuhler. IPC: C07C 41/01. US patent 4551561. 1985-11-05. United States Patent and Trademark Office [seen on 2018-02-26]. Access via: https://patents.google.com/patent/US4551561A

121. PISZCZYK, L., A. HEJNA, M. DANOWSKA, M. STRANKOWSKI, K. FORMELA. Polyurethane/ground tire rubber composite foams based on polyglycerol: Processing, mechanical and thermal properties. *Journal of Reinforced Plastics and Composites*. 2015, 34(9), 708-717. ISSN: 0731-6844.

122. AUVERGNE, R., S. CAILLOL, G. DAVID, B. BOUTEVIN, J. P. PASCAULT. Biobased thermosetting epoxy: present and future. *Chemical reviews*. 2014, 114(2), 1082-1115. E-ISSN: 1520-6890.

123. DE ARAUJO FILHO, C. A., S. HEREDIA, K. ERANEN, T. SALMI. Advanced millireactor technology for the kinetic investigation of very rapid reactions: Dehydrochlorination of 1,3-dichloro-2-propanol to epichlorohydrin. *Chemical Engineering Science.* 2016, 149, 35-41. ISSN: 0009-2509.

124. BELL, B., J. R. BRIGGS, R. CAMPBELL, S. M. CHAMBERS, P. D. GAARENSTROOM, J. G. HIPPLER, B. D. HOOK, K. KEARNS, J. M. KENNY, W. J. KRUPER, D. J. SCHRECK, C. N. THERIAULT, C. P. WOLFE. Glycerin as a renewable feed stock for epichlorohydrin production. The GTE Process. *CLEAN – Soil, Air, Water*. 2008, 36, 657–661. ISSN: 1863-0669.

125. SANTACESARIA, E., R. VITIELLO, R. TESSER, V. RUSSO, R. TURCO, M. DI SERIO. Chemical and Technical Aspects of the Synthesis of Chlorohydrins from Glycerol. *Industrial & Engineering Chemistry Research*. 2014, 53(22), 8939-8962. ISSN: 0888-5885.

126. PASCAULT, J. P., R. J. J. Williams. Epoxy polymers: new materials and innovations. In *Wiley Enciclopedia of Composites*. Weinheim, Germany: Wiley-VCH, 2010. ISBN: 978-3-527-32480-4.

127. MAY, C. A. *Epoxy resins: chemistry and technology*. New York: Marcel Dekker, 1988. ISBN 10: 0824776909 1-1288.

128. PASCAULT, J. P., H. SAUTEREAU, J. VERDU, R. J. J. WILLIAMS. *Thermosetting polymers*. New York: Marcel Dekker, 2002. ISBN: 0-8247-0670-6.

129. MAITRA, J., V. K. SHUKLA. Cross-linking in hydrogels - A Review. *American Journal of Polymer Science*. 2014, 4(2). 25-31. ISSN: 21631344.

130. BALANI, K., V. VERMA, A. AGARWAL, R. NARAYAN. Physical, thermal, and mechanical properties of polymers. In *Biosurfaces : A Materials Science and*

Engineering Perspective, (pp. 329-344). New Jersey: Hoboken, 2015. ISBN: 9781118299975.

131. SHAKER, Z. G., R. M. BROWNE, H. A. STRETZ, P. E. CASSIDY, M. T. BLANDA. Epoxy-toughened, unsaturated polyester interpenetrating networks. *Journal of Applied Polymer Science*. 2002, 84(12), 2283-2286. ISSN: 0021-8995.

132. VIJAYAN, P. P., D. PUGLIA, M. A. S. A. AL-MAADEED, J. M. KENNY, S. THOMAS. Elastomer/thermoplastic modified epoxy nanocomposites: The hybrid effect of 'micro' and 'nano' scale. *Materials Science & Engineering R*. 2017, 116, 1-29. ISSN: 0927-796X.

133. LIU, D., G. LI, B. LI, Y. LUAN, H. LING, X. YANG. In-situ toughened CFRP composites by shear-calender orientation and fiber-bundle filtration of PA microparticles at prepreg interlayer. *Composites Part A*. 2016, 84, 165-174. ISSN: 1359-835X.

134. ARNEBOLD, A., K. THIEL, E. KENTZINGER, A. HARTWIG. Morphological adjustment determines the properties of cationically polymerized epoxy resins. *RSC Advances*. 2015, 5(53), 42482-42491. ISSN: 2046-2069.

135. HARTWIG, A., A. LUHRING, J. TRAUTMANN. Nanoparticles in Epoxide-Based Adhesives. *Macromolecular Materials and Engineering*. 2009, 294(6-7), 363-379. ISSN: 1438-7492.

136. MA, J., M. S. MO, X. S. DU, P. ROSSO, K. FRIEDRICH, H. C. KUAN. Effect of inorganic nanoparticles on mechanical property, fracture toughness and toughening mechanism of two epoxy systems. *Polymer*. 2008, 49(16), 3510-3523. ISSN: 0032-3861.

137. OZEREN OZGUL, E., M. H. OZKUL. Effects of epoxy, hardener, and diluent types on the workability of epoxy mixtures. *Construction and Building Materials*. 2018, 158, 369-377. ISSN: 0950-0618.

138. FACHE, M., R. AUVERGNE, B. BOUTEVIN, S. CAILLOL. New vanillin-derived diepoxy monomers for the synthesis of biobased thermosets. *European Polymer Journal*. 2015, 67, 527-538. ISSN: 0014-3057.

139. KUMAR, A., T. VLACH, P. RYPAROVA, A. S. ŠKAPIN, J. KOVAČ, S. ADAMOPOULOUS, H. P. STERGIOS, M. PETRIČ. Influence of liquefied wood polyol on the physical-mechanical and thermal properties of epoxy based polymer. *Polymer Testing*. 2017, 64, 207-216. ISSN: 0142-9418.

140. NG, F., G. COUTURE, C. PHILIPPE, B. BOUTEVIN, S. CAILLOL. Bio-Based Aromatic Epoxy Monomers for Thermoset Materials. *Molecules*. 2017, 22(1), 1-49. ISSN: 14203049.

141. GASSMAN, N. R., E. COSKUN, D. F. STEFANICK, J. K. HORTON, P. JARUGA, M. DIZDAROGLU, S. H. WILSON. Bisphenol a promotes cell survival following oxidative DNA damage in mouse fibroblasts. *PloS one*. 2015, 10(2), 1-14. E-ISSN: 1932-6203.

142. MIKOLAJEWSKA, K., J. STRAGIEROWICZ, J. GROMADZINSKA. Bisphenol A - Application, sources of exposure and potential risks in infants, children and

pregnant women. *International journal of occupational medicine and environmental health*. 2015, 28(2), 209-241. E-ISSN: 1896-494X.

143. XIAO, Q., Y. LI, H. OUYANG, P. XU, D. WU. High-performance liquid chromatographic analysis of bisphenol A and 4-nonylphenol in serum, liver and testis tissues after oral administration to rats and its application to toxicokinetic study. *Journal of Chromatography B*. 2006, 830(2), 322-329. ISSN: 1570-0232.

144. U.S. Food and Drug Administration. (2018). *Questions & Answers on Bisphenol A (BPA) Use in Food Contact Applications* [seen on 2018-03-05]. Access via: https://www.fda.gov/Food/IngredientsPackagingLabeling/FoodAdditivesIngredients/ucm355155.htm

145. AMERICAN CHEMISTRY COUNCIL, INC. (2018). *U. S. Federal Government Research Provides Strong Support for BPA Safety* [seen on 2018-03-05]. Access via: https://www.factsaboutbpa.org/safety-assessments/fda-research-bpa-safety

146. JIN, N. J., J. YEON, I. SEUNG, K. S. YEON. Effects of curing temperature and hardener type on the mechanical properties of bisphenol F-type epoxy resin concrete. *Construction and Building Materials*. 2017, 156, 933-943. ISSN: 0950-0618.

147. AUDEBERT, M., L. DOLO, E. PERDU, J. CRAVEDI, D. ZALKO. Use of the γH2AX assay for assessing the genotoxicity of bisphenol A and bisphenol F in human cell lines. *Archives of Toxicology*. 2011, 85(11), 1463-1473. ISSN: 0340-5761.

148. ZHANG, L., F. PAN, X. LIU, L. YANG, X. JIANG, J. YANG, W. SHI. Multi-walled carbon nanotubes as sorbent for recovery of endocrine disrupting compound-bisphenol F from wastewater. *Chemical Engineering Journal*. 2013, 218, 238-246. ISSN: 1385-8947.

149. JIN, F. L., X. LI, S. J. PARK. Synthesis and application of epoxy resins: A review. *Journal of Industrial and Engineering Chemistry*. 2015, 29, 1-11. ISSN: 1226-086X.

150. GUO, B., D. JIA, W. FU, Q. QIU. Hygrothermal stability of dicyanate-novolac epoxy resin blends. *Polymer Degradation and Stability*. 2003, 79(3), 521-528. ISSN: 0141-3910.

151. GUAN, Z., L. LIU, L. HES. YANG. Amphiphilic hollow carbonaceous microspheres for the sorption of phenol from water. *Journal of Hazardous Materials*. 2011, 196, 270-277. ISSN: 0304-3894.

152. MORITA, Y. Cationic polymerization of hydrogenated bisphenol-A glycidyl ether with cycloaliphatic epoxy resin and its thermal discoloration. *Journal of Applied Polymer Science*. 2005, 97(3), 1395-1400. ISSN: 0021-8995.

153. BARONCINI, E. A., Y. KUMAR, P. SANTOSH, R. GIUSEPPE, J. F. STANZIONE. Recent advances in bio-based epoxy resins and bio-based epoxy curing agents. *Journal of Applied Polymer Science*. 2016, 44103, 1-19. ISSN: 0021-8995.

154. VAN DER PAS, D. J., K. M. TORR. Biobased Epoxy Resins from Deconstructed Native Softwood Lignin. *Biomacromolecules*. 2017, 18(8), 2640-2648. E-ISSN: 1526-4602.

155. ALGER, M. *Polymer science dictionary*. London: Chapman & Hall, 1997. ISBN: 0412608707.

156. LIU, S., V. S. CHEVALI, Z. XU, D. HUI, H. WANG. A review of extending performance of epoxy resins using carbon nanomaterials. *Composites Part B*. 2018, 136, 197-214. ISSN: 1359-8368.

157. AMERICAN CHEMISTRY COUNCIL, Polycarbonate-BPA Global Group. (No year given). *Bisphenol A (BPA)* [seen on 2018-03-05]. Access via: https://www.americanchemistry.com/Product-Groups-and-Stats/PolycarbonateBPA-Global-Group/

158. GERGELY, A., I. BERTOTI, T. TOROK, E. PFEIFER, E. KALMAN. Corrosion protection with zinc-rich epoxy paint coatings embedded with various amounts of highly dispersed polypyrrole-deposited alumina monohydrate particles. *Progress in Organic Coatings*. 2013, 76(1), 17-32. ISSN: 0300-9440.

159. LIU, S., H. YAN, Z. FANG, Z. GUO, H. WANG. Effect of graphene nanosheets and layered double hydroxides on the flame retardancy and thermal degradation of epoxy resin. *RSC Advances*. 2014, 4(36), 18652-18659. ISSN: 2046-2069.

160. LIU, W., Y. WANG, P. WANG, Y. LI, Q. JIANG, X. HU, Y. WEI, Y. QIU, S. I. S. SHAHABADI, X. LU. A biomimetic approach to improve the dispersibility, interfacial interactions and toughening effects of carbon nanofibers in epoxy composites. *Composites Part B*. 2017, 113, 197-205. ISSN: 1359-8368.

161. GUL, S., A. KAUSAR, M. MEHMOOD, B. MUHAMMAD, S. JABEEN. Progress on Epoxy/Polyamide and Inorganic Nanofiller-Based Hybrids: Introduction, Application, and Future Potential. *Polymer-Plastics Technology and Engineering*. 2016, 55(17), 1842-1862. ISSN: 0360-2559.

162. SUH, S. W., J. J. KIM, S. H. KIM, B. K. PARK. Effect of PI film surface on printing of Pd(II) catalytic ink for electroless copper plating in the printed electronics. *Journal of Industrial and Engineering Chemistry*. 2012, 18(1), 290-294. ISSN: 1226-086X .

163. JIN, N. J., I. SEUNG, Y. S. CHOI, J. YEON. Prediction of early-age compressive strength of epoxy resin concrete using the maturity method. *Construction and Building Materials*. 2017, 152, 990-998. ISSN: 0950-0618.

164. LUO, S., Z. QIAN, X. YANG, Q. LU. Fatigue behavior of epoxy asphalt concrete and its moisture susceptibility from flexural stiffness and phase angle. *Construction and Building Materials*. 2017, 145, 506-517. ISSN: 0950-0618.

165. LEE, S. H., Y. T. CHOI, H. M. LEE, D. W. PARK. Performance evaluation of directly fastened asphalt track using a full-scale test. *Construction and Building Materials*. 2016, 113, 404-414. ISSN: 0950-0618.

166. YOU, D., H. LIANG, W. MAI, R. ZENG, M. TU, J. ZHAO, Z. ZHA. Microwave-assisted functionalization of polyurethane surface for improving blood

compatibility. *Journal of Industrial and Engineering Chemistry*. 2013, 19(5), 1587-1592. ISSN: 1226-086X.

167. VAN WACHEM, P. B., R. ZEEMAN, P. J. DIJKSTRA, J. FEIJEN, M. HENDRIKS, P. T. CAHALAN, M. J. A. VAN LUYN. Characterization and biocompatibility of epoxy-crosslinked dermal sheep collagens. *Journal of Biomedical Materials Research*. 1999, 47(2), 270–277. ISSN: 1552-4965.

168. YAGCI, Y., S. JOCKUSCH, N. J. TURRO. Photoinitiated Polymerization: Advances, Challenges, and Opportunities. *Macromolecules*. 2010, 43(15), 6245-6260. ISSN: 0024-9297.

169. SANGERMANO, M., N. RAZZA, J. V. CRIVELLO. Cationic UV-Curing: Technology and Applications. *Macromolecular Materials Engineering*. 2014, 299, 775-793. ISSN: 1438-7492.

170. ARSU, N., I. REETZ, Y. YAGCI, M. K. MISHRA. Photoinitiated Radical Vinyl Polymerization. In *Handbook of Vinyl Polymers: Radical Polymerization, Process, and Technology*, (pp. 141-204). Boca Raton, FL: CRC Press, 2009. ISBN: 9780824725952.

171. MORSELLI, D. F. BONDIOLI, M. SANGERMANO, M. MESSORI. Photo-cured epoxy networks reinforced with TiO$_2$ in-situ generated by means of non-hydrolytic sol–gel process. *Polymer*. 2012, 53, 283-290. ISSN: 0032-3861.

172. GOLAZ, B., V. MICHAUD, J. A. E. MANSON. Photo-polymerized epoxy primer for adhesion improvement at thermoplastics/metallic wires interfaces. *Composites Part A*. 2013, 48, 171-180. ISSN: 1359-835X.

173. BAHRIA, H., Y. ERBIL. UV technology for use in textile dyeing and printing: Photocured applications. *Dyes and Pigments*. 2016, 134, 442-447. ISSN: 0143-7208.

174. POLYKAPROV, A., A. TIWARI. Photocured materials: a general perspective. In *Photocured materials*, (pp. 1-14). USA: Royal Society of Chemistry, 2015. ISBN: 978-1-78262-001-3.

175. LALEVEE, J., M. A. TEHFE, A. ZEIN-FAKIH, B. BALL, S. TELITEL, F. MORLET-SAVARY, B. GRAFF, J. P. FOUASSIER. N -Vinylcarbazole: An Additive for Free Radical Promoted Cationic Polymerization upon Visible Light. *ACS Macro Letters*. 2012, 1(7), 802-806. ISSN: 2161-1653.

176. SANGERMANO, M. Advances in cationic photopolymerization. *Pure and Applied Chemistry*. 2012, 84(10), 2089-2101. ISSN: 00334545.

177. SHI, S., C. CROUTXE-BARGHORN, X. ALLONAS. Photoinitiating systems for cationic photopolymerization: Ongoing push toward long wavelengths and low light intensities. *Progress in Polymer Science*. 2017, 65, 1-41. ISSN: 0079-6700.

178. CRIVELLO, J. V., E. REICHMANIS. Photopolymer Materials and Processes for Advanced Technologies. *Chemistry of Materials*. 2014, 26(1), 533-548. ISSN: 0897-4756.

179. PARK, C. H., S. TAKAHARA, T. YAMAOKA. The participation of the anion and alkyl substituent of diaryliodonium salts in photo-initiated cationic polymerization reactions. *Polymers for Advanced Technologies*. 2006, 17(3), 156-162. ISSN: 1042-7147.

180. CRIVELLO, J. V., J. MA, F. JIANG. Synthesis and photoactivity of novel 5-arylthianthrenium salt cationic photoinitiators. *Journal of Polymer Science Part A: Polymer Chemistry*. 2002, 40(20), 3465-3480. ISSN: 0887-624X.

181. GOMURASHVILI, Z., J. V. CRIVELLO. Phenothiazine photosensitizers for onium salt photoinitiated cationic polymerization. *Journal of Polymer Science Part A: Polymer Chemistry*. 2001, 39(8), 1187-1197. ISSN: 0887-624X.

182. CRIVELLO, J. V. UV and electron beam-induced cationic polymerization. *Nuclear Instruments and Methods in Physics Research B*. 1999, 151, 8-21. ISSN: 0168-583X.

183. ABADIE, M. J. M., N. K. CHIA, F. BOEY. Cure kinetics for the ultraviolet cationic polymerization of cycloliphatic and diglycidyl ether of bisphenol-A (DGEBA) epoxy systems with sulfonium salt using an auto catalytic model. *Journal of Applied Polymer Science*. 2002, 86(7), 1587-1591. ISSN: 0021-8995.

184. HARTWIG, A. Influence of moisture present during polymerisation on the properties of a photocured epoxy resin. *International Journal of Adhesion and Adhesives*. 2002, 22(5), 409-414. ISSN: 0143-7496.

185. TAKAHASHI, E., F. SANDA, T. ENDO. Photocationic and radical polymerizations of epoxides and acrylates by novel sulfonium salts. *Journal of Polymer Science Part A: Polymer Chemistry*. 2003, 41(23), 3816-3827. ISSN: 0887-624X.

186. LALEVEE, J., A. DIRANI, M. EL-ROZ, X. ALLONAS, J. P. FOUASSIER. Germanes as efficient coinitiators in radical and cationic photopolymerizations. *Journal of Polymer Science Part A: Polymer Chemistry*. 2008, 46(9), 3042-3047. ISSN: 0887-624X.

187. HARIKRISHNA, R., S. PONRATHNAM, S. S. TAMBE. Reaction kinetics and modeling of photoinitiated cationic polymerization of an alicyclic based diglycidyl ether. *Nuclear Instruments and Methods in Physics Research: B*. 2014, 318, 263-268. ISSN: 0168-583X.

188. YILDIZ, Z., H. A. ONEN. Dual-curable PVB based adhesive formulations for cord/rubber composites: The influence of reactive diluents. *International Journal of Adhesion and Adhesives*. 2017, 78, 38-44. ISSN: 0143-7496.

189. QIN, Y., T. YANG, M. FAN, J. CHENG, J. ZHANG. The effect of a renewable fatty acid derivatives based epoxy diluent on the curing kinetics and thermal properties of epoxy/anhydride systems. *Thermochimica Acta*. 2015, 614, 37-44. ISSN: 0040-6031.

190. QIAN, J. W., Y. M. MIAO, L. ZHANG, H. L. CHEN. Influence of viscosity slope coefficient of CA and its blends in dilute solutions on permeation flux of their films for MeOH/MTBE mixture. *Journal of Membrane Science*. 2002, 203(1), 167-173. ISSN: 0376-7388.

191. SHAW, S. J. Additives and modifiers for epoxy resins. In *Chemistry and Technology of Epoxy Resins*. Dordrecht: Springer, 1993. ISBN: 978-94-011-2932-9.

192. HARIKRISHNA, R. Kinetics of Photocationically Curable Formulations Involving Glycerol Diglycidyl Ether and Phenyl Glycidyl Ether. *Journal of Macromolecular Science: Part A*. 2014, 51(10), 788-795. ISSN: 1060-1325.

193. KIM, D., S. KIM. Vitrification effect on the curing reaction of epoxy resin. *Polymer Bulletin*. 1987, 18(6), 533-539. ISSN: 0170-0839.

194. HARIKRISHNA, R. Cationic photopolymerization kinetics of neat coating formulations involving poly(propylene glycol) diglycidyl ether and glycerol diglycidyl ether. *Journal of Thermal Analysis and Calorimetry*. 2015, 122(3), 1445-1454. ISSN: 1388-6150.

195. DEMENGEOT, E. A. C., I. BALIUTAVICIENE, J. OSTRAUSKAITE, L. AUGULIS, V. GRAZULEVICIENE, L. RAGELIENE, J. V. GRAZULEVICIUS. Crosslinking of epoxidized natural oils with diepoxy reactive diluents. *Journal of Applied Polymer Science*. 2010, 115(4), 2028-2038. ISSN: 0021-8995.

196. REMEIKYTE, A., J. OSTRAUSKAITE, V. GRAZULEVICIENE. Synthesis and properties of photocross-linked polymers of epoxidized linseed oil with different reactive diluents. *Journal of Applied Polymer Science*. 2013, 129(3), 1290-1298. ISSN: 0021-8995.

197. KOWALCZYK, K., A. KOWALCZYK. UV-curable epoxy varnishes modified with polyvinyl resins. *Progress in Organic Coatings*. 2015, 89, 100-105. ISSN: 0300-9440.

198. KUBISA, P. Hyperbranched polyethers by ring-opening polymerization: Contribution of activated monomer mechanism. *Journal of Polymer Science Part A: Polymer Chemistry*. 2003, 41(4), 457-468. ISSN: 0887-624X.

199. SANGERMANO, M., M. A. TASDELEN, Y. YAGCI. Photoinitiated curing of mono- and bifunctional epoxides by combination of active chain end and activated monomer cationic polymerization methods. *Journal of Polymer Science Part A: Polymer Chemistry*. 2007, 45(21), 4914-4920. ISSN: 0887-624X.

200. ARNEBOLD, A., K. THIEL, E. KENTZINGER, A. HARTWIG. Morphological adjustment determines the properties of cationically polymerized epoxy resins. *RSC Advances*. 2015, 5(53), 42482-42491. ISSN: 2046-2069.

201. ARNEBOLD, A., S. WELLMANN, A. HARTWIG. Covalent integration of differently structured polyester polyols improves the toughness and strength of cationically polymerized, amorphous epoxy networks. *Journal of Applied Polymer Science*. 2016, 133(38), 1-11. ISSN: 0021-8995.

202. PRADHAN, D., B. SAMANTARAY, R. CHOUDHARY, N. KARAN, R. THOMAS, R. KATIYAR. Effect of plasticizer on structural and electrical properties of nanocomposite solid polymer electrolytes. *Ionics*. 2011, 17(2), 127-134. ISSN: 0947-7047.

203. LIM, H., S. HOAG. Plasticizer Effects on Physical–Mechanical Properties of Solvent Cast Soluplus® Films. *AAPS PharmSciTech*. 2013, 14(3), 903-910. E-ISSN: 1530-9932.

204. REPKA, M. A., S. K. BATTU, S. B. UPADHYE, S. THUMMA, M. M. CROWLEY, F. ZHANG, C. MARTIN, J. W. MCGINITY. Pharmaceutical Applications of Hot-Melt Extrusion: Part II. *Drug Development and Industrial Pharmacy*. 2007, 33(10), 1043-1057. ISSN: 0363-9045.

205. TILBROOK, D. A., R. L. CLARKE, N. E. HOWLE, M. BRADEN. Photocurable epoxy–polyol matrices for use in dental composites I. *Biomaterials*. 2000, 21(17), 1743-1753. ISSN: 0142-9612

206. WANG, Z., X. LIN, W. LIU. Synthesis of bis(2,3-epoxycyclohexyl) and its cationic photopolymerization in the presence of different diols. *Polymer International*. 2009, 58(1), 74-80. ISSN: 0959-8103.

207. SANGERMANO, M., M. L. B. DUARTE, R. A. ORTIZ, A. G. S. GOMEZ, A. E. G. VALDEZ. Diol spiroorthocarbonates as antishrinkage additives for the cationic photopolymerization of bisphenol-A–diglycidyl ether. *Reactive and Functional Polymers*. 2010, 70(2), 98-102. ISSN: 1381-5148.

208. CHIANG, T. H., T. E. HSIEH. A study of monomer's effect on adhesion strength of UV-curable resins. *International Journal of Adhesion and Adhesives*. 2006, 26(7), 520-531. ISSN: 0143-7496.

209. NASH, H., H. DOCKTOR, D. WEBSTER. Effect of composition on performance properties in cationic UV-curable coating systems. *JCT Research*. 2004, 1(3), 153-161. ISSN: 1547-0091.

210. CHEN, Z., D. C. WEBSTER. Study of the effect of hyperbranched polyols on cationic UV curable coating properties. *Polymer International*. 2007, 56(6), 754-763. ISSN: 0959-8103.

211. DILLMAN, B., J. L. P. JESSOP. Chain transfer agents in cationic photopolymerization of a bis-cycloaliphatic epoxide monomer: Kinetic and physical property effects. *Journal of Polymer Science Part A: Polymer Chemistry*. 2013, 51(9), 2058-2067. ISSN: 0887-624X.

212. CRIVELLO, J. V., J. MA, F. JIANG, H. HUA, J. AHN, R. ACOSTA ORTIZ. Advances in the Design of Photoinitiators, Photo-Sensitizers and Monomers for Photoinitiated Cationic Polymerization. *Macromolecular Symposia*. 2004, 215(1), 165-178. ISSN: 1022-1360.

213. VAN WIJK, A., I. VAN WIJK. *3D printing with biomaterials towards a sustainable and circular economy*. Amsterdam, The Netherlands: IOS Press, 2015. ISBN 978-1-61499-486-2.

214. LIGON, S. C., R. LISKA, J. STAMPFL, M. GURR, R. MULHAUPT. Polymers for 3D Printing and Customized Additive Manufacturing. *Chemical reviews*. 2017, 117(15), 10212-10290. E-ISSN: 1520-6890.

215. WANG, X., M. JIANG, Z. ZHOU, J. GOU, D. HUI. 3D printing of polymer matrix composites: A review and prospective. *Composites Part B*. 2017, 110, 442-458. ISSN: 1359-8368.

216. WANG, K., C. C. HO, C. ZHANG, B. WANG. A Review on the 3D Printing of Functional Structures for Medical Phantoms and Regenerated Tissue and Organ Applications. *Engineering*. 2017, 3(5), 653-662. ISSN: 2095-8099.

217. SAKIN, M., Y. C. KIROGLU. 3D Printing of Buildings: Construction of the Sustainable Houses of the Future by BIM. *Energy Procedia*. 2017, 134, 702-711. ISSN: 1876-6102.

218. TAHAYERI, A., M. MORGAN, A. P. FUGOLIN, D. BOMPOLAKI, A. ATHIRASALA, C. S. PFEIFER, J. L. FERRACANE, L. E. BERTASSONI. 3D printed versus conventionally cured provisional crown and bridge dental materials. *Dental Materials*. 2018, 34(2), 192-200. ISSN: 0109-5641.

219. HASHEMI SANATGAR, R., C. CAMPAGNE, V. NIERSTRASZ. Investigation of the adhesion properties of direct 3D printing of polymers and nanocomposites

on textiles: Effect of FDM printing process parameters. *Applied Surface Science*. 2017, 403, 551-563. ISSN: 0169-4332.

220. LILLE, M., A. NURMELA, E. NORDLUND, S. METSA-KORTELAINEN, N. SOZER. Applicability of protein and fiber-rich food materials in extrusion-based 3D printing. *Journal of Food Engineering*. 2018, 220, 20-27. ISSN: 0260-8774.

221. NGO, T. D., A. KASHANI, G. IMBALZANO, K. T. Q. NGUYEN, D. HUI. Additive manufacturing (3D printing): A review of materials, methods, applications and challenges. *Composites Part B*. 2018, 143, 172-196. ISSN: 1359-8368.

222. NIESLER, F., M. HERMATSCHWEILER, A. WERNER. (2014). *Lasers for 3D Printing: Additive manufacturing with NIR lasers forms micro-sized parts* [seen on 2018-03-28]. Access via: https://www.laserfocusworld.com/articles/print/volume-50/issue-08/features/lasers-for-3d-printing-additive-manufacturing-with-nir-lasers-forms-micro-sized-parts.html

223. THIEL, M., M. HERMATSCHWEILER. Three-dimensional laser lithography. *Optik & Photonic*. 2011, 6(4), 36-39. ISSN:2191-1975.

224. SENIUTINAS, G., A. WEBER, C. PADESTE, I. SAKELLARI, M. FARSARI, C. DAVID. Beyond 100 nm resolution in 3D laser lithography — Post processing solutions. *Microelectronic Engineering*. 2018, 191, 25-31. ISSN: 0167-9317.

225. FREY, S. (2017). *Laser SLA vs DLP vs Masked SLA 3D Printing Technology* [seen on 2018-03-28]. Access via: http://theorthocosmos.com/laser-sla-vs-dlp-vs-masked-sla-3d-printing-technology-compared/

226. MELCHELS, F. P. W., J. FEIJEN, D. W. GRIJPMA. A review on stereolithography and its applications in biomedical engineering. *Biomaterials*. 2010, 31(24), 6121-6130. ISSN: 0142-9612.

227. CHO, Y. H., I. H. LEE, D. W. CHO. Laser scanning path generation considering photopolymer solidification in micro-stereolithography. *Microsystem Technologies*. 2005, 11(2), 158-167. ISSN: 0946-7076.

228. *PR48-Clear Clear Prototyping Material (Technical Data Sheet)*. (no year given). [seen on 2018-03-28]. Access via: http://cpspolymers.com/PR48%20TDS.pdf

229. *RenShape® SL 5170 (Technical Data Sheet)*. (2002). [seen on 2018-03-29]. Access via: http://www-eng.lbl.gov/~dw/projects/DW4219_RP_Materials_Testing/Project_final/Material%20data%20sheets/SL%205170%20(US)_250_final.pdf

230. *SU-8 2000 Permanent Epoxy Negative Photoresist (Processing guidelines)*. (no year given). [seen on 2018-03-29]. Access via: http://www.microchem.com/pdf/SU-82000DataSheet2000_5thru2015Ver4.pdf

231. *SOMOS® Products*. (no year given). [seen on 2018-03-29]. Access via: https://www.dsm.com/products/somos/en_US/products.html

232. *MATERIALS for Stereolithography*. (2016). [seen on 2018-03-29]. Access via: https://proto3000.com/sla-photopolymer-materials.php

233. *3D Printing and Additive Manufacturing*. (2018). [seen on 2018-03-29]. Access via: https://www.paragon-rt.com/Stereolithography-SLA

234. JACKS, C. V., W. D. BRIND, R. SMITH. (1955). Mulching. *Technical Communication No.49 of the commonwealth bureau of the soil science* [seen on

2018-03-30]. Access via: http://krishikosh.egranth.ac.in/bitstream/1/2034248/1/565.pdf

235. CHALKER-SCOTT, L. (2007). Impact of Mulches on Landscape Plants and the Environment — A Review. *Journal of Environmental Horticulture*, 25(4), 239-249. [seen on 2018-03-30]. Access via: http://hrijournal.org/doi/pdf/10.24266/0738-2898-25.4.239

236. ADEKALU, K. O., I. A. OLORUNFEMI, J. A. OSUNBITAN. Grass mulching effect on infiltration, surface runoff and soil loss of three agricultural soils in Nigeria. *Bioresource Technology*. 2007, 98(4), 912-917. ISSN: 0960-8524.

237. KADER, M. A., M. SENGE, M. A. MOJID, K. ITO. Recent advances in mulching materials and methods for modifying soil environment. *Soil & Tillage Research*. 2017, 168, 155-166. ISSN: 0167-1987.

238. CUELLO, J. P., H. Y. HWANG, J. GUTIERREZ, S. Y. KIM, P. J. KIM. Impact of plastic film mulching on increasing greenhouse gas emissions in temperate upland soil during maize cultivation. *Applied Soil Ecology*. 2015, 91, 48-57. ISSN: 0929-1393.

239. BRODHAGEN, M., M. PEYRON, C. MILES, D. INGLIS. Biodegradable plastic agricultural mulches and key features of microbial degradation. *Applied Microbiology and Biotechnology*. 2015, 99(3), 1039-1056. ISSN: 0175-7598.

240. TAN, Z., Y. YI, H. WANG, W. ZHOU, Y. YANG, C. WANG. Physical and Degradable Properties of Mulching Films Prepared from Natural Fibers and Biodegradable Polymers. *Applied Sciences*. 2016, 147(6), 1-11. ISSN 2076-3417.

241. AZLIN-HASIM, S., M. C. CRUZ-ROMERO, E. CUMMINS, J. P. KERRY, M. A. MORRIS. The potential use of a layer-by-layer strategy to develop LDPE antimicrobial films coated with silver nanoparticles for packaging applications. *Journal of Colloid And Interface Science*. 2016, 461, 239-248. ISSN: 0021-9797.

242. MA, Z., Y. MA, L. QIN, J. LIU, H. SU. Preparation and characteristics of biodegradable mulching films based on fermentation industry wastes. *International Biodeterioration & Biodegradation*. 2016, 111, 54-61. ISSN: 0964-8305.

243. ABRUSCI, C., J. L. PABLOS, T. CORRALES, J. LOPEZ-MARIN, I. MARIN, F. CATALINA. Biodegradation of photo-degraded mulching films based on polyethylenes and stearates of calcium and iron as pro-oxidant additives. *International Biodeterioration & Biodegradation*. 2011, 65(3), 451-459. ISSN: 0964-8305.

244. SCARASCIA-MUGNOZZA, G., C. SICA, G. RUSSO. Plastic materials in European agriculture: actual use and perspectives. *Journal of Agricultural Engineering*. 2012, 42 (3), 15-28. ISSN: 1974-7071.

245. KASIRAJAN, S., M. NGOUAJIO. Polyethylene and biodegradable mulches for agricultural applications: a review. *Agronomy for Sustainable Development*. 2012, 32, 501-529. ISSN: 1774-0746.

246. FRANCA, D. C., T. G. ALMEIDA, G. ABELS, E. L. CANEDO, L. H. CARVALHO, R. M. R. WELLEN, K. HAAG, K. KOSCHEK. Tailoring PBAT/PLA/Babassu films for suitability of agriculture mulch application. *Journal of Natural Fibers*. 2018, 1-11. ISSN: 1544-0478.

247. CHIELLINI, E., P. CINELLI, S. MAGNI, S. MIELE, C. PALLA. Fluid biomulching based on poly(vinyl alcohol) and fillers from renewable resources. *Journal of Applied Polymer Science*. 2008, 108(1), 295-301. ISSN: 0021-8995.

248. DANG, X., Z. SHAN, H. CHEN. The Preparation and Applications of One Biodegradable Liquid Film Mulching by Oxidized Corn Starch-Gelatin Composite. *Applied Biochemistry and Biotechnology*. 2016, 180(5), 917-929. ISSN: 0273-2289.

249. WEI, D., H. WANG, Z. ZIAEE, F. CHIBANTE, A. ZHEG, H. XIAO. Non-leaching antimicrobial biodegradable PBAT films through a facile and novel approach. *Materials Science & Engineering C*. 2016, 58, 986-991. ISSN: 0928-4931.

250. KIJCHAVENGKUL, T., R. AURAS, M. RUBINO, M. NGOUAJIO, R. T. FERNANDEZ. Assessment of aliphatic–aromatic copolyester biodegradable mulch films. Part I: Field study. *Chemosphere*. 2008, 71(5), 942-953. ISSN: 0045-6535.

251. EGUES, I., M. GONZALEZ ALRIOLS, Z. HERSECZKI, G. MARTON, J. LABIDI. Hemicelluloses obtaining from rapeseed cake residue generated in the biodiesel production process. *Journal of Industrial and Engineering Chemistry*. 2010, 16(2), 293-298. ISSN: 1226-086X.

252. RASHAD, A. M. Phosphogypsum as a construction material. *Journal of Cleaner Production*. 2017, 166, 732-743. ISSN: 0959-6526.

253. HOLKAR, C. R., S. S. JAIN, A. J. JADHAV, D. V. PINJARI. Valorization of keratin based waste. *Process Safety and Environmental Protection*. 2018, 115, 85-98. ISSN: 0957-5820.

254. KOLAY, A.K. *Manures and fertilizers*. India: Atlantic Publishers & Distributors, 2007. ISBN-10: 8126908106.

255. KORNILLOWICZ-KOWALSKA, T., J. BOHACZ. Biodegradation of keratin waste: Theory and practical aspects. *Waste Management*. 2011, 31(8), 1689-1701. ISSN: 0956-053X.

256. WOLICKA, D. Biotransformation of phosphogypsum in wastewaters from the dairy industry. *Bioresource Technology*. 2008, 99(13), 5666-5672. ISSN: 0960-8524.

257. WIAZ, M., W. MROCZYK, D. JOZEFIAK, A. RUTKOWSKI. Composition of rapeseed cakes and meals manufactured under different technological conditions. *Journal of Animal and Feed Sciences*. 2005, 14(1), 507-510.

258. TREINYTE, J., V. GRAZULEVICIENE, I. GRIGALAVICIENE, E. MISKINE, D. BRIDZIUVIENE. Polymer Composites from Poly(vinyl alcohol), Horn Meal and Crude Glycerol for Mulching Coatings. *Waste and Biomass Valorization*. 2017, 8, 1225-1235. ISSN: 1877-2641.

259. TREINYTE, J., L. CESONIENE, D. BRIDZIUVIENE, J. OSTRAUSKAITE, A. BUCINSKAS, E. RAINOSALO, V. GRAZULEVICIENE. Applicability of crude glycerol as the multifunctional additive for the preparation of mulching coatings. *Waste and Biomass Valorization*. 2018, 1-11. Access via doi: 10.1007/s12649-017-9966-1.

260. TREINYTE, J., V. GRAZULEVICIENE, J. OSTRAUSKAITE. Biodegradable polymer composites with nitrogen- and phosphorus-containing waste materials as

the fillers. *Ecological Chemistry and Engineering S*. 2014, 21(3), 515-528. ISSN: 1898-6196.

261. SKLIUTAS, E., S. KASETAITE, L. JONAUSKAS, J. OSTRAUSKAITE, M. MALINAUSKAS. Photosensitive naturally derived resins toward optical 3-D printing. *Optical engineering*. 2018, 57(4), 1-9. ISSN: 0091-3286.

262. FLORY, P. J. *Principles of Polymer Chemistry*. Ithaca, United States: Cornell University Press, 1953. ISBN-0801401348.

263. MOY, E., NEUMANN, A. W. Solid/liquid interfacial tensions from contact angle data and direct force measurements. *Journal of Colloid and Interface Science*. 1987, 119(1), 296-297. Access via doi: 10.1016/0021-9797(87)90273-6.

264. LI, D., A. W. NEUMANN. Equation of state for interfacial tensions of solid-liquid systems. *Advances in Colloid and Interface Science*. 1992, 39, 299-345. Access via doi: 10.1016/0001-8686(92)80064-5.

265. OWENS, D. K., R. C. WENDT. Estimation of the surface free energy of polymers. *Journal of Applied Polymer Science*. 1969, 13(8), 1741-1747. Access via doi: 10.1002/app.1969.070130815.

266. KAELBLE, D. H. Dispersion-Polar Surface Tension Properties of Organic Solids. *Journal of Adhesion*. 1970, 2(2), 66-81. Access via doi: 10.1080/0021846708544582.

267. WU, S. Calculation of interfacial tension in polymer systems. *Journal of Polymer Sciece*. 1971, 34(1), 19-30. Access via doi: 10.1002/polc.5070340105.

268. WU, S. Polar and Nonpolar Interactions in Adhesion. *Journal of Adhesion*. 1973, 5(1), 39-55. Access via doi: 10.1080/00218467308078437.

269. YOUNG, T. An essay on the cohesion of fluids. *Philosophical Transactions of the Royal Society of London*. 1805, 95, 65-87. Access via doi: 10.1098/rstl.1805.0005.

270. BOTELLA, A., J. DUPUY, A. A. ROCHE, H. SAUTEREAU, V. VERNEY. Photo-Rheometry/NIR Spectrometry: An in situ Technique for Monitoring Conversion and Viscoelastic Properties during Photopolymerization. *Macromolecular Rapid Communications*. 2004, 25(12), 1155-1158. ISSN: 1022-1336.

271. MEYERS, M. A., K. K. CHAWLA. *Mechanical Behavior of Materials*. New Jersey: Prentice-Hall, 1999. ISBN 978-0-521-86675-0.

272. CANDAN, Z., D. J. GARDNER, S. M. SHALER. Dynamic mechanical thermal analysis (DMTA) of cellulose nanofibril/nanoclay/pMDI nanocomposites. *Composites Part B*. 2016, 90, 126-132. ISSN: 1359-8368.

273. KREUTZER, J., X. H. QIN, C. GORSCHE, H. PETERLIK, R. LISKA, U. SCHUBERT. Variation of the crosslinking density in cluster-reinforced polymers. *Materials Today Communications*. 2015, 5, 10-17. ISSN: 2352-4928.

274. MEZGER, T. G. *The Rheology Handbook*. 3rd ed. Hanover: Vincentz Network, 2011. ISBN 978-3-86630-890-9.

275. RIEGER, J. The glass transition temperature T_g of polymers—Comparison of the values from differential thermal analysis (DTA, DSC) and dynamic mechanical measurements (torsion pendulum). *Polymer Testing*. 2001, 20(2), 199-204. ISSN: 0142-9418.

276. KARSLI, N. G., A. AYTAC. Tensile and thermomechanical properties of short carbon fiber reinforced polyamide 6 composites. *Composites Part B: Engineering*. 2013, 51, 270-275. ISSN: 1359-8368.

277. MENG, Q., I. ZAMAN, J. R. HANNAM, S. KAPOTA, L. LUONG, O. YOUSSF, J. MA. Improvement of adhesive toughness measurement. *Polymer Testing*. 2011, 30(2), 243-250. ISSN: 0142-9418.

278. KEMEI, S. K., M. S. K. KIRUI, F. G. NDIRITU, P. M. ODHIAMBO, R. G. NGUMBU, D. M. G. LEITE, A. L. J. PEREIRA. Storage moduli, loss moduli and damping factor of GaAs and GaMnAs thin films using DMA 2980. *Materials Science in Semiconductor Processing*. 2014, 20, 23-27. ISSN: 13698001.

279. POLYMER PROPERTIES DATABASE. (2015). *Rubbery Plateau and Entanglements* [seen on 2018-04-17]. Access via: http://polymerdatabase.com/polymer%20physics/RubberyPlateau.html

280. BARRIOS-ESTRADA, C., M. D. J. ROSTRO-ALANIS, A. L. PARRA, M. P. BELLEVILLE, J. SANCHEZ-MARCANO, H. M. N. IQBAL, R. PARRA-SALDIVAR. Potentialities of active membranes with immobilized laccase for Bisphenol A degradation. *International Journal of Biological Macromolecules*. 2018, 108, 837-844. ISSN: 0141-8130.

281. TOYAMA, T., Y. SATO, D. INOUE, K. SEI, Y. C. CHANG, S. KIKUCHI, M. IKE. Biodegradation of bisphenol A and bisphenol F in the rhizosphere sediment of Phragmites australis. *Journal of Bioscience and Bioengineering*. 2009, 108(2), 147-150. ISSN: 1389-1723.

282. STAPLES, C. A., P. B. DOME, G. M. KLECKA, S. T. OBLOCK, L. R. HARRIS. A review of the environmental fate, effects, and exposures of bisphenol A. *Chemosphere*. 1998, 36(10), 2149-2173. ISSN: 0045-6535.

283. *DISSOCIATION CONSTANTS OF ORGANIC ACIDS AND BASES*. (no year given). [seen on 2018-04-23]. Access via: https://www.zirchrom.com/organic.htm

284. EPPINK, M. H. M., E. CAMMAART, D. VAN WASSENAAR, W. J. MIDDELHOVEN, W. J. H. VAN BERKEL. Purification and properties of hydroquinone hydroxylase, a FAD-dependent monooxygenase involved in the catabolism of 4-hydroxybenzoate in *Candida parapsilosis* CBS604. *European Journal of Biochemistry*. 2000, 267(23), 6832-6840. ISSN: 0014-2956.

285. KAMADA, F., S. ABE, N. HIRATSUKA, H. WARIISHI, H. TANAKA. Mineralization of aromatic compounds by brown-rot basidiomycetes - mechanisms involved in initial attack on the aromatic ring. *Microbiology*. 2002, 148 (6), 1939-1947. ISSN: 0026-2617.

286. LEITAO, A. L., M. P. DUARTE, J. S. OLIVEIRA. Degradation of phenol by a halotolerant strain of Penicillium chrysogenum. *International Biodeterioration & Biodegradation*. 2007, 59(3), 220-225. ISSN: 0964-8305.

287. NAKAMURA, T., H. ICHINOSE, H. WARIISHI. Flavin-containing monooxygenases from Phanerochaete chrysosporium responsible for fungal metabolism of phenolic compounds. *Biodegradation*. 2012, 23(3), 343-350. ISSN: 0923-9820.

288. CHEVIGNY, C., N. JOUAULT, F. DALMAS, F. BOUE, J. JESTIN. Tuning the mechanical properties in model nanocomposites: Influence of the polymer-filler

interfacial interactions. *Journal of Polymer Science Part B: Polymer Physics*. 2011, 49, 781-791. ISSN:1099-0488.

289. *CALCULATION OF SURFACE FREE ENERGY (SFE) FROM CONTACT ANGLE RESULTS*. (no year given). [seen on 2018-04-26]. Access via: http://www.surface-tension.org/article/65.html

LIST OF SCIENTIFIC PUBLICATIONS

Publications on the theme of the dissertation in the journals of the main list of *Clarivate Analytics Web of Science* database

1. **Kašėtaitė, Sigita**; Ostrauskaitė, Jolita; Gražulevičienė, Violeta; Svedienė, Jurgita; Bridžiuvienė, Danguolė. Photocross-linking of glycerol diglycidyl ether with reactive diluents // Polymer bulletin. Berlin : Springer. ISSN 0170-0839. 2015, vol. 72, iss. 12, p. 3191-3208.

2. **Kašėtaitė, Sigita**; Ostrauskaitė, Jolita; Gražulevičienė, Violeta; Bridžiuvienė, Danguolė; Rainosalo, Egidija. Biodegradable glycerol-based polymeric composites filled with industrial waste materials // Journal of Composite Materials. London : SAGE. ISSN 0021-9983. 2017, vol. 51, iss. 29, p. 4029-4039.

3. **Kašėtaitė, Sigita**; Ostrauskaitė, Jolita; Gražulevičienė, Violeta; Bridžiuvienė, Danguolė; Budreckienė, Rūta; Rainosalo, Egidija. Biodegradable photocross-linked polymers of glycerol diglycidyl ether and structurally different alcohols // Reactive and Functional Polymers. Amsterdam : Elsevier. ISSN 1381-5148. 2018, vol. 122, p. 42-50.

4. Skliutas, Edvinas; **Kašėtaitė, Sigita**; Jonušauskas, Linas; Ostrauskaitė, Jolita; Malinauskas, Mangirdas. Photosensitive naturally derived resins toward optical 3-D printing // Optical Engineering. Bellingham : SPIE. ISSN 0091-3286. 2018, vol. 57, iss. 4, p. 1-9.

Articles in conference proceedings

1. **Kašėtaitė, Sigita**; Ostrauskaitė, Jolita; Gražulevičius, Juozas Vidas. Photocross-linked polymers of glycerol diglycidyl ether // Baltic polymer symposium 2014: Laulasmaa, Estonia, September 24-26, 2014 : program and abstracts / Tallinn University of Technology. Tallinn: Tallinn University of Technology. 2014, p. 98.

2. **Kašėtaitė, Sigita**; Ostrauskaitė, Jolita; Gražulevičienė, Violeta. Glycerol-based polymeric composites reinforced with production wastes // Chemistry and chemical technology 2015 : programme and proceedings of the international conference, Vilnius, Lithuania, January 23, 2015 / Vilnius University, Lithuanian Academy of Sciences, Kaunas University of Technology, Center for Physical Sciences and Technology. [S.l. : s.n.], 2015. ISBN 9786094594618. p. 299-300.

3. **Kašėtaitė, Sigita**; Ostrauskaitė, Jolita; Gražulevičienė, Violeta. Glycerol-based polymeric composites filled with industrial waste materials // Baltic polymer symposium 2015: Sigulda, Latvia, September 16-18 : programme and

proceedings / Riga Technical University. Institute of Polymer Materials. Riga : [s.n.], 2015. ISBN9789934542121. p. 146.

4. **Kašėtaitė, Sigita**; Ostrauskaitė, Jolita; Gražulevičienė, Violeta. Photorheometrical study of compositions based on glycerol diglycidyl ether and di- or trihydroxylic alcohols // Chemistry and chemical technology : international conference of Lithuanian Society of Chemistry : Lithuanian Academy of Science, Vilnius, Lithuania, April 28-29, 2016 : book of abstracts / Fizinių ir technologijos mokslų centras, Vilniaus universitetas, Lietuvos mokslų akademija, Kauno technologijos universitetas. 2016, p. 181.

5. Skliutas, Edvinas; **Kašėtaitė, Sigita**; Ostrauskaitė, Jolita; Malinauskas, Mangirdas. 3D optical printing and custom made resins // Open readings 2016 : 59th scientific conference for students of physics and natural sciences : programme and abstracts. Vilnius : Vilniaus universiteto leidykla. ISSN 2029-4425. 2016, p. 197.

6. **Kašėtaitė, Sigita**; Ostrauskaitė, Jolita; Gražulevičienė, Violeta. Photorheometrical study of compositions based on glycerol diglycidyl ether and industrial waste materials // BiPoCo 2016 : 3rd international conference "Bio-based polymers and composites, August 28 - September 1, 2016, Szeged, Hungary : abstract book. [Budapest] : [BiPoCo]. 2016, p. 332-333.

7. **Kašėtaitė, Sigita**; Ostrauskaitė, Jolita; Gražulevičienė, Violeta. Photo-curable glycerol-based polymers with structurally different alcohols // Baltic polymer symposium 2016 : Klaipeda, September 21-24, 2016 : programme and abstracts / Kaunas University of Technology, Vilnius University, Klaipeda University. Kaunas : Kaunas University of Technology, 2016. ISBN 9786090212356. p. 71.

8. Skliutas, Edvinas; **Kašėtaitė, Sigita**; Grigalevičiūtė, Giedrė; Jonušauskas, Linas; Rekštytė, Sima; Ostrauskaitė, Jolita; Malinauskas, Mangirdas. Bioresists from renewable resources as sustainable photoresins for 3D laser microlithography: material synthesis, cross-linking rate and characterization of the structures // Proceedings of SPIE : Advanced fabrication technologies for micro/nano optics and photonics X, Jan 28 - Feb 2, 2017, San Francisco, California, United States / Editors: Georg von Freymann, Winston V. Schoenfeld, Raymond C. Rumpf. Bellingham, WA : SPIE. ISSN 0277-786X. 2017, vol. 10115, article 1011514, p. 1-11. DOI: 10.1117/12.2249600.

9. Malachovskienė, Eglė; Bridžiuvienė, Danguolė; **Kašėtaitė, Sigita**; Ostrauskaitė, Jolita. Degradative impact of fungi on newly synthesized copolymers of glycerol diglycidyl ether and different diols // COINS : international conference of Life sciences : abstract book. [S.l : s.n. 2017, p. 82-84.

10. Skliutas, Edvinas; **Kašėtaitė, Sigita**; Jonušauskas, Linas; Rekštytė, Sima; Ostrauskaitė, Jolita; Malinauskas, Mangirdas. Bioresists from renewable resources as sustainable photoresins for 3d laser microlithography: material synthesis, cross-linking rate and characterization of the structures // Open readings 2017 : 60 scientific conference for students of physics and natural

sciences, March 14-17, 2017 Vilnius, Lithuania : programme and abstracts. Vilnius : Vilnius University. ISSN 2029-4425. 2017, p. 228.

11. **Kašėtaitė, Sigita**; Ostrauskaitė, Jolita; Gražulevičienė, Violeta. DMTA analysis of glycerol diglycidyl ether based photocross-linked polymers // Proceedings of the 3rd World Congress on Mechanical, Chemical, and Material Engineering, MCM'17, Rome, Italy, June 8–10, 2017. Ottawa : International ASET Inc. ISSN 2369-8136. 2017, article ICCPE106, p. 1-5. DOI: 10.11159/iccpe17.106.

12. Skliutas, Edvinas; **Kašėtaitė, Sigita**; Jonušauskas, Linas; Ostrauskaitė, Jolita; Malinauskas, Mangirdas. Link 3D gamtinės kilmės dervų fotostruktūrinimo dinaminės projekcinės litografijos būdu = Towards 3D photostructuring of naturally derived resins employing dynamic projection lithography // 42-oji Lietuvos nacionalinė fizikos konferencija, 2017 m. spalio 4-6 d., Vilnius : programa ir pranešimų tezės. Vilnius : Vilniaus universitetas, 2017. ISBN 9786094598807. p. 260. DOI: 0.15388/proceedings/LNFK.42.

Other publications and articles in conference proceedings

1. **Kašėtaitė, Sigita**; Ostrauskaitė, Jolita; Gražulevičienė, Violeta; Švedienė, Jurgita; Bridžiuvienė, Danguolė. Camelina oil- and linseed oil-based polymers with bisphosphonate crosslinks // Journal of applied polymer science. Malden : Wiley-Blackwell. ISSN 0021-8995. 2014, vol. 131, iss. 17, p.1-8.

2. **Kašėtaitė, Sigita**; De la Flor, Silvia; Serra, Angels; Ostrauskaitė, Jolita. Effect of selected thiols on cross-linking of acrylated epoxidized soybean oil and properties of resulting polymers // Polymers. Basel : MDPI AG. ISSN 2073-4360. 2018, Vol. 10, iss. 4, p. 1-13.

3. **Kašėtaitė, Sigita**; Ostrauskaitė, Jolita; Pečiulytė, Laura; Juknienė, Indrė; Grigonis, Aidas; Matusevičius, Algimantas Petras. Polymeric composites for reconstruction of hooves // Baltic polymer symposium 2016 : Klaipeda, September 21-24, 2016 : programme and abstracts / Kaunas University of Technology, Vilnius University, Klaipeda University. Kaunas : Kaunas University of Technology, 2016. ISBN 9786090212356. p. 72.

4. Miežinytė, Greta; **Kašėtaitė, Sigita**; Ostrauskaitė, Jolita. Photorheometrical study of cross-linking kinetics of acrylated soybean oil and aromatic dithiols // Chemistry and chemical technology 2017 : proceedings of the international conference, April 28th, 2017, Kaunas. Kaunas : Kauno technologijos universitetas. ISSN 2538-7359. 2017, p. 62.

5. Miežinytė, Greta; **Kašėtaitė, Sigita**; Ostrauskaitė, Jolita. Photocross-linked polymers of acrylated soybean oil and aromatic dithiols as promising materials for optical 3D printing // Frontiers in Polymer Science in association with the journal Polymer: 17-19 May, 2017, Seville, Spain / organised by Elsevier. [S.l.] : [s.n.]. 2017, P3.043, p. 1.

6. **Kašėtaitė, Sigita**; Ostrauskaitė, Jolita; Serra, A.; De la Flor, S. Bio-based polymers from acrylated epoxidized soybean oil and structurally different thiols // Baltic polymer symposium 2017: Tallinn, Estonia, 20-22 September, 2017 / Co-organized by Tallinn University of Technology and COST action CA15107. Tallinn : TTU. 2017, p. 90.

7. Valaitytė, Deimantė; **Kašėtaitė, Sigita**; Ostrauskaitė, Jolita. Photorheometrical study of cross-linking kinetics of acrylated soybean oil and squalene hexathiol // Open readings 2018: 61st international conference for students of physics and natural sciences, March 20-23, 2018, Vilnius, Lithuania : programme and abstracts. [S.l.] : [s.n.]. 2018, p. 274.
8. **Kašėtaitė, Sigita**; Ostrauskaitė, Jolita; Serra, Angels; De la Flor, Silvia. Cross-linked polymers of acrylated epoxidized soybean oil and different thiols // Chemical sciences journal: 8th European chemistry congress, June 21-23, 2018, Paris, France. London : OMICS International. ISSN 2150-3494. 2018, 9, p. 67.

ACKNOWLEDGEMENTS